BIOCOMPATIBILITY OF OCULAR BIOMEDICAL DEVICES

by

Nathan Williams Gooch

A dissertation submitted to the faculty of
The University of Utah
in partial fulfillment of the requirements for the degree of

Doctor of Philosophy

Department of Bioengineering

The University of Utah

August 2013

The University of Utah Graduate School

STATEMENT OF DISSERTATION APPROVAL

The dissertation of **Nathan Williams Gooch**

has been approved by the following supervisory committee members:

Balamurali Ambati	, Chair	**5/1/2013** Date Approved
Bruce Gale	, Member	**5/1/2013** Date Approved
Vladimir Hlady	, Member	**5/1/2013** Date Approved
Robert Hitchcock	, Member	**5/1/2013** Date Approved
Brenda Mann	, Member	**5/1/2013** Date Approved

and by **Patrick Tresco**, Chair of the Department of **Bioengineering**

and by Donna M. White, Interim Dean of The Graduate School.

ABSTRACT

Biocompatibility is a key aspect in determining the success of a biomedical device. In this work the development, manufacture, designs, and biocompatibility of two devices are discussed. As protein adsorption to a material surface is the first step in the host wound healing and inflammatory response this phenomenon was additionally examined.

The capsule drug ring (CDR) is a reservoir and delivery agent which is designed to be placed within the capsular bag during cataract surgery. Prototypes were manufactured by hot melt extrusion of Bionate® II (DSM), a polycarbonate urethane. The devices have been optimized using Avastin® as the drug of interest. In vitro biocompatibility was assessed with human lens epithelial cell (B-3), mouse macrophage (J774A.1), and mouse fibroblast (L-929) cell lines. Cell migration and proliferation were assessed after in vitro culture. Proinflammatory cytokines (i.e., MIP-1β, MIP-1α, MCP-1, IL-1β, TNF, and TGF-β1) were quantified using cytometric bead array (CBA). Preliminary *in vivo* biocompatibility and pharmacokinetics testing has been performed in rabbits.

Cataract extraction uses ultrasound energy and vacuum to liquefy, emulsify, and aspirate the cloudy lens. During phacoemulsification, thermal energy and fluidic currents within the eye can damage the postmitotic corneal endothelium. This results in corneal edema, compromised vision, and a potential need for corneal transplantation. Viscoelastics are used to stabilize the anterior chamber, to maintain the eye pressurization, and to help absorb and dissipate thermal energy. However, the fragile

corneal endothelium is often damaged despite the use of viscoelastics. This work discusses the development of a foldable 100 micron transparent shield for use during phacoemulsification. This endo-contact lens is designed to float in the anterior chamber to allow for surgical access, and to absorb and deflect thermal energy to protect the fragile corneal endothelium.

TABLE OF CONTENTS

LIST OF TABLES

LIST OF FIGURES

LIST OF SYMBOLS AND ABBREVIATIONS

ρ	Density
A	Amps
AMD	Age-Related Macular Degeneration
anti-VEGF	Anti-Vascular Endothelial Growth Factor
C	Carbon
C	Celcius
C_P	Specific Heat
CBA	Cytometric Bead Array
CCD	Charge-Coupled Device
CDE	Cumulative Dissipated Energy
CDR	Capsule Drug Ring
CMV	Cytomegalovirus
CNC	Computer Numerical Control
CO_2	Carbon Dioxide
DMA	Direct Memory Access
DPBS	Dulbecco's Phosphate-Buffered Saline
ELISA	Enzyme-Linked Immunoabsorbant Assay
EPT	Effective Phaco Time
EU	Endotoxin Units
eV	Electron Volts
FDA	Food and Drug Administration
FGN	Fibrinogen
g	Grams
H & E	Hematoxylin and Eosin
HSAA	Human Serum Albumin
IgG	Immunoglobulin G
IL-1β	Interleukin-1β
IND	Investigational New Drug
IOP	Intraocular Pressure
ISO	International Organization for Standardization
IVT	Intravitreal Injections
J	Joules
K	Kelvin
k	Thermal Conductivity
L	Liters
LAL	Limulus Amebocyte Lysate
LPS	Lipopolysaccharide

m	Meters
MCP-1	Monocyte Chemotactic Protein-1
MEM	Minimum Essential Medium
MEMS	Microelectromechanical System
min	Minutes
MIP-1α	Macrophage Inflammatory Protein-1α
MIP-1β	Macrophage Inflammatory Protein-1β
MTS	Mercaptopropyltrimethoxysilane
O	Oxygen
OAG	Open-Angle Glaucoma
OD	Optical Density
PBS	Phosphate-Buffered Saline
PCU	Polycarbonate Urethane
PDMS	Polydimethylsiloxane
PEG	Polyethylene Glycol
PES	Polyethersulfone
PVA	Polyvinyl Alcohol
Q	Heat
Q_{bio}	Biological Heat
RCF	Relative Centrifugal Force
S	Sulfur
S/N	Signal-to-Noise
SEM	Standard Electron Microscopy
T	Temperature
t	Time
TCPS	Tissue Culture Polystyrene
TGF-β1	Transforming Growth Factor-β1
TIRF	Total Internal Reflection Fluorescence
TNF	Tumor Necrosis Factor
u	Heat Transfer Coefficient
UV	Ultraviolet
V	Volts
VEGF	Vascular Endothelial Growth Factor
W	Watts
XPS	X-ray Photoelectron Spectroscopy

CHAPTER 1

INTRODUCTION

Background

Age-Related Macular Degeneration

Of noncataract blindness, age-related macular degeneration (AMD), glaucoma, and corneal disease each account for 20-25% of world blindness. AMD, the leading cause of blindness in the US, has 2 principal forms: "wet" or exudative (characterized by angiogenesis or growth of new blood vessels), and "dry" or nonexudative (characterized by geographic atrophy and drusen, and a steady rate of progression to "wet" disease). In the US, there are over 2 million people with advanced AMD (expected to double by 2020), and worldwide, there are ~30 million people with this condition. Further, 7.5 million Americans are affected by intermediate AMD and are thus at risk for developing advanced AMD. This disease is a major public health epidemic with vast socioeconomic impact. Present antiangiogenic modalities offer significant benefit to many patients with neovascular AMD, indefinite monthly intravitreal injections. However, treatment of AMD requires monthly intravitreal (IVT) injections, which can have serious risks (e.g., retinal detachment, endophthalmitis, hemorrhage, and cataractogenesis), are not well accepted by patients, and costly. The AMD population is in need of safer and easier to use drug delivery technologies that can deliver the anti-VEGF compounds into the target

tissues at a minimum as effectively as the IVT injection. Such technology will revolutionize the treatment of AMD and reduce health care costs locally and globally for AMD with the introduction of anterior-segment based alternatives to IVT injections and the ability to decrease monthly office visits.

Current FDA-approved therapies include the anti-VEGF aptamer (pegaptanib (Macugen; OSI)) and the anti-VEGF Fab fragment (ranibizumab (Lucentis; Genentech)), and photodynamic therapy. Use of Macugen and photodynamic therapy has been eclipsed by intravitreal injections of Lucentis, as it is the first drug to demonstrate significant visual acuity improvement in patients with neovascular AMD. Lucentis costs approximately $2,500 per injection (prospective annual cost approximating $30,000), thus demonstrating the potential of a large market (Lucentis sales are expected to approach $1 billion annually). This has triggered a pipeline of 24 INDs (Investigational New Drugs) with at least 20 drug projects in preclinical stages. While the future space in pharmaceutical management of AMD may become crowded, drug delivery platforms are needed to improve ease of administration, convenience, and patient quality of life, for patients now accept monthly intravitreal injections only because there is no choice. In addition, off-label use of bevacizumab (Avastin; Genentech), an anti-VEGF antibody has become common as it much less expensive, but nonetheless this requires regular intravitreal injections.

Current intraocular drug delivery devices include Retisert, Vitrasert, Posurdex, Medidur, and Neurotech's NT-501. All of these devices require intravitreal procedures and often suturing. These are single drug agents targeting chronic eye inflammation (fluocinolide – Retisert & dexamethasone - Posurdex), CMV retinitis (ganciclovir -

Vitrasert), diabetic macular edema (Medidur), and the dry form of macular degeneration (CNTF- NT-501). Surmodics has also recently developed the Eureka device delivering steroids for uveitis. None of these devices are refillable, nor do they target glaucoma or the wet (exudative) form of macular degeneration, which are the leading causes of severe visual loss.

Glaucoma: The Silent Thief of Sight

Glaucoma is a slowly progressive pathology that can result in the loss of peripheral vision, decreased contrast sensitivity, and loss of visual acuity. Due to the asymptomatic nature of the early phases of the disease most patients experience undiagnosed loss of vision until the advanced stages of the disease have occurred. Thus the disease is known as the "silent thief of sight." This indolent optic neuropathy is characterized structurally by a loss of retinal ganglion cells and optic nerve axons. Glaucoma is the second leading cause of the world's blindness with nearly 70 million cases worldwide and accounting for 12% of all cases of preventable blindness [1-3]. It is estimated that by 2020, close to 4 million Americans will have glaucoma with 50% undiagnosed and approximately 120,000 individuals developing blindness. [4, 5].

Glaucoma's strong correlation with raised intraocular pressure (IOP) has been demonstrated by large prospective randomized trials [6-11]. Increased IOP and IOP variability are now recognized as significant risk factors both for the development and the progression of glaucoma, with open-angle glaucoma (OAG) in particular [6, 9-11]. At present, the majority of OAG treatment modalities focus on the management and reduction of IOP. The standard goal of treatment is to reduce IOP by 20–50% from which

damage was sustained. Current pharmacotherapies such as pharmaceutical treatment with eye drops and gels, laser treatment, or incisional surgery achieve a lower IOP by either decreasing aqueous production or improving aqueous outflow [12, 13].

In developing countries, where the access to adequate care and therapies is limited, people are going blind from a disease that can be successfully treated. Patients in these countries may not have the ability to get to their clinics routinely for refills and exams [14]. However, even in the US with ready access to medical care and pharmaceuticals, glaucoma continues to progress in many patients [15]. Often poor IOP control is due to poor compliance and adherence to daily topical treatment regimes or inadequate, complex dosing regimens [16]. Despite effective monotherapy agents, data have shown that upwards of 40% of OAG patients require combination therapy for IOP reduction with close to 75% of glaucoma patients requiring adjunctive therapy after five years [7]. The complexity, cost, and administration issues with multiple medications further reduce patient compliance and adherence. Prescribing pharmacy claims data show the vast majority of patients do not take their topical medications or renew their prescriptions, resulting in patients regularly missing doses. Pharmacy records indicate that close to two months can go by between refills even for simple to use once a day prostaglandins analogs (PGAs) [17]. Of patients discontinuing their initially prescribed medication, more than half failed to restart any topical therapy (827/1624 [51%]) in the span of one year [18]. Retrospective population based data suggests a minority of patients consistently adhere to their topical medication [19]. A sustained mode of delivery where the patient's dependence on daily self instillation is eliminated could dramatically improve these statistics.

Data confirm that many patients are unable to self-administer drops effectively, including the arthritic aging population and uncooperative pediatric glaucoma patients [20]. Patient videos and questionnaires have demonstrated the inability for patients to effectively self dose and administer the drops accurately and as prescribed [21]. Recent data revealed that only 71% of 204 glaucoma patients were able to get a drop into the eye, and only 39% did so without touching the bottle to the surface of the eye [22]. Such studies confirm eye drop wastage, potential contamination of the eye drop bottles, and poor understanding of the situation among participants.

Side effects of glaucoma medications are also undermining patient compliance [23]. They can range from local minor effects such as redness, dry eye, burning, and foreign body sensation, to more serious systemic effects such as shortness of breath, fatigue, and low blood pressure or heart rate. An alternative delivery mode could substantially improve the local ocular and systemic safety and tolerability profile by decreasing the amount of drug delivered locally thus limiting systemic exposure.

There are currently several novel and innovative sustained release (SR) delivery methods in various stages of development. This paper will review some broad drug delivery platforms, the current landscape for treating glaucoma with these alternative delivery modes, and will discuss what data are needed in development to allow such a novel technology to be a clinically viable marketed product.

Ocular Drug Delivery

Current innovation in glaucoma treatment is focused on the improvement of drug delivery methods. The aim is to deliver drugs locally in a controlled manner while

mitigating the challenge of poor patient adherence, compliance, and persistence. Currently, the patient who is receiving maximal medical therapy may use up to four different classes of topical medications. A medication's cost, the complexity of a medical regimen, and the side effects of medications are all factors that may contribute to noncompliance. Innovative technologies may address these issues by ultimately leading to better patient outcomes, a better quality of life, and cost savings to society. To develop a viable, reproducible, SR technology one must consider: (1) formulation work; standardizing the release kinetics, and duration of action; (2) clinical study design (determining the timing of replacement or refill, and identifying the acceptable safety risk profile compared to the topical comparator); (3) encouraging physician and patient acceptance of perhaps a more invasive procedure; and (4) navigation of reimbursement issues to establish the rationale of a perhaps more costly product over the generic comparator.

From a technology perspective, the development of IOP lowering SR therapies is one of the fastest growing segments of the glaucoma market. This is due to the abundance of generic IOP lowering agents, first line branded drugs coming off patent, and the need to improve the compliance rates for these conventional therapies [24]. When considering total glaucoma-related pharmaceutical revenues, the market is actually declining due to drugs losing patent protection with subsequent generic competition. Significant revenue opportunities exist for first to market products that are able to show safety and efficacy in lowering IOP with generic SR reformulations. Furthermore, from a clinical and regulatory perspective, these drugs are being repurposed for the same indication (IOP lowering based on local delivery to the target ocular tissue) albeit with novel release

delivery profiles and bioequivalency data. Well established safety risk benefit profiles exist for daily topical pharmacotherapies with extensive clinical data thus eliminating much of the concern and evaluation that is associated with a novel chemical entity. First steps in improving adherence and local tolerability could be as simple as changing the formulation thus improving ocular residence time.

When a topical medication is chosen as a first-line therapy for a patient with OAG a stepladder approach is used [25]. Typically monotherapy is attempted before additional agents are added. Medications are selected based on their potential contribution to IOP reduction and the tolerability of their side effects.

There are currently five main classes of topical medications for the treatment of glaucoma. Most pharmacotherapies either decrease aqueous production (beta blockers (BB), alpha agonists (AA), and carbonic anhydrase inhibitors (CAIs)) or improve aqueous outflow (cholinergics, PGAs). There are also combined medications such as BB with AA or CAIs. Topical BB and CAIs are associated with fewer systemic side-effects than their oral forms and are better tolerated by many patients. PGAs have the advantage of effectiveness in lowering IOP with once daily dosing. However, some patients experience an irreversible change in iris color and periorbital dermal darkening with PGAs [26]. Recent research in topical delivery for glaucoma is focused on new drug carriers and formulations that will improve cornea penetration in a SR manner. Many of these approaches include the use of nanospheres, liposomes, and permeability enhancers to work in tandem with the drug formulation.

Conventional eye drops face rapid tear turnover. Only 1–3% of the topical dosage penetrates to target tissues [27]. A wide variety of novel ocular drugs, including nucleic

acids such as antisense oligonucleotides and siRNAs, are being investigated in tandem with nanosphere and microsphere ocular drug delivery methods to enhance cellular penetration, protect against degradation, and improve the solubility of normally poorly soluble drugs in order to allow for long-term delivery [28]. Liposomes are vesicular lipid systems of a diameter ranging between 50 nm and a few micrometers. They provide a convenient way of obtaining slow drug release from a relatively inert depot. Research has shown that drugs within neutrally charged liposomes result in similar IOP reduction and lasted twice as long as the conventional eye drop, suggesting that the liposomes increased the residence time of the drug [29]. This could reduce dosing frequency. Surfactants, bile acids, chelating agents, and preservatives have all been used as permeability enhancers. Cyclodextrins, cylindrical oligonucleotides with a hydrophilic outer surface and a lipophilic inner surface that form complexes with lipophilic drugs, are among the more popular permeability enhancers. They increase chemical stability and bioavailability and decrease local irritation [30].

Delivery Devices in Preclinical Development

Several innovative technologies are currently in preclinical development. The Replenish, Inc. (Pasadena, CA, U.S.) device consists of a reservoir for IOP lowering medication, a hydrolysis-based pump system and a cannula that delivers the drug into the anterior chamber. The device is designed to be a nonabsorbed, semipermanent, refillable device. It is implanted much like a tube shunt under the conjunctiva. It can be refilled in the office and can be noninvasively tuned to modulate the drug release rate. Clinically, IOP regulating pharmaceuticals have never been administered intracamerally, hence

safety studies will need to be conducted prior to clinical use.

In general, manually and electrically controlled mini drug pumps, like the Replenish device, are designed, fabricated, and tested using principles of microelectromechanical systems (MEMS) engineering [31]. A reservoir can be implanted subconjunctivally and a cannula is then inserted through an incision into either the anterior or posterior segment. Once the drug reservoir is depleted it can be refilled through a check valve (a one way valve), perhaps refilled over months to years. Electrically controlled pumps incorporate implanted batteries into the design. These devices can also drive electrolysis by wireless inductive power transfer. Electrolysis results in the electrochemically induced phase change of water to hydrogen, and oxygen gas generates pressure in the reservoir, forcing the drug through the cannula. Drug delivery is achieved simply by adjusting the applied current. Prototypes of MEMS (*i.e.*, Replenish) with ocular hypotensive agents, 0.5% timolol or 0.004% travoprost, were implanted in two dogs under the temporal conjunctiva with the cannula inserted into the anterior chamber [32]. The reduction of IOP was achieved for 8 hours with no complications observed out to 3 months. Device concerns include the potential of traumatic damage to intraocular structures during implantation, as well as for the risk of endophthalmitis from continued external contact to the anterior chamber from the reservoir.

Replenish, Inc. soon plans to enter trials for FDA approval of a refillable programmable pump that is implanted onto the surface of the globe to deliver IOP lowering agents directly to the trabecular meshwork. The Replenish device is expected to be implanted for extended periods of time, extending to more than 5 years before needing replacement [32].

Contact lenses are currently in preclinical stages as replaceable drug delivery devices. As a drug delivery vehicle, they are desirable because they are a patient accepted, noninvasive, and a relatively safe product. Contact lenses that are commonly used today for vision correction are often composed of poly-2-hydroxyethylmethacrylate (p-HEMA) hydrogels. *In vitro* testing has shown that drug can diffuse from the hydrogel at therapeutic levels for up to 4 days [33]. Furthermore, researchers have shown that p-HEMA can be synthesized in the presence of drug nanoparticles for the purpose of reducing water solubility of drugs and lengthening elution profiles [33]. This is one method of increasing the residence time of drug particles inside the contact lens, thus increasing the duration of continued SR.

In an effort to further increase the duration of therapeutic drug delivery and improve the drug delivery kinetics, other contact lens designs have been attempted such as creating a drug depot in a degradable poly(lactic-co-glycolic) acid (PLGA) and coating the depot in p-HEMA, which is nondegradable [33]. *In vitro* studies of these lenses showed drug release with zero-order kinetics for up to 4 weeks [34, 35]. A limitation to the usage of contact lenses as drug delivery devices is that it requires patients to have steady hands and wear the contact lenses at all times possibly limiting the utility of other drugs being administered concurrently and raising safety concerns (e.g., corneal abrasion, neovascularization, and infection).

Conjunctival or subconjunctival administration of IOP lowering agents with SR for 3–4 months is another attractive alternative to daily eye drops. A time frame of 3–4 months of delivery is consistent with the frequency of routine glaucoma visits. Delivery over this extended time period is theoretically possible considering the volume available

in and under the conjunctival space, as well as degradation rates of biocompatible polymers. Injections in this region are minimally invasive and well tolerated by most patients. In spite of the potential advantages of bypassing patient compliance issues and the simplicity of in office administration, to date there are no subconjunctival delivery systems in clinical trials.

The ideal subconjunctival delivery of an IOP lowering drug would allow the drug to maintain suitable stability, be permeable across the sclera, provide SR out to 3–4 months, and minimize systemic and lymphatic absorption. Possibly the most significant challenge is a lack of clinical evidence to date supporting 3–4 months of IOP reduction. Although target *in vitro* SR rates are achievable and continuous IOP reduction has been shown in animal models, it is yet to be seen if this translates to clinical studies [36].

There are currently several technologies in development to achieve targeted release profiles with approved IOP lowering drugs. Timolol maleate has been incorporated into PLGA microparticles with a double water-in-oil emulsion technique [37]. One such formulation of PLGA exhibited SR for over 100 days in vitro with 100% of drug release at this point. Disadvantages to this method are a burst effect of 30% of the total drug after one day and only a 20% loading efficiency. Timolol eye drops have known cardio-pulmonary adverse side effects from excessive systemic absorption and these bursts could potentially lead to systemic adverse events.

Another SR formulation in preclinical development is liposomal latanoprost [36]. The formulation, which involves encapsulation of lipophilic latanoprost within a lipid bilayer, was tested *in vivo* in normotensive New Zealand white rabbits. IOP was lowered by 2–3 mmHg when compared to the nontreated rabbits and showed greater IOP reduction than

topical latanoprost drops. The IOP reduction from a single injection continued for 50 days at which point another injection was administered and a similar IOP lowering effect was shown out to 80 days. No adverse side effects were recorded even considering that a significant burst effect was suggested. However, the authors did not report any pharmacokinetic data. An advantage of this liposomal formulation is that the excipient benzalkonium (BAK) is not needed considering that the injection is a single use product. BAK is used in many topical multidose eye drop formulations as a preservative and has been implicated in ocular surface disease [38]. Products devoid of BAK offer an improved safety profile eliminating this unwanted side effect [39]. A drawback of a liposomal formulation is that its ocular safety and biocompatibility is less established than PLGA and other polymers.

Scleral permeability mechanisms are poorly understood making it difficult to predict a drug's interaction in the subconjunctival space and subsequent intraocular penetration. Physicochemical properties such as hydrophilicity/lipophilicity, acid/base characteristics, and molecular weight alter a drugs ability to permeate the sclera. Hydrophilic drugs better penetrate the sclera and have more pronounced burst effects where lipophilic drugs generally have smaller burst effects but poor scleral permeability [40, 41]. This creates a design paradigm when considering the ideal formulation because both good scleral permeability and a low burst effect are crucial to achieve safety and efficacy clinically. Strategies to minimize burst effects could be through excipient selection and multiple elements of controlled release (*i.e.*, degradation of microspheres and diffusion through a membrane) [42-44].

Delivery Devices in Clinical Development

Several prospective products are already in clinical development attempting to be the first to market as a sustained delivery of a generic IOP lowering agent (Table 1.1). The precise developmental status of many of these candidates is uncertain as they work through technical and clinical hurdles. Some of these products have encountered challenges with the mode of delivery. These have included such issues as long term device retention, which brings into suspect the ability of the drug to actually get to the ocular tissue continuously. Other challenges such as the insertion process have limited the ability of clinicians to affectively and safely place the device or depot.

Other opportunities to hasten clinical development incorporate generic drugs with nonproprietary polymers such as PLGA, Polycaprolactone (PCL), and chitosan. These polymers are attractive because their established ocular biocompatibility profiles and well recognized release kinetics can hasten the development path.

In terms of clinical progress, QLT is the furthest along. Punctal plugs have long been used for the treatment of dry eye syndrome and are a device that could be easily accepted by both patients and physicians. Punctal plugs are tiny, biocompatible devices inserted

Table 1.1. Glaucoma intraocular pressure (IOP) lowering sustained release (SR) platforms that have reached clinical development.

Company	Drug	Delivery Method	Clinical Development
pSivida Corp.	Latanoprost	Subconjunctival/Perilimbal	Phase I/II
Alcon	Anecortave	Subconjunctival/Subtenons	Phase II/III
Allergan	Brimonidine	Intravitreal	Phase II
QLT	Latanoprost	Punctal plug	Phase II
Aerie	Latanoprost	Subconjunctival suture fixation	Projected to start Phase I/II in 2012

into the lid puncta to block tear drainage. The use of punctal plugs for the delivery of ophthalmic medications offers a novel approach for chronic treatment of various eye diseases including glaucoma, postoperative therapy, and dry eye syndrome. Punctal plugs have several potential advantages over eye drops, including dose reduction, enhanced efficacy, and better patient compliance. Those made from silicone, hydroxyethyl methacrylate, polycaprolactone are intended for 180 day use [45], while punctal plugs made from animal collagen last for 7–10 days and disintegrate [46]. Recently, punctal plugs made from thermosensitive, hydrophobic acrylic polymer were used to avoid extrusion problems (Cylindrical Smartplug®) and improve retention. This polymer changes from a rigid solid to a soft, cohesive gel when its temperature changes from room temperature to body temperature. Excessive tearing (epiphora) and displacement or loss of plugs are common and can occur for many reasons. Canaliculitis, bacterial build up from punctual occlusion, can also be a concern. Punctal plug drug delivery systems are usually coated with a material that is impermeable to the drug and tear fluid on all sides except the head portion through which the drug is released into the tear film. The release of the drug from a punctal plug is controlled by drug diffusion to the tear fluid. The drug can be in the form of solutions, suspensions, microemulsions, nanoparticles, or liposomes. Some plugs can be soaked in drug solution before insertion; however, these drug-loading approaches, when performed in the outer coat alone, result in limited drug loading. Most punctal plugs have shown near zero-order drug release rates for drug molecules [47, 48]. QLT has had some issues with punctal plug retention. Punctal plug-mediated ocular delivery of latanoprost is in Phase II clinical study (QLT, Inc., BC, Canada) with a revised and custom fit plug delivering latanoprost. Recent reports show

60% of subjects at 4 weeks showed an IOP reduction of 5 mmHg or greater with a higher plug retention rate. The IOP lowering efficacy however is still inferior to topically daily administered Xalatan®.

Ophthalmic inserts are sterile preparations, with thin, multilayered, drug-impregnated devices placed into cul-de-sac or conjuctival sac in order to contact the bulbar conjunctiva. Ophthalmic inserts can be divided into three primary categories: soluble, insoluble, and bioerodible. For insoluble inserts, usually the core is a drug reservoir and sandwiched between rate limiting membranes. Ocular inserts allow for controlled sustained release, reduced dosing frequency, and increased contact time with ocular tissue (*i.e.*, better bioavailability). Expulsion and discomfort are the two greatest problems associated with their use.

Ocusert® (ALZA Corporation) is an insoluble insert and was the first ocular sustained release therapy. Ocusert devices are constructed of plastic membranes about one-third the size of a contact lens and inserted into the eye and worn under the upper or lower lid, where they cannot be seen. Ocusert never overcame topical drops as the delivery method of choice because of patient discomfort, the requirement of manual dexterity, patient education requirements regarding device placement and premature device displacement [49].

LACRISERT® (ATON Pharma) is a sterile, translucent, rod-shaped, water soluble, ophthalmic insert made of hydroxypropyl cellulose, for administration into the inferior cul-de-sac of the eye once daily and marketed for dry eye. It reduces the signs and symptoms resulting from moderate to severe dry eye syndromes, such as conjunctival hyperemia, corneal and conjunctival staining. It also has received minimal to moderate

market up take. Conceptually, other compounds, such as IOP lowering agents, could be formulated in such a device to help address the issues raised in this paper.

Subconjunctival inserts could allow for the use of implants in place of viscoelastic depot delivery injections. The qualities of an ideal subconjunctival injection could be obtained, but with the added risks of performing a minimally invasive surgery as opposed to an in office procedure. pSivida announced a collaboration with Pfizer in mid 2011 to deliver latanoprost via a unique patented drug delivery subconjunctival insert. According to public disclosures they initiated an ongoing Phase I/II study for safety, tolerability and initial efficacy at the University of Kentucky [50]. Aerie Pharmaceuticals has developed a latanoprost ocular insert said to be in preclinical development with plans to be in the clinic in 2012 [51]. An analysis of the company's publicly available information reveals an ocular insert made by compressing pellets of latanoprost then coating them with a membrane such as ethylene vinyl acetate [52]. This type of insert could provide a solution to the burst effect-hydrophilicity/lipophilicty paradigm with improved ability to control the burst effect through porosity and membrane thickness of hydrophilic drugs that readily permeate the sclera.

Topically administered daily ophthalmic brimonidine (Alphagan, Allergan) is indicated for IOP reduction in patients with ocular hypertension and or OAG. Brimonidine works by decreasing the amount of aqueous fluid in the eyes. Generally brimonidine is administered as a topical eye drops 2–3 times per day. Ophthalmic brimonidine has recently been shown to have potential neuroprotective mechanisms in glaucoma patients in addition to IOP lowering. In the Low Tension Glaucoma study, subjects randomized to Alphagan had equal IOP lowering as timolol yet less visual field

progression [53]. Neuroprotective treatments are designed to increase cell survival by protecting or enhancing cell injury resistance mechanisms or by helping to inhibit cell death.

Ozurdex, a degradable dexamethasone intravitreal implant, is used to treat macular edema and noninfectious uveitis. This device is one of two that have been approved by the US Food and Drug Administration (FDA) for intraocular implantation. Ozurdex slowly degrades in the vitreous releasing dexamethasone. Allergan is currently undergoing clinical trials of brimonidine tartrate in the Ozurdex PLGA platform for the treatment of geographic atrophy due to AMD [54]. This device could also translate into glaucoma management as a neuroprotective modality delivering brimondine.

Anecortave acetate (AnA), delivered as an anterior subtenons depot for the treatment of elevated IOP (Alcon Laboratories, Inc), showed promise in several initial pilot IOP-lowering studies. This insoluble compound had the benefit of acting as a sustained release suspension when given as a depot for upwards of 6 weeks. Its angiostatic properties originally were being investigated for wet age-related macular degeneration (AMD), but observations of IOP lowering effect led to glaucoma clinical investigations. Chemical modifications to eliminate the glucocorticoid activity and its mechanism of action were thought to enhance outflow at the trabecular meshwork [55, 56]. The hydrophobic molecule resisted diffusion and could therefore create a sustained release depot when injected in the juxtascleral or subtenons space.

An uncontrolled prospective case series wherein seven eyes of six subjects were treated with AnA via a juxtascleral delivery method was studied in 2009. Multiple perilimbal injections providing 24 cumulative mg were administered with a 30-gauge

needle under topical anesthesia [56]. IOP dropped an average of 9.5 ± 4.5 mmHg within the first week with effective IOP control maintained for a minimum of 3 but up to 19 months. Another study showed that a similar treatment resulted in 34% IOP reduction for one month in 7/8 eyes suffering uncontrolled steroid-induced ocular hypertension (OHT) [56].

Results of Phase II clinical trials were not as encouraging as prospective studies. The safety and efficacy study involved 200 patients who each received one anterior juxtascleral injection. It confirmed sustained IOP lowering at the highest dosage of 60 mg. However the mean reduction was only 3.8 mmHg [57]. In July 2009 Alcon announced that the benefit was insufficient to justify further development [58].

Conclusions

Glaucoma is a chronic pathology with few symptoms until late in the disease. Treatment is designed to prevent worsening rather than to improve visual function. Due to the fact that an immediate benefit is not felt by the patient, glaucoma is by nature a disease where compliance is a problem. SR of glaucoma therapies may be an answer to the issues of poor compliance, poor adherence, and even glaucoma progression through better and sustained IOP control. Despite glaucoma medications lowering IOP effectively, they are often unable to flatten the diurnal curve of IOP and if doses are missed due to noncompliance longer term IOP control is even worse [59]. With IOP variability and fluctuation both over 24 hours and over the course of weeks to months, glaucoma will most likely progress thus impacting the patient's visual outcomes. Outcomes data from large multicenter prospective studies support the notion that

consistent IOP lowering controlling for variability and fluctuation, may improve visual outcomes [6, 60, 61]. These SR technologies could show effectiveness in better IOP control both over 24 hours as well as longitudinally thus improving outcomes.

However, efficacy will not be enough to get these products on the market, as there are economic and health care issues that need to be considered. A novel delivery would need to be economically favorable to society and improve upon the standard of care. The U.S. health care system is currently relying on comparative effectiveness data to demonstrate improved quality of life, better outcomes for patients, and more cost effective means of providing care when considering reimbursements [62]. Thus outcomes research and data will need to be gathered during clinical development.

Currently, in the US, eye drops are generally the first choice for treating patients with OAG and generics are reasonably inexpensive. Despite effective therapies, patents progress and it is the cost of potential and future visual impairment resources that has the greatest cost to society. Studies have confirmed that the cost of care for people with glaucoma, over their expected lifetime, is higher than that of people without OAG [63]. Furthermore, with glaucoma progression and more aggressive interventions, the costs increase [64]. Hence therapies that affect outcomes and have the greatest likelihood of slowing progression through better IOP control will have the greatest cost savings to society.

With the possibility of improved patient outcomes, the argument can then be made that a more expensive drug device would have better long term efficacy, IOP control and less glaucoma progression, thus encouraging payers to reimburse more over the generic standard of care. These results could support a viable reimbursement proposition for a SR

commercial product given the significant number of patients with glaucoma on topical IOP lowering therapies that could benefit. The unmet medical need and the potential cost saving to society would cancel out the higher initial upfront cost of the device.

In summary, the ideal marketed SR drug delivery for glaucoma would have to show comparative efficacy to the topical daily comparator and have an acceptable safety risk profile that would allow it to be accepted by patients and physicians. It would need to demonstrate an advantage over the daily topical generic comparators such as an advantage for long term benefits, *i.e.*, better IOP control, less IOP fluctuation and hence better patient outcomes. It would need to be easy to administer, minimally invasive, and preferably given as an in office procedure every few months. It would have an acceptable safety and efficacy profile and perhaps even decrease the associated local tolerability and systemic safety concerns of the active compound when delivered as a daily topical.

The incidence of glaucoma is expected to rise dramatically in the next two decades. Thus, there is an urgent need to develop novel ocular delivery systems that meet the poly-pharmacy needs of the population with better patient compliance and better sustained long term IOP control initially. This paper has only focused on treating glaucoma with the current mainstay of therapy, IOP lowering agents. However, it must be recognized that glaucoma is a neurologic condition with retinal ganglion cell loss. Studies have indicated that glaucoma is a complex neurologic disease that affects optic nerves, optic radiations, and the lateral geniculate nucleus as well. Central nervous system (CNS) damage associated with glaucoma has been detected by alterations in optic nerves using magnetic resonance imaging [65]. Since retinal ganglion cell degeneration and vision loss can continue despite IOP normalization some propose that nervous system-based factors

can also mediate glaucomatous degeneration. This CNS damage may in itself contribute to the progression of glaucoma raising the opportunity for non IOP focused compounds being delivered in a SR manner and aimed at the neuronal preservation and or protection in glaucoma in the future [66].

Regardless of the compound and or mechanism of action, the ideal ocular delivery system is one that achieves and maintains effective drug concentrations at the target site for desired time intervals, minimizes systemic exposure and affords good patient tolerance, acceptance and compliance while maintaining a reasonable quality of life. The challenge as pharmaceutical scientists is to circumvent the protective transport barriers of the eye without inducing undesirable and unattractive side effects and still achieve a safe and effective therapy.

In conclusion, considering what the next steps for glaucoma treatment could be, ophthalmologists, health care providers, and researchers must remember the main therapeutic goal: to prevent or slow vision loss in a patient. Given the recognized high unmet need for improved glaucoma drug delivery, there is much activity, research and excitement in this area. As researchers, we need to look at new delivery technologies in terms of safety and risk, IOP and non-IOP efficacy, and development timelines as well as cost. Although various factors and hurdles will continue to play a role in furthering SR development, excitement remains for these novel delivery technologies in the future.

Motivation

Lately, there has been significant progress in the development of ocular biomedical devices. A number of these devices have been reported that show a great potential for a

wide range of applications. However, there is still a considerable scope for the development of improved ocular biomedical devices for the purpose of improving patient treatment options. The current state of clinical treatment of glaucoma, AMD, and cataracts could be much improved with advances in the development of ocular biomedical devices. This dissertation will answer some of these issues by discussing the development of new ocular biomedical devices with particular emphasis on biocompatibility.

Scope of Work and Significance

In this dissertation, I discuss two new biomedical devices (i) a capsule drug ring (CDR) placed within the capsular bag during cataract surgery for the purpose of sustained drug release for treatment of ocular disease and (ii) the endo-contact lens, a lens placed under the corneal endothelium prior to cataract surgery for the protection of the delicate cell layer. Design, fabrication and characterization of both of these devices are detailed. The motivation and significance of the development of both systems is also described. Hot-melt extrusion of polycarbonate urethane and soft lithography-based rapid prototyping techniques are used to fabricate the proposed medical devices. Polyethylene glycol (PEG) is also evaluated as a protein inert surface coating. These surfaces are used as a simplified model for complex biological protein adsorption phenomena involved in early biocompatibility host responses. PEG density gradients are evaluated in their ability to reduce protein adsorption.

Both theoretical and experimental results are used in the development of these biomedical devices to evaluate efficacy in their intended roles. A model is developed in

SolidWorks and COMSOL to predict the thermal effects of the use of the endo-contact lens. The state of the field of ocular disease treatment is reviewed in detail.

This work opens up the potential of new avenues for the treatment of ocular disease. Age-related macular degeneration, glaucoma, and cataracts are some of the ocular diseases that can benefit from the methods and devices developed as part of this work.

Chapter Outlines

This dissertation is organized such that each chapter, except the last chapter which states the conclusions and recommendations for future work, is either a published work or in preparation for publication. Chapter 1 is a portion of a comprehensive review on the state of the field of ocular disease management that was published as a peer reviewed scientific review article [67]. Chapter 2 describes the development of the Capsular Drug Ring (CDR) [68]. This device is under development as a sustained release device for the treatment of age-related macular degeneration, glaucoma, or cystoid macular edema. This chapter is under review for publication. Chapter 3 discusses the development of the endo-contact lens, a temporary lens for use during cataract surgery for the purpose of protecting the corneal endothelium from thermal damage during phacoemulsification. Future work for this device includes an evaluation of biocompatibility and efficacy under *in vivo* conditions. This chapter will be considered for publishing upon completion of this work. Chapter 4 examines the effect of polyethylene glycol (PEG) as a protein inert surface coating. This chapter focuses on the effect of PEG surface density as a function of its protein inert qualities. Chapter 4 is also being prepared as a journal paper in addition to inclusion in this dissertation. Chapter 5 is a summary of the important findings of this

dissertation work and suggests future efforts related to this work.

References

[1] Cedrone C, Mancino R, Cerulli A, Cesareo M, Nucci C. Epidemiology of primary glaucoma: prevalence, incidence, and blinding effects. Progress in Brain Research 2008;173:3–14.

[2] Quigley HA, Broman AT. The number of people with glaucoma worldwide in 2010 and 2020. The British Journal of Ophthalmology 2006;90:262–7.

[3] Friedman DS, Wolfs RC, O'Colmain BJ, Klein BE, Taylor HR, West S, et al. Prevalence of open-angle glaucoma among adults in the United States. Archives of Ophthalmology 2004;122:532–8.

[4] National Eye Institute, N.I.o.H. National Eye Institute. Available online: http://www.nei.nih.gov/ (accessed on 4 November 2011).

[5] Prevent Blindness America. Prevent Blindness America. 2011; Available online: http://www.preventblindness.org/ (accessed on 4 November 2011).

[6] AGIS Investigators. The Advanced Glaucoma Intervention Study (AGIS): 7. The relationship between control of intraocular pressure and visual field deterioration.The AGIS Investigators. American Journal of Ophthalmology 2000;130:429–40.

[7] CNTGS Group. The effectiveness of intraocular pressure reduction in the treatment of normal-tension glaucoma. American Journal of Ophthalmology 1998;126:498–505.

[8] Heijl A, Leske MC, Bengtsson B, Hyman L, Hussein M. Reduction of intraocular pressure and glaucoma progression: results from the Early Manifest Glaucoma Trial. Archives of Ophthalmology 2002;120:1268–79.

[9] Kass MA, Heuer DK, Higginbotham EJ, Johnson CA, Keltner JL, Miller JP, et al. Ocular Hypertension Treatment Study: a randomized trial determines that topical ocular hypotensive medication delays or prevents the onset of primary open-angle glaucoma. Archives of Ophthalmology 2002;120:701–13.

[10] Medeiros FA, Weinreb RN, Zangwill LM, Alencar LM, Sample PA, Vasile C, et al. Long-term intraocular pressure fluctuations and risk of conversion from ocular hypertension to glaucoma. Ophthalmology 2008;115:934–40.

[11] Musch DC, Gillespie BW, Niziol LM, Lichter PR, Varma R. Intraocular pressure control and long-term visual field loss in the Collaborative Initial Glaucoma Treatment Study. Ophthalmology 2011;118:1766–73.

[12] European Glaucoma Society. Terminology and guidelines for glaucoma (3rd edition). Editrice Dogma S.r.l. Savona, Italy, 2008 Available online: http://www.eugs.org/eng/aims.asp (accessed on 2 September 2011).

[13] Glaucoma Panel, A.A.o.O. Primary Open-Angle Glaucoma Suspect. Preferred Practice Pattern® Guidelines 2010 Available online: http://one.aao.org/ce/practiceguidelines/ppp_content.aspx?cid=e2387c8a-e51c-4c21-be20-c30fbf4f3260/ (accessed on 15 November 2011).

[14] Robin A, Grover DS. Compliance and adherence in glaucoma management. Indian Journal of Ophthalmology 2011;59 Suppl:S93–6.

[15] Leske MC, Heijl A, Hyman L, Bengtsson B, Dong L, Yang Z. Predictors of long-term progression in the early manifest glaucoma trial. Ophthalmology 2007;114:1965–72.

[16] Tsai JC, McClure CA, Ramos SE, Schlundt DG, Pichert JW. Compliance barriers in glaucoma: a systematic classification. Journal of Glaucoma 2003;12:393–8.

[17] Walt J, Wilensky J, Fiscella R, Chiang T, Guckian A. Refill Rates and Budget Impact of Glaucoma Lipid Therapy. Clinical Drug Investigation 2007;27:819–25.

[18] Schwartz GF, Platt R, Reardon G, Mychaskiw MA. Accounting for restart rates in evaluating persistence with ocular hypotensives. Ophthalmology 2007;114:648–52.

[19] Wilensky J, Fiscella RG, Carlson AM, Morris LS, Walt J. Measurement of persistence and adherence to regimens of IOP-lowering glaucoma medications using pharmacy claims data. American Journal of Ophthalmology 2006;141:S28–33.

[20] Hennessy A., Katz J, Covert D, Kelly CA, Suan EP, Speicher MA, et al. A video study of drop instillation in both glaucoma and retina patients with visual impairment. American Journal of Ophthalmology 2011;152:982–8.

[21] Robin AL, Novack GD, Covert DW, Crockett RS, Marcic TS. Adherence in glaucoma: objective measurements of once-daily and adjunctive medication use. American Journal of Ophthalmology 2007;144:533–40.

[22] Hennessy AL, Katz J, Covert D, Protzko C, Robin AL. Videotaped evaluation of eyedrop instillation in glaucoma patients with visual impairment or moderate to severe visual field loss. Ophthalmology 2010;117:2345–52.

[23] Zimmerman TJ, Hahn SR, Gelb L, Tan H, Kim EE. The impact of ocular adverse effects in patients treated with topical prostaglandin analogs: changes in prescription patterns and patient persistence. Journal of Ocular Pharmacology and Therapeutics 2009;25:145–52.

[24] Visiongain. Ophthalmic pharmaceuticals, market analysis, forecasts and dynamics - 2009-2023; Visiongain, Ltd: London, UK, 2009; 148.

[25] Coleman AL, Caprioli J. The logic behind target intraocular pressure. American Journal of Ophthalmology 2009;147:379–80.

[26] Bean GW, Camras CB. Commercially available prostaglandin analogs for the reduction of intraocular pressure: similarities and differences. Survey of Ophthalmology 2008;53 Suppl1:S69–84.

[27] Kreuter. J. Particulates (Nanoparticles and Microparticles), in Ophthalmic Drug Delivery Systems, A.K. Mitra, Editor. Marcel Dekker: New York, 1993,. 275-285.

[28] Fattal E, Bochot A. Ocular delivery of nucleic acids: antisense oligonucleotides, aptamers and siRNA. Advanced Drug Delivery Reviews 2006;58:1203–23.

[29] Monem AS, Ali FM, Ismail MW. Prolonged effect of liposomes encapsulating pilocarpine HCl in normal and glaucomatous rabbits. International Journal of Pharmaceutics 2000;198:29–38.

[30] Short BG. Safety evaluation of ocular drug delivery formulations: techniques and practical considerations. Toxicologic Pathology 2008;36:49–62.

[31] Saati S, Lo R, Li PY, Meng E, Varma R, Humayun MS. Mini drug pump for ophthalmic use. Transactions of the American Ophthalmological Society 2009;107:60–71.

[32] Kuno N, Fujii S. Recent advances in ocular drug delivery systems. Polymers 2011;3:193–221.

[33] Gulsen D, Chauhan A. Ophthalmic Drug Delivery through Contact Lenses. Investigative Ophthalmology & Visual Science 2004;45:2342–7.

[34] Ciolino JB, Hoare TR, Iwata NG, Behlau I, Dohlman CH, Langer R, et al. A drug-eluting contact lens. Investigative Ophthalmology & Visual Science 2009;50:3346–52.

[35] Ciolino JB, Hudson SP, Mobbs AN, Hoare TR, Iwata NG, Fink GR, et al. A prototype antifungal contact lens. Investigative Ophthalmology & Visual Science 2011;52:6286–91.

[36] Natarajan J V, Chattopadhyay S, Ang M, Darwitan A, Foo S, Zhen M, et al. Sustained release of an anti-glaucoma drug: demonstration of efficacy of a liposomal formulation in the rabbit eye. PloS One 2011;6:e24513.

[37] Bertram J, Saluja S. Sustained delivery of timolol maleate from poly (lactic-co-glycolic acid)/poly (lactic acid) microspheres for over 3 months. Journal of Microencapsulation 2009;26:18–26.

[38] Horsley MB, Kahook MY. Effects of prostaglandin analog therapy on the ocular surface of glaucoma patients. Clinical Ophthalmology 2009;3:291–5.

[39] Henry JC, Peace JH, Stewart JA, Stewart WC. Efficacy, safety, and improved tolerability of travoprost BAK-free ophthalmic solution compared with prior prostaglandin therapy. Clinical Ophthalmology 2008;2:613–21.

[40] Islam S. Hydrophilic drug loaded PLA/PLGA in situ implants: studies on thermal behavior of drug & polymer and observation of parameters influencing drug burst. International Journal of Pharmacy and Pharmaceutical Sciences 2011;3:181–8.

[41] Kadam RS, Cheruvu NPS, Edelhauser HF, Kompella UB. Sclera-choroid-RPE transport of eight β-blockers in human, bovine, porcine, rabbit, and rat models. Investigative Ophthalmology & Visual Science 2011;52:5387–99.

[42] Frank A, Rath SK, Venkatraman SS. Controlled release from bioerodible polymers: effect of drug type and polymer composition. Journal of Controlled Release : Official Journal of the Controlled Release Society 2005;102:333–44.

[43] Fu K, Harrell R, Zinski K, Um C, Jaklenec A, Frazier J, et al. A potential approach for decreasing the burst effect of protein from PLGA microspheres. Journal of Pharmaceutical Sciences 2003;92:1582–91.

[44] Peng Y, Ang M, Foo S, Lee WS, Ma Z, Venkatraman SS, et al. Biocompatibility and biodegradation studies of subconjunctival implants in rabbit eyes. PloS One 2011;6:e22507.

[45] Borgia, M.J., Chaouk, H., Cui, H., Laredo, W., Li, Z., Nathan, A. M.J.T. II. Punctal Plugs for the Delivery of Active Agents. Johnson & Johnson New Brunswick, NJ, USA, 2008, 10.

[46] The Eye Digest. Punctal Plugs. 05/19/2009 Available online: http://www.agingeye.net/dryeyes/plugsetc.php/ (accessed on 1 November 2011).

[47] Chauhan A, Zhu H. Dry Eye Treatment by Puncta Plugs. University of Florida Research Foundation: Gainsville, FL, US, 2010; 15.

[48] Rodstrom TR, Smith L, Tian Y, Allen D, Weiner L, Bakshi S. Punctal Plugs and Methods of Delivering Therapeutic Agents. Alcon Research, Ldt, Fort Worth, TX, US, 2008; 13.

[49] Pollack I, Quigley H, Harbin T. The Ocusert pilocarpine system: advantages and disadvantages. Southern Medical Journal 1976;69:1296–8.

[50] University of Kentucky Clinical Trial, Safety Study of Latanoprost Slow Release Insert (Latanoprost SR). 2010, ClinicalTrials.gov (accessed on 15 December 2011).

[51] Aerie Pharmaceuticals. Aerie Pharmaceuticals, Inc. 2011; Available online: http://www.aeriepharma.com/ (accessed on 15 December 2011).

[52] Kopezynski C, Lin CW, Sutay C. Drug Delivery Devices for Delivery of Therapeutic Agents. Chapel Hill, NC, USA, 2010.

[53] Krupin T, Liebmann JM, Greenfield DS, Ritch R, Gardiner S. A randomized trial of brimonidine versus timolol in preserving visual function: results from the Low-Pressure Glaucoma Treatment Study. American Journal of Ophthalmology 2011;151:671–81.

[54] Allergan Clinical Trial, Safety and Efficacy of Brimonidine Intravitreal Implant in Patients With Geographic Atrophy Due to Age-related Macular Degeneration (AMD). 2008, ClinicalTrials.gov (accessed on 4 November 2011).

[55] Hennessy AL, Robin AL. Anecortave Acetate: A New Approach for the Medical Treatment of Glaucoma, in The Glaucome Book: A Practical, Evidence-Based Approach to Patient Care, P.N. Schanknow and J.R. Samples, Editors. 2010, Springer: New York. 988-994.

[56] Robin AL, Clark AF, Covert DW, Krueger S, Bergamini MVW, Landry T a, et al. Anterior juxtascleral delivery of anecortave acetate in eyes with primary open-angle glaucoma: a pilot investigation. American Journal of Ophthalmology 2009;147:45–50.e2.

[57] Smit B. Anecortave Acetate for Steroid-Induced OHT, in Glaucoma Today. Bryn Mawr Communications LLC Wayne, PA, 2010, 43-44

[58] Alcon Inc., Alcon Discontinues Development of Anecortave Acetate for Intraocular Pressure Reduction., Business Wire: press release, 2009.

[59] Stewart WC, Konstas AGP, Nelson LA, Kruft B. Meta-analysis of 24-hour intraocular pressure studies evaluating the efficacy of glaucoma medicines. Ophthalmology 2008;115:1117–1122.e1.

[60] Caprioli J, Coleman AL. Intraocular pressure fluctuation a risk factor for visual field progression at low intraocular pressures in the advanced glaucoma intervention study. Ophthalmology 2008;115:1123–1129.e3.

[61] Caprioli J, Varma R. Intraocular pressure: modulation as treatment for glaucoma. American Journal of Ophthalmology 2011;152:340–344.e2.

[62] Wu AW, Snyder C, Clancy CM, Steinwachs DM. Adding the patient perspective to comparative effectiveness research. Health Affairs (Project Hope) 2010;29:1863–71.

[63] Kymes SM, Plotzke MR, Li JZ, Nichol MB, Wu J, Fain J. The increased cost of medical services for people diagnosed with primary open-angle glaucoma: a decision analytic approach. American Journal of Ophthalmology 2010;150:74–81.

[64] Traverso CE, Walt JG, Kelly SP, Hommer AH, Bron AM, Denis P, et al. Direct costs of glaucoma and severity of the disease: a multinational long term study of resource utilisation in Europe. The British Journal of Ophthalmology 2005;89:1245–9.

[65] Garaci F, Bolacchi F, Cerulli A, Melis M, Spano A, Cedrone C, et al. Optic nerve and optic radiation neurodegeneration in patients with glaucoma: in vivo analysis with 3-T diffusion-tensor MR imaging1. Radiology 2009;252:496–501.

[66] Yücel Y, Zhang Q, Weinreb R, Kaufman P, Gupta N. Effects of retinal ganglion cell loss on magno-, parvo-, koniocellular pathways in the lateral geniculate nucleus and visual cortex in glaucoma. Progress in Retinal and Eye Research 2003;22:465–81.

[67] Gooch N, Molokhia SA, Condie R, Burr RM, Archer B, Ambati BK, et al. Ocular drug delivery for glaucoma management. Pharmaceutics 2012;4:197–211.

[68] Gooch N, Burr R, Holt D, Gale B, Ambati B. Design and in vitro biocompatibility of a novel ocular drug delivery device. Journal of Functional Biomaterials 2013;4:14–27.

CHAPTER 2

DEVELOPMENT OF THE CAPSULE DRUG RING (CDR) BASED ON KNOWN OCULAR-BIOCOMPATIBLE MATERIALS

Abstract

The capsule drug ring (CDR) is a reservoir and delivery agent which is designed to be placed within the capsular bag during cataract surgery. Prototypes were manufactured by hot melt extrusion of Bionate® II (DSM), a polycarbonate urethane. The devices have been optimized using Avastin® as the drug of interest. In vitro biocompatibility was assessed with human lens epithelial cell (B-3), mouse macrophage (J774A.1), and mouse fibroblast (L-929) cell lines. Cell migration and proliferation were assessed after in vitro culture. Proinflammatory cytokines (i.e., MIP-1β, MIP-1α, MCP-1, IL-1β, TNF, and TGF-β1) were quantified using cytometric bead array (CBA). Preliminary *in vivo* biocompatibility and pharmacokinetics testing has been performed in rabbits.

Introduction

Of the diseases that result in vision loss, those which affect the retina and retinal function are of particular research interest due to the resultant permanent loss of visual function for which there is no definitive treatment. Current therapies restrict the progression of the disease, but due to limitations inherent in current pharmaceutical

delivery modalities, cannot cure it [1–5]. Continuous or repeated treatment is an implication of this form of therapy. Age-related macular degeneration (AMD) is the leading cause of blindness and significant visual impairment in developed nations. There are 30 million worldwide cases of AMD; in the United States, there are over 2 million current cases of advanced AMD with 200,000 new cases every year [3]. AMD is expressed in two principle forms. The “wet” or exudative form of the disease is characterized by the formation of new blood vessels, also known as angiogenesis. The “dry” or nonexudative form of the disease is characterized by the formation of drusen and often progresses into wet AMD. Rates of blindness due to retinal degeneration are expected to rise as the population ages over the next few decades [1].

The primary location of pharmaceutical action for the treatment of AMD is the posterior segment and the retina, with particular focus on the retinal pigment epithelium (RPE). The primary goal of treatment is to preserve the macula. While there are multiple methods of treatment under investigation, the current clinical treatment for this disease is indefinite frequent intravitreal injections (Figure 2.1).

Current treatments of AMD focus on pharmacological approaches. Due to the impact of angiogenesis in wet AMD, a significant amount of successful research has been focused on the use of antivascular endothelial growth factor (anti-VEGF) therapies as viable treatments for patients [2,5–8]. However, the current method of pharmaceutical delivery is indefinite intravitreal injections which are performed as often as monthly which can result in resistance [3,9]. These injections must be performed by retinal specialists due to the serious risks associated with these injections (e.g., retinal detachment, endophthalmitis, and vitreal hemorrhaging). Modern antiangiogenic

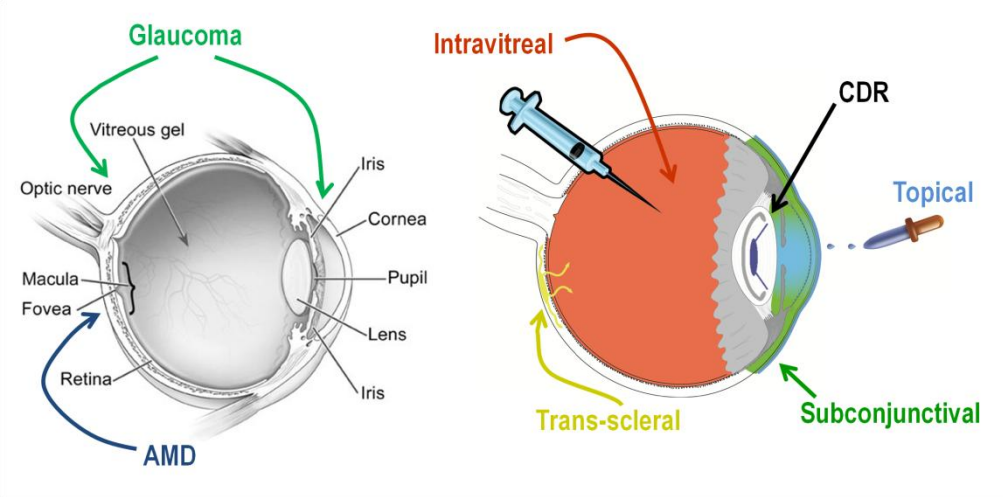

Figure 2.1. AMD and glaucoma locations of treatment are shown.

therapies offer significant benefit to many patients with neovascular AMD but would be much improved with a drug delivery modality which supported sustained and extended release profiles. Improvement in the treatment of AMD and other ocular diseases can have an immediate positive impact on the quality of life of patients.

Currently, there are implantable intraocular drug delivery devices on the market but none of these commercialized ocular drug delivery devices deliver anti-VEGF, nor are they refillable, versatile, and implantable by general ophthalmologists. In addition, these devices target AMD, which is the leading cause of blindness in the United States [10–18]. The Capsule Drug Ring (CDR) is a novel drug delivery device which is focused on the treatment of wet AMD by the sustained delivery of anti-VEGF. The device is designed to reside within the unused periphery of the capsular bag after cataract surgery. This can be implanted during standard intraocular lens (IOL) implantation which eliminates the need of an additional surgery. The CDR resides in the anterior chamber's capsular bag which reduces implantation and refilling costs as retinal specialists are not needed. This device

is intended to be a permanent, refillable implantation. This approach takes advantage of the frequency of cataract surgeries (3,000,000 annually in the United States) eliminating the need for additional surgeries or sutures. The incorporation of long term release kinetics will be a driving factor in the success of this device. Lucentis costs approximately $2,500 per injection (prospective annual cost approximating $30,000 per patient); Avastin costs approximately $150 per injection (prospective annual cost approximating $1,800 per patient). The CDR has been designed with the goal of reducing the frequency of injections thereby reducing the cost of treatment. With the goal of reducing the number of injections from monthly to once every 6 months, the annual cost of AMD treatment could be reduced by as much as 50%.

To test our idea of an implantable permanent intraocular drug delivery device we chose materials which have shown *in vivo* biocompatibility in other bodily tissues and screened their *in vitro* ocular biocompatibility via cell culture. We also tested the ability of Avastin, a ~150 kDa antibody, to permeate from the anterior chamber to the posterior chamber of the eye. Finally, we studied preliminary *in vitro* and *in vivo* drug release kinetics from the CDR.

Experimental

Materials and Design

CDR Mark I devices were constructed of Carbothane, a polyurethane carbonate; polyethersulfone (PES) membrane; and Loctite UV curable glue. This first generation device had a drug reservoir of 50-100 uL with ports for refilling the device. However, the device suffered from inconsistent leaking and filter fouling due to inconsistencies

inherent to the manufacturing process. The device also needs to be less than 50 mg in weight such that, in combination with the drug in the reservoir, the device does not exceed a weight of 200 mg within the capsular bag. The typical weight of a cataractous lens is 200 mg and can exceed 250 mg.

Despite not being currently prescribed for ocular use, Avastin (bevacizumab) was used as the pharmacological agent in this study. Lucentis (ranibizumab), the Fab fragment of Avastin, is an FDA-approved treatment for AMD. While Lucentis is a prescription medicine for the treatment of AMD, Avastin is being investigated as a lower-cost potential alternative therapy and is often used off-label for the clinical treatment of AMD [3]. Recent studies show similar outcomes in the ocular antiangiogenic efficacies and safety of the two drugs [3].

The CDR Mark I devices were manufactured using 4 μm sheets of Carbothane. Ten layers of these Carbothane sheets were pressed together onto a 2.3 mm glass plate without excessive tension or the inclusion of air bubbles. The plate and Carbothane was then placed into a CO_2 VLS 3.60 (Versa Laser) and stabilized using tape. The laser followed specific preprogrammed parameters to manufacture the core of the CDR devices as shown in Figure 2.2 and Table 2.1. The heat from the laser was also used to seal and laminate the layers of Carbothane together.

After the shell of the CDR was generated, the PES membranes were attached. To complete the device manufacture, the final layer of Carbothane was then attached to the top sealing the shell to form a reservoir (Figure 2.3). Islets were incorporated into the device design for the purpose of manipulation by the surgeon as the other regions of the device would be vulnerable to puncture by ophthalmic instruments.

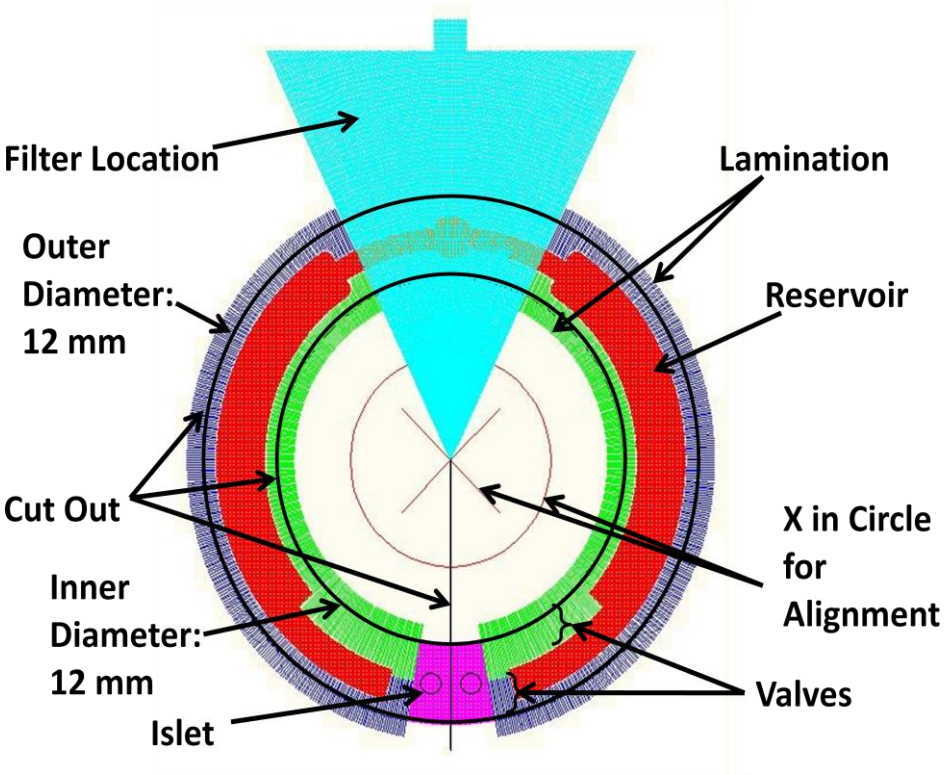

Figure 2.2. CO_2 laser parameters for the generation of the prototype CDRs.

Table 2.1. CO_2 laser parameters for manufacture of prototype CDRs.

	Power (%)	Speed (%)	Pulses per Inch	Z-axis (mm)
Filter Location	2	11	700	3
Reservoir	3.5 and 3	13 and 15	700	3.1 and 2.6
Reservoir below filter	2	10	700	3.1
Lamination: Outer	3	23	700	3.1
Lamination: Inner	3	26	700	3.1
Cut Out	13	10	700	3.1 and 2.6
Islet Area	3	15	700	3
X in Circle	2	10	700	2.3

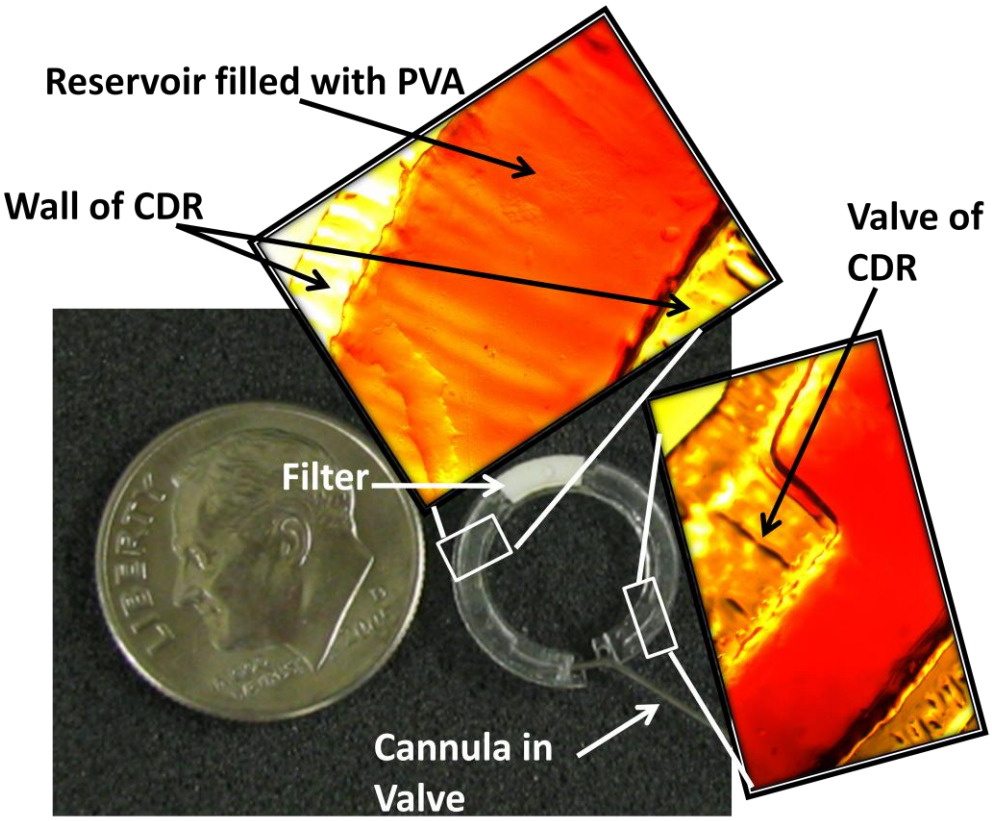

Figure 2.3. Completed CDR prototype design showing the sealed device and valves.

CDR Mark I devices persisted in suffering from fouling of the filter and fluid leaking from the reservoir despite design optimizations. In order to rectify these issues, the method of manufacture was changed. The Mark II CDRs were manufactured of three materials: Bionate® II, polyethersulfone, and Loctite® 4307™. Bionate II (DSM - Biomedical) 80A, a polycarbonate urethane (PCU) was synthesized by DSM Biomedical into pellets using DSM's proprietary technology and subsequently extruded into tubes using hot melt extrusion (Haake Minilab II Micro Compounder, Thermo Scientific). Tubing was extruded using a long land die (Guill Tool and Engineering) with a 0.750 outer diameter (420 SS) and a bullet nose tip. As the Bionate II tubing was extruded from

the dye it was wrapped around an 8 mm pipe to incorporate the correct inner and outer diameters into the polymer before fully setting. This extrusion/die setup formed tubing with an outer diameter of 1.4 mm, a wall thickness of 0.2 mm, and an inner diameter of 1.0 mm (Figure 2.4). Additional Bionate II films were extruded to a thickness of approximately 250 μm for use in biocompatibility assays. All the materials were synthesized and extruded without extrusion additives. Bionate II tubing was coated with Vitrostealth (DSM), a polyethylene glycol coating, after extrusion using DSM's proprietary technology.

Polyethersulfone (PES) (Sterlitech, PES0032005) was purchased from Sterlitech Corporation. The membrane has passed USP Class VI tests and is commonly used for hemodialysis membrane filters. The PES filter had 30nm pore-sized holes at a density of ~70%. Loctite 4307 (Henkel Corporation), a UV sensitive medical grade adhesive, has a history of being used in medical devices and is ISO 10993 compliant. This material served as the medium of adhesion between the Bionate II tubing and the PES membrane. The CDRs were assembled by cutting the Bionate II tubing into 360° segments yielding

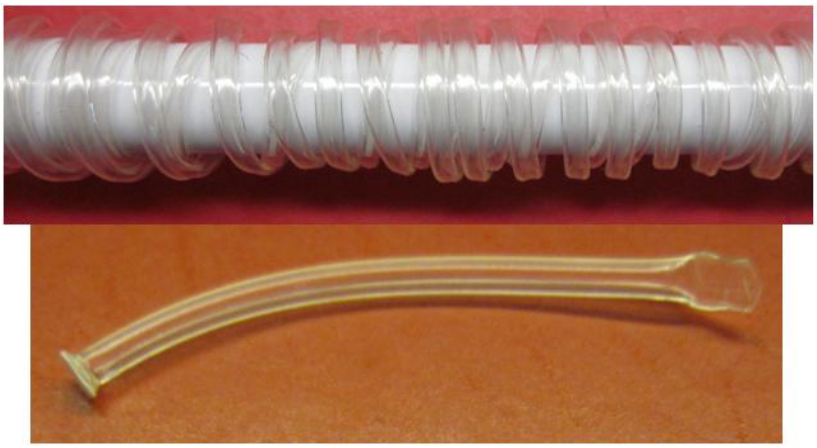

Figure 2.4. Bionate II the tubing after hot melt extrusion showing curvature and a linear section showing the attached membrane and the seal end.

a circular area of 0.79mm^2. PES membranes were cut to fit around one of the two open ends of the tubing segment and adhered into place using Loctite 4307. The other end of tubing was sealed closed using a heat press. CDRs were then cleansed by rinsing the devices three times in 200 proof ethanol. The devices were dried between each rinse. The devices were then sterilized using standard ethylene oxide treatment methods as part of a larger batch for the University of Utah Hospital.

Endotoxin Assessment

After manufacture, the devices were tested for presence of endotoxin. CDR device components and fully manufactured devices were placed in LAL water in separate endotoxin free containers and placed on a shaker plate at room temperature for 3 days. The samples were then placed in sonication for 2 hours and 30 minutes at 37 degrees Celsius. Meanwhile, a standard curve was formed from known endotoxin concentrations of 0, 0.005, 0.1, 0.25, 0.5, 1, 5, and 50 EU/mL. Afterwards the rinsate from the samples was extracted. The filter began to degrade after sonication and was centrifuged at 13,000 RCF to remove debris and the supernatant was used for the experiment. Each sample rinsate was read using a microplate reader at 405nm. The reaction onset time of each sample was recorded at n=3. The onset time is the time taken to reach the OD value (usually 0.03 OD units). Using the standard curve the endotoxin levels of the samples were determined.

In Vitro Cytotoxicity

In vitro cytotoxicity of the device components was assessed by the incubation (37.0°C; air, 95%; carbon dioxide (CO_2), 5%) of J774A.1 mouse macrophage and L-929 mouse fibroblast cell lines onto the major components of the CDR's. J774A.1 macrophages and L-929 fibroblasts and appropriate growth media were purchased from ATCC. J774A.1 macrophages were incubated in 10% fetal bovine serum in Dulbecco's Modified Eagle's Medium. L-929 fibroblasts were incubated in 10% horse serum in Eagle's Minimum Essential Medium. CDR components were sterilized using standard ethylene oxide treatment methods as previously discussed prior to cell plating. Cell media were harvested each day for 5 days at which time negative controls had reached full confluency. Inflammatory cytokines (i.e., MIP-1β, MIP-1α, MCP-1, IL-1β, TNF, and TGF-β1) secreted by cells into media were quantified using cytometric bead array (CBA) as a measure of the *in vitro* biocompatibility of these materials. Each *in vitro* cytotoxicity assessment was performed in the absence of Avastin. While it is possible that the presence of this anti-VEGF pharmaceutical agent could impact the biocompatibility of the CDR device, eliminating the use of Avastin in this study allows for a clearer picture of the impact of each device material. *In vitro* cytotoxicity was evaluated in the context of surface roughness and surface energy. Surface roughness was determined using a Tencor P-10 Surface Profilometer. Surface energy was inferred through the measurement of interfacial contact angles of deionized water on each surface using an AmScope MD900.

Drug Release Kinetics – *In Vitro*

To predict the *in vivo* release kinetics of Avastin from the CDR, several *in vitro* release studies were conducted ranging from 1 – 4 months with novel Avastin formulations. Avastin was frozen at -80 ^{o}C and lyophilized overnight. High molecular weight polyvinyl alcohol (140 – 158 kDa, Sigma) was added to balanced salt solution (BSS), a commonly used irrigating solution isotonic to the eye, at a final concentration of 50 mg/mL. The BSS was heated to 85 ^{o}C and stirred vigorously as the PVA was slowly added until completely solubilized. The PVA solution was cooled to room temperature and the Avastin lyophilate was added to a final concentration of 100 mg/mL. Approximately 35 uL of the formulations were filled in Bionate extruded tubes with polyethersulfone (PES) membranes attached to one end by UV curing adhesive and the other end sealed by heat press after filling (Figure 2.4). Each tube was immersed in 4 mL of BSS in closed vials and stored at room temperature on an oscillatory shaker at low speed. Samples from each vial were taken at predetermined time points and vial volume was maintained by addition of fresh BSS, thus maintaining sink conditions. A sample size of 3 was used per formulation tested.

Drug Release Kinetics – *In Vivo*

A preliminary *in vivo* drug distribution study was conducted following the *in vitro* studies to verify if therapeutically relevant quantities of Avastin can be achieved in the retina/choroid. CDRs were sterilized using ethylene oxide and filled with drug the night before surgery. Standard cataract surgery with phacoemulsification was performed on all rabbits. CDRs were filled with ~35 µL of the aforementioned reformulated Avastin. Of

the 8 rabbits used, 2 were sacrificed at the time points of 1, 4, 8 and 12 weeks. Upon sacrifice, tissues were segmented into the iris, cornea, sclera, retina, choroid, aqueous (anterior), and vitreous (posterior) humor and stored separately at -80° C.

Ocular drug distribution was gathered upon sacrifice of the rabbits at the predetermined time points. Histopathology was collected and showed some signs of long term inflammation and retinal hemorrhaging (data not shown). As a small preliminary study, it is unclear if the tissue aberrations are a result of the phacoemulsification/cataract surgery, CDR material/surgery, or some other factor.

Both *in vitro* and *in vivo* Avastin sample concentrations were measured using an enzyme-linked immunoabsorbant assay (ELISA). Avastin concentration was detected with a goat antihuman IgG/Fc antiobody labeled with horseradish peroxidase (Pierce Biotechnology Inc.) and chemiluminescent signal was detected on the EL800 Absorbance Microplate Reader (Biotek).

Results and Discussion

Despite not being currently FDA approved for ocular applications, Avastin (bevacizumab; Genentech) was used as the pharmacological agent in this study. Lucentis® (ranibizumab; Genentech), the Fab fragment of Avastin, is an FDA-approved treatment for AMD. While Lucentis is a prescription medicine for the treatment of AMD, Avastin is being investigated as a lower-cost potential alternative therapy and is often used off-label for the clinical treatment of AMD [3]. Recent studies show similar outcomes in the ocular antiangiogenic efficacies and safety of the two drugs [3].

Design and Manufacture

The CDR devices were designed and manufactured to be placed within the capsular bags of cataract patients prior to IOL insertion. In order to be successful the devices have very specific size requirements. To that end, polymer tubes were extruded with an outer diameter of 1.4 mm, a wall thickness of 0.2 mm, and an inner diameter of 1.0 mm. This allowed for the devices to fit around the periphery of the capsular bag, maximizing reservoir size without obstructing vision. Standard electron microscopy (SEM) was performed on the devices to show appropriate adhesion of Bionate II to PES filters to confirm that the reservoir contents were not leaking from the device, but were indeed being released only through the membrane which was carefully selected to generate our desired drug release kinetics. SEM also confirmed that adhesive did not foul our PES filter restricting drug flow from the device (Figure 2.5).

Endotoxin Assessment

Manufactured CDRs should be free of adventitious microbial agents for the protection of ocular tissues and for the reduction of the host inflammatory and immune responses. Adventitious microbes could be introduced by the raw CDR materials or the manufacture process. In an attempt to reduce microbial presence the CDRs were treated with ethanol washes and ethylene oxide after manufacture. In order to determine the efficacy of this method of cleansing, the manufacture method of the device and the raw CDR materials were tested for contamination with endotoxin. Endotoxins are the lipo-polysaccharides (LPS) from gram-negative bacteria. Endotoxin assays test for the presence of viable gram-negative bacteria and additionally detect the LPS from dead

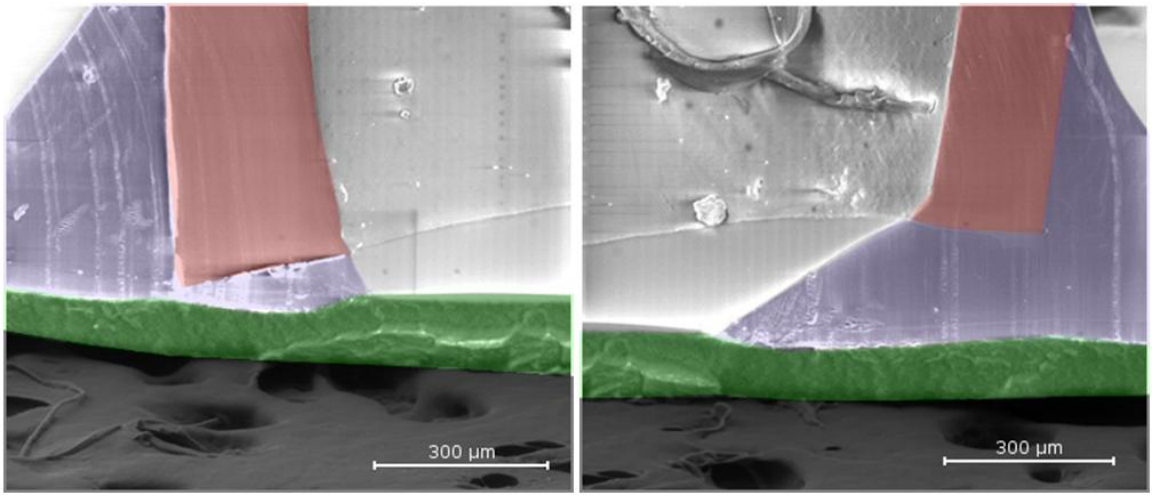

Figure 2.5. SEM images show appropriate adhesion of Bionate II tubing using the device membrane. Bionate II is shown in red, UV adhesive is shown in blue, the PES membrane is highlighted in green, and the SEM mount is shown in dark grey.

gram-negative bacteria. LPS is one of the most common causes of toxic reactions due to the presence of pyrogens. Therefore, the absence of detected LPS indicates an absence of pyrogens. For this study samples of each material and fully manufactured CDRs were quantified for endotoxin presence using a Limulus Amebocyte Lysate (LAL) assay. The result of the assay is shown in Figure 2.6. Each sample contained very low levels ofendotoxin. The highest concentration of detected endotoxin in our samples was 0.0344 EU/mL which is a full order of magnitude lower than what is considered to be endotoxin free, 0.5 EU/mL. The assay also detected less than half of the endotoxin contamination in each device component when compared to the fully manufactured devices. This would indicate that the method of device manufacture is introducing some small degree of bacterial contamination, but contamination levels are still well below what is considered endotoxin free.

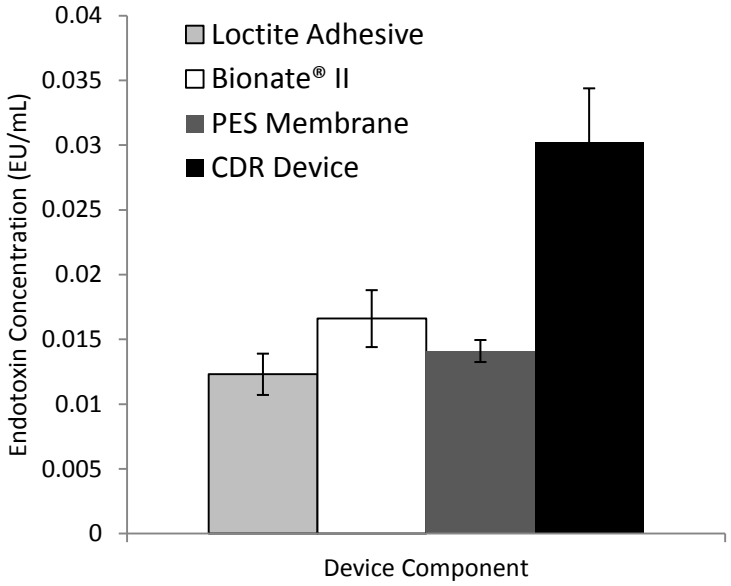

Figure 2.6. Endotoxin contamination levels of each component of the CDR. Each component is at levels which are considered to be endotoxin free (<0.5 EU/mL).

In Vitro Cytotoxicity

The interface between an implanted material and the surrounding biological tissue is the site of action wherein the host's response to an implant is most markedly manifested. Materials implanted into both hard and soft tissues generate some degree of cellular response. The severity of the host's response to an implant can be attributed to a number of factors including the surgical technique, the size, shape, and surface properties of the implant, and the nature of the tissues at the implant location. The interfacial interactions are a major factor in determining the success or failure of an implant. Therefore, the determination of an implant's impact on the host tissues is important to evaluate. This impact can only fully be anticipated through statistically powered *in vivo* usage of the implant; however, first step biocompatibility testing of biomedical devices can be shown through the use of *in vitro* cytotoxicity testing as discussed in ISO 10993.Implantation

into a host tissue generates a host cellular response. Activated cells produce cytokines including MCP-1, TGF-β1, IL-1β, TNF, MIP-1α, and MIP-1β. These cytokines are influential in regulating the host's wound healing response. Wound healing involves a number of cells including fibroblasts, monocytes, macrophages, and endothelial cells. For this study we performed cell culture with L-929 fibroblasts and J774A.1 macrophages. Both cell lines were individually cultured on the primary component of the CDR, Bionate II (DSM). Cell culture media were harvested after each day of the experiment and assay cytokines were quantified through the use of CBA on media harvested from days 1, 3, and 5. Fibroblast cell culture media were quantified for the presence of MCP-1 and TGF-β1; macrophage cell culture media were quantified for the presence of MCP-1, TNF, MIP-1α, and MIP-1β cytokines. These cytokine concentrations were compared to concentrations produced by cells cultured on incubation gold standard tissue culture polystyrene (TCPS).

L-929 fibroblasts were incubated on each surface and growth media were quantified 1, 3, and 5 days postincubation for inflammatory cytokines (Figure 2.7). The production of MCP-1 and TGF-β1 proinflammatory cytokines had a general increasing trend over incubation time which was to be expected as the cell populations increased over time. It was expected that a PEG coating (Vitrostealth®) of the biomaterial would decrease the production of proinflammatory cytokines but this correlation was not seen with our data. The production of TGF-β1 appeared to increase most dramatically for the fibroblasts cultured with the Vitrostealth coating. For both fibroblast produced quantified cytokines the cellular populations appear to show little difference from the negative control. J774A.1 macrophages were cultured experimentally similar to the L-929 fibroblasts and

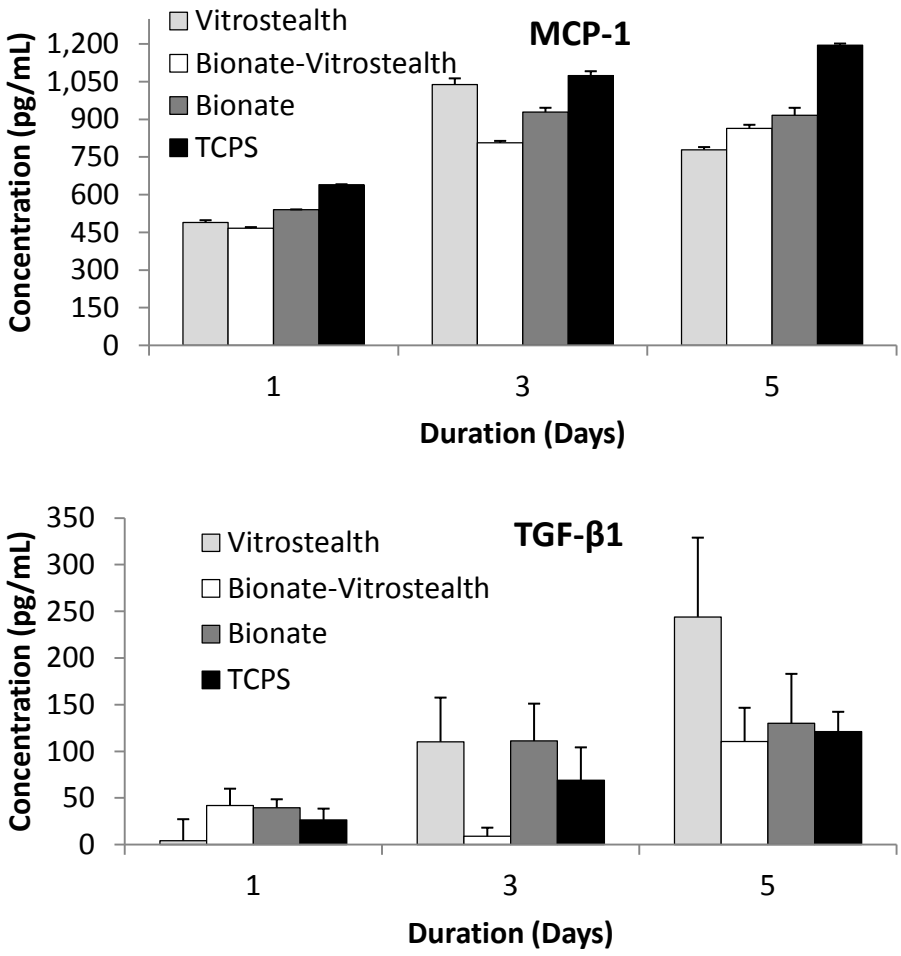

Figure 2.7. MCP-1 and TGF-β1 proinflammatory cytokines produced by L-929 fibroblasts as quantified by CBA.

media were harvested and quantified for days 1, 3, and 5. MCP-1, TNF, MIP-1α, and MIP-1β proinflammatory cytokines were measured using CBA (Figure 2.8). Cells cultured on the Bionate II material tended to show similar cytokine concentrations to the negative control throughout the duration of the experiment. In addition the macrophage cells cultured on each surface did not show signs of proliferative or morphological toxicity. This would indicate that the polycarbonate urethane (Bionate II) was not

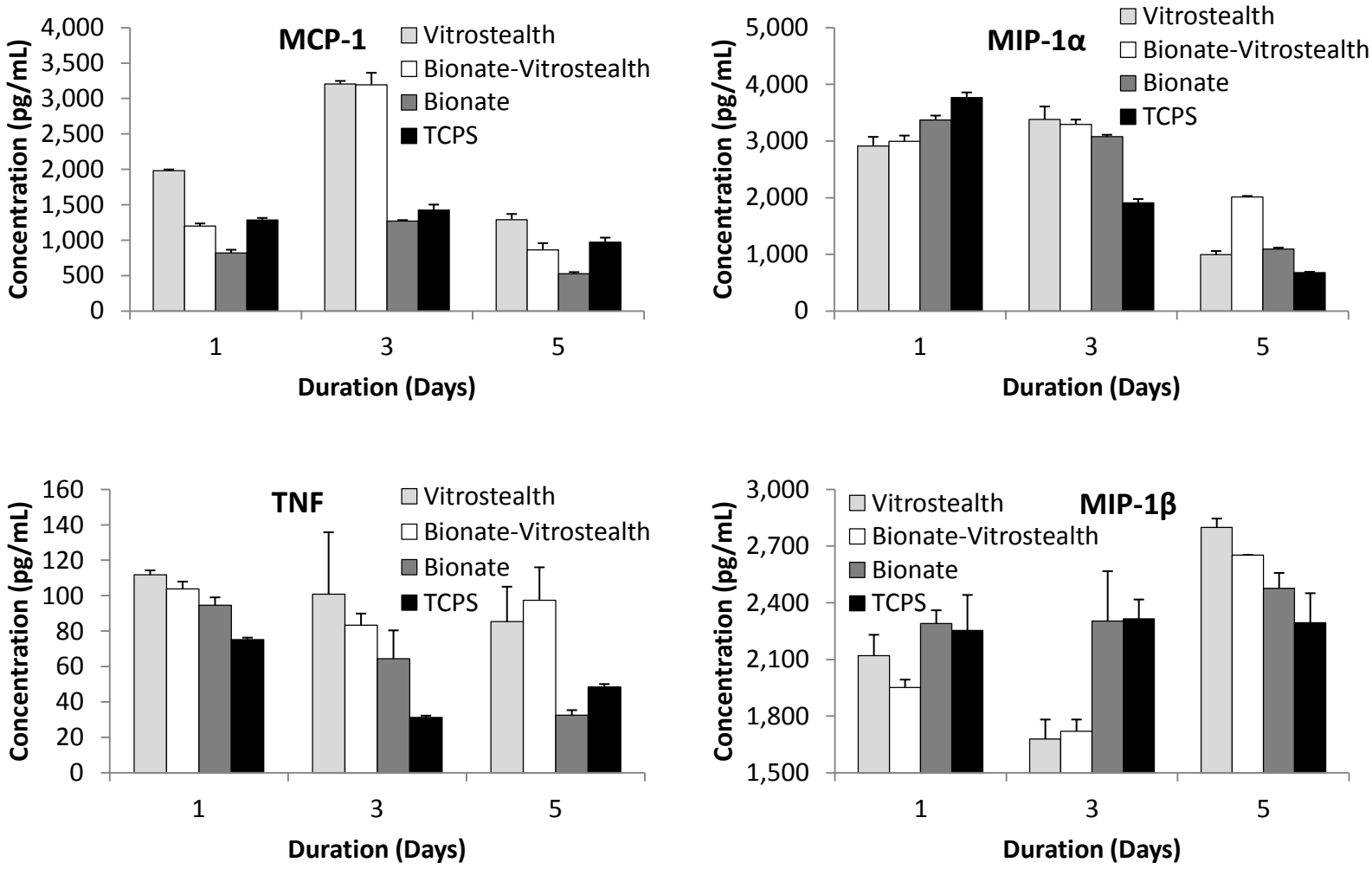

Figure 2.8. MCP-1, TNF, MIP-1α, and MIP-1β proinflammatory cytokines produced by J774A.1 macrophages as quantified by CBA.

aggravating the cells. However, cells that were cultured on Vitrostealth generally tended to express higher concentrations of TNF and MCP-1. However, this increase in TNF (~100 pg/mL) and MCP-1 (~60 pg/mL) is not significant on these volume scales. While no material is perfectly biocompatible, these *in vitro* data indicate that each of the tested biomaterials has a very similar impact on cultured fibroblasts and macrophages as the gold standard in cell culture, TCPS. This is seen in the similar levels of cytokine production in each of the samples.

It should be noted that cellular adhesion is also an important indicator of material biocompatibility. During this study this property was not implicitly measured for quantitative analysis but a qualitative analysis shows cellular adhesion on each material surface to be comparable. Macrophage cell adhesion was unaffected by the material type showing similar growth and adhesion on each of the materials. Fibroblast cellular adhesion appears to be impacted by each of the materials resulting in a slight morphological change despite remaining viable (Figure 2.9).

Surface roughness was measured for samples of TCPS, Bionate II, and Vitrostealth-coated Bionate II. Contact angle measurements were also taken for TCPS and Bionate II samples. These data are shown in Table 2.2. The data indicate that Bionate II was relatively rough in comparison to the other two surfaces. This may have induced some degree of increased cellular toxicity in comparison to the other samples; however, surface contact angles for both Bionate II and TCPS were very similar and the cellular release of proinflammatory cytokines also indicates that the increased roughness of the Bionate II samples had little effect on the cytotoxicity of the samples.

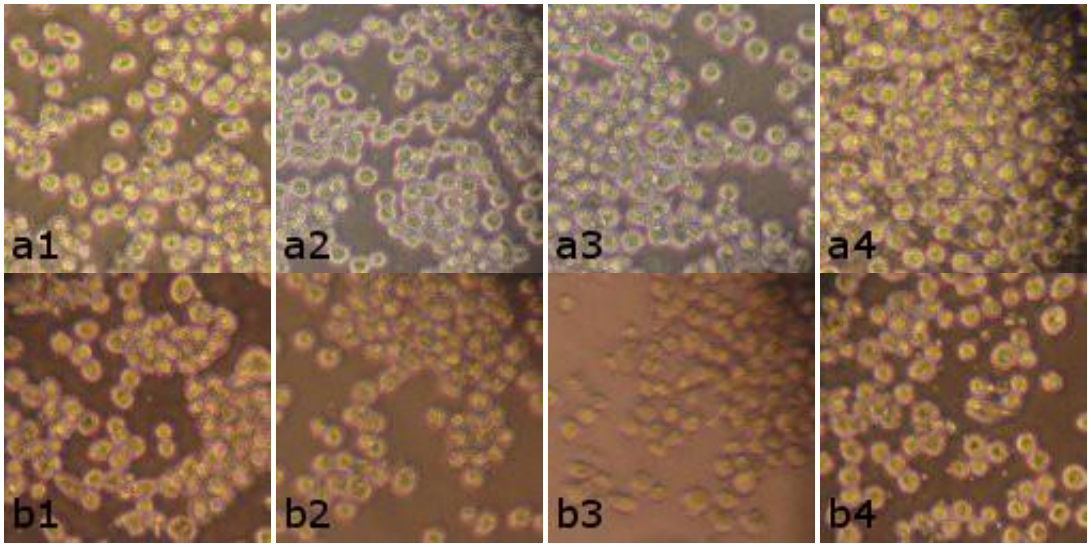

Figure 2.9. Photographs of L-929 fibroblast (a) and J774A.1 macrophage (b) showing representative cellular adhesion on Bionate II (1), Vitrostealth (2), Vitrostealth-coated Bionate II (3), and TCPS (4).

Table 2.2. Surface measurements of roughness and hydrophilicity.

	Surface Roughness (Ra, Å)	RMS Roughness (Rq, Å)	Contact Angle (degrees)
TCPS	177.7 ± 46.6	227.1 ± 62.6	76.5 ± 2.3
Bionate II	754.3 ± 372.2	953.5 ± 452.3	77.0 ± 2.5
Vitrostealth	98.8 ± 36.4	123.1 ± 47.0	N/A

Drug Release Kinetics – *In Vitro/In Vivo*

The current standard of care for the treatment of AMD is monthly intravitreal injections of Lucentis (ranibizumab; Genentech). However, Avastin (bevacizumab; Genentech) is a drug that is increasingly being used off label as a replacement for Lucentis for AMD treatment. For our drug release kinetics assessments we have used Avastin. For clinical treatment, each monthly bolus injection contains 1.25 mg and thus

the daily rate delivered is 41.7 ug/day. We used this as an initial target rate to be further refined with future *in vivo* experimentation. It is unclear if more or less drug than this is needed as the implant location is intended for the capsular bag as compared to intravitreally placed. Furthermore, sustained release drug delivery generally requires less drug and therefore a clinically relevant delivery rate will likely differ. Delineating macromolecular drug delivery from CDRs placed in the capsular bag at the time of cataract surgery is ongoing.

CDR drug release kinetics were assessed *in vitro* and *in vivo*. These experiments were performed as a first assessment of CDR device efficacy. *In vitro* media were harvested over time as previously described and assessed for Avastin concentrations at predetermined time points. The cumulative *in vitro* drug release accounts for ~30% of the total loaded drug where release plateaued at day 42 (Figure 2.10). Explanations for the unaccounted drug include nonspecific binding with the CDR, protein degradation from elevated temperatures and aggregation from the elevated concentration of 100 mg/mL. The presence of these phenomena was confirmed but not quantified explicitly. This study showed a two phase drug release profile. The first 10 days show a drug release of about 80 μg/day. After the first 10 days the rate of drug release slows down to about 16.5 μg/day. Future work with the CDR will include the tuning of the rate of drug release to incorporate near-zero order release kinetics and stability optimization as measured by charge variance analysis to maintain a therapeutic effect as determined in an appropriate disease model.

In vivo drug concentrations were quantified after implantation into 4 rabbits, concurrent to our *in vitro* assessment. The rabbits were sacrificed at 1, 4, 8, and 12

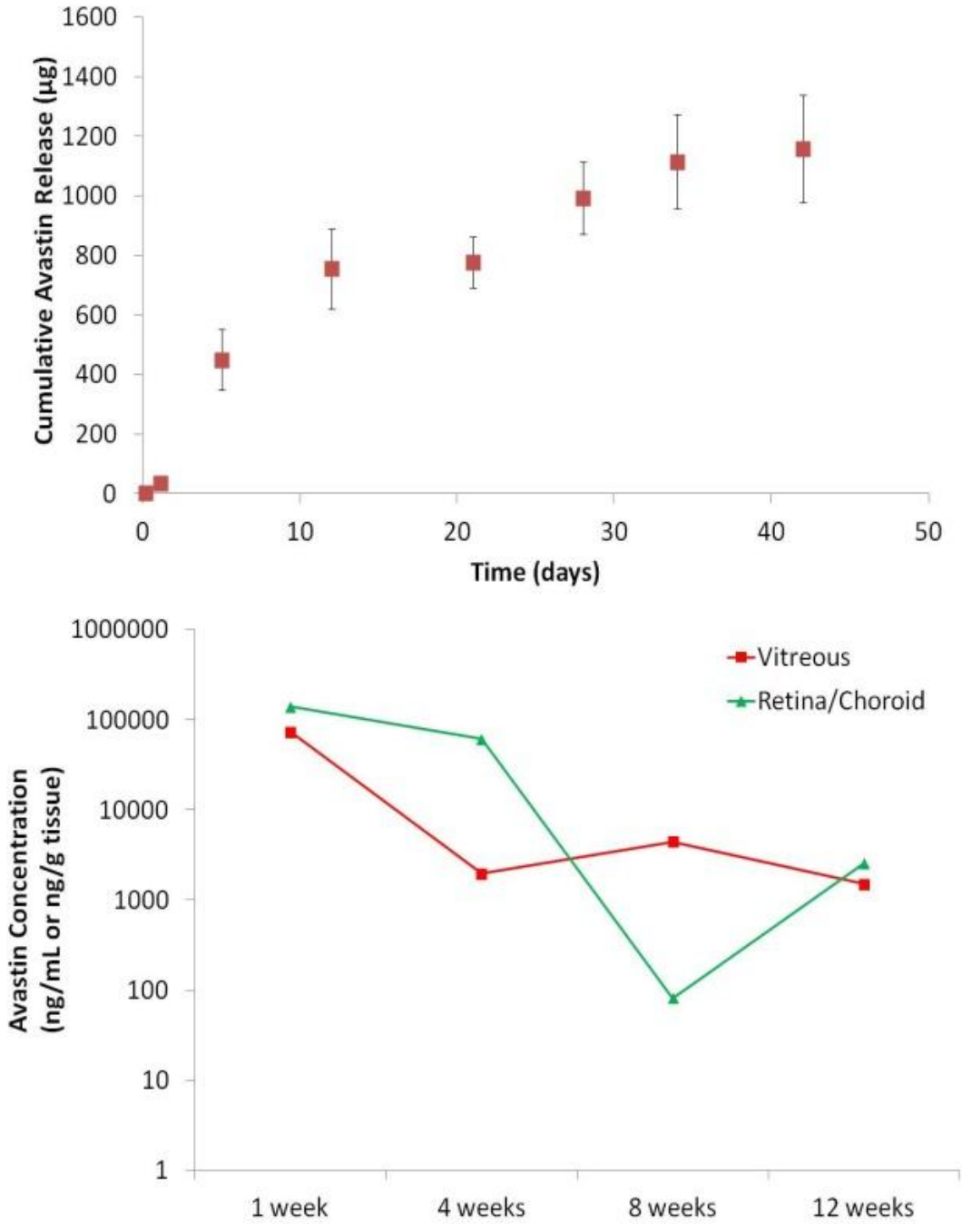

Figure 2.10. CDR sustained drug release was quantified by measuring Avastin release over time.

weeks. Tissues were harvested and ELISA was performed. Ocular drug distribution was assessed upon sacrifice of implanted rabbits at predetermined time points as shown in Figure 2.10. To the best of our knowledge there is no published work showing the penetration of a large molecule from the anterior chamber to the posterior chamber. This experiment clearly shows the ability of a large molecule such as Avastin (149 kDa) to penetrate into retinal tissues. During week 1 the drug concentration is found to be about 100 μg/mL and over the course of 12 weeks decreased to a concentration of about 1 μg/mL. However, for this experiment, only a single rabbit (n=2 eyes) was assessed for each timepoint and a statistically powered experiment will need to be performed in order to determine a correlation between the *in* vitro and *in* vivo release profiles.

Conclusions

Today AMD continues to be the leading cause of blindness and significant visual impairment in developed nations. While current treatments are able to slow the progression of the disease and improve the quality of life of many patients, the treatment process is far from perfect. Significant improvement can be made in patient health outcomes through the development of an extended release device. The development of the Capsule Drug Ring continues to be a work in progress but preliminary results of key *in vitro* device biocompatibility and efficacy assessments demonstrate the potential of the device. Future work with the device includes the incorporation of Avastin into *in vitro* biocompatibility assays, development of improved drug release kinetics to improve the long-term efficacy of the device, and the complete statistically powered *in vivo* biocompatibility and efficacy assessment of the device.

The results of this study show the successful manufacture of the CDR, a potentially refillable drug delivery device. The device is able to deliver Avastin out to 90+ days while showing acceptable biocompatibility. With a strategy of refilling the device only once over this 90-day period the burden of the cost of healthcare resulting from AMD treatments could be reduced by 25%. *In vitro* results show the devices and their individual components to be highly biocompatible with cells showing little difference in migration, proliferation, and proinflammatory cytokine generating behaviors when compared to gold standard culture methods. Future work will include the incorporation of Avastin into *in vitro* biocompatibility assays to determine the effect of the drug presence. In addition, improved drug release kinetics to improve the long-term efficacy of the device will need to be developed. The CDR shows great potential as an implantable ocular device for drug delivery.

References

[1] Congdon NG, Friedman DS, Lietman T. Important causes of visual impairment in the world today. JAMA 2003;290:2057–60.

[2] Ferrara N, Heinsohn H, Walder CE, Bunting S, Thomas GR. The regulation of blood vessel growth by vascular endothelial growth factor. Annals of the New York Academy of Sciences 1995;752:246–56.

[3] Kaufman SR. Developments in age-related macular degeneration: Diagnosis and treatment. Geriatrics 2009;64:16–9.

[4] Nagy JA, Dvorak AM, Dvorak HF. VEGF-A and the induction of pathological angiogenesis. Annual Review of Pathology 2007;2:251–75.

[5] Qazi Y, Maddula S, Ambati BK. Mediators of ocular angiogenesis. Journal of Genetics 2009;88:495–515.

[6] Dvorak HF. Vascular permeability factor/vascular endothelial growth factor: a critical cytokine in tumor angiogenesis and a potential target for diagnosis and therapy. Journal of Clinical Oncology 2002;20:4368–80.

[7] Ellis LM, Hicklin DJ. VEGF-targeted therapy: mechanisms of anti-tumour activity. Nature Reviews Cancer 2008;8:579–91.

[8] Ferrara N, Gerber HP, LeCouter J. The biology of VEGF and its receptors. Nature Medicine 2003;9:669–76.

[9] Bergers G, Hanahan D. Modes of resistance to anti-angiogenic therapy. Nature Reviews Cancer 2008;8:592–603.

[10] Bourges JL, Bloquel C, Thomas A, Froussart F, Bochot A, Azan F, et al. Intraocular implants for extended drug delivery: therapeutic applications. Advanced Drug Delivery Reviews 2006;58:1182–202.

[11] Campbell M, Nguyen ATH, Kiang AS, Tam LCS, Gobbo OL, Kerskens C, et al. An experimental platform for systemic drug delivery to the retina. Proceedings of the National Academy of Sciences of the United States of America 2009;106:17817–22.

[12] Daugherty AL, Mrsny RJ. Formulation and delivery issues for monoclonal antibody therapeutics. Advanced Drug Delivery Reviews 2006;58:686–706.

[13] Gorle AP, Gattani SG. Design and evaluation of polymeric ocular drug delivery system. Chemical & Pharmaceutical Bulletin 2009;57:914–9.

[14] Jaffe GJ, Yang CH, Guo H, Denny JP, Lima C, Ashton P. Safety and pharmacokinetics of an intraocular fluocinolone acetonide sustained delivery device. Investigative Ophthalmology & Visual Science 2000;41:3569–75.

[15] Kimura H, Ogura Y. Biodegradable polymers for ocular drug delivery. Ophthalmologica Journal International D'ophtalmologie International Journal of Ophthalmology Zeitschrift Für Augenheilkunde 2001;215:143–55.

[16] Lavik E, Kuehn MH, Kwon YH. Novel drug delivery systems for glaucoma. Eye (London, England) 2011;25:578–86.

[17] Li PY, Shih J, Lo R, Adams B, Agrawal R, Saati S, et al. An electrochemical intraocular drug delivery device. Sensors and Actuators A: Physical 2008;143:41–8.

[18] Saettone MF, Salminen L. Ocular inserts for topical delivery. Advanced Drug Delivery Reviews 1995;16:95–106.

CHAPTER 3

DEVELOPMENT OF THE ENDO-CONTACT LENS BASED ON KNOWN OCULAR-BIOCOMPATIBLE MATERIALS

Abstract

Cataract surgery can damage corneal endothelium, which can limit corneal clarity and vision and potentially cause need for corneal transplantation. A contact lens designed to shield the cornea from thermal and fluidic injury would be a great benefit to patients.

Cataract extraction, also known as phacoemulsification, uses ultrasound energy and vacuum to liquefy, emulsify, and aspirate the cloudy lens. During phacoemulsification, thermal energy and fluidic currents within the eye can damage the postmitotic corneal endothelium. This results in corneal edema, compromised vision, and a potential need for corneal transplantation. Viscoelastics are used to stabilize the anterior chamber, to maintain the eye pressurization, and to help absorb and dissipate thermal energy. However, the fragile corneal endothelium is often damaged despite the use of viscoelastics.

A foldable 100 micron transparent shield (the endo-contact lens) has been developed for use during phacoemulsification. This device has been designed to float in the anterior chamber, for the purpose of allowing surgical access, while hydroplaning and not sticking to the corneal endothelium, thus protecting this fragile cell layer. The device has been designed to be 5 mm in diameter, have a 6.42 mm radius of curvature, and be

manufactured from medical grade polydimethylsiloxane (PDMS). The endo-contact lens is a disposable implant which is designed to protect the cornea and potentially eliminate the need for viscoelastic.

Introduction

Cataracts develop as a clouding within the natural lens within the eye. This is most often caused by protein aggregation within the lens [1]. Cataracts tend to develop slowly, so vision gets worse gradually. Over time, the amount of aggregation increases to a point where vision becomes sufficiently blurry or dull to warrant the extraction of the cataract and replacement with an artificial lens.

Cataract extraction, also known as phacoemulsification, uses ultrasound energy and vacuum to liquefy, emulsify, and aspirate the cloudy lens. During phacoemulsification, thermal energy is generated by the conversion of electrical energy to mechanical energy and by frictional heat between the vibrating needle and the probe sleeve [2,3]. Temperatures can rise to over 100° C. This thermal energy and the fluidic currents induced by phacoemulsification within the eye can damage the postmitotic corneal endothelium [4,5].

The corneal endothelium consists of a delicate monolayer of cells on the posterior corneal surface. During phacoemulsification many of these cells are damaged; furthermore, the corneal endothelial cell layer is unable to regenerate after injury [6]. The body's mechanism for repair involves the enlargement of residual cells, cellular migration, and an influx of fluid which results in a lower cell density and a disruption of the natural cell structural patterns. Sufficient damage to this delicate cell layer can cause

corneal edema, compromise vision, and prompt a need for corneal transplantation. The lens endothelium normally has a cell density of 2500 cells per mm^2 and endothelial cell loss is typically 8-13% after cataract extraction; however in complex cases cell loss can be greater than 40% [7]. Corneal edema and decomposition begin to occur when the cellular density falls below 500 cells per mm^2.

Within the United States the elderly population continues to increase; that population increase results in an enlarged population of patients with cataracts. There are 3 million cataract surgeries annually within the United States and this number is expected to rise [8]. As cataract surgery can damage corneal endothelium, the increased numbers of operations will yield increasing patient populations with decreased corneal clarity and can potentially cause an increased need for corneal transplantations. The development of a contact lens designed to shield the cornea from thermal and fluidic injury would be a great benefit to patients and healthcare providers as the number of operations increase.

Design Rationale

Sodium hyaluronate and other viscoelastic materials have long been used during cataract surgeries and have become the standard of care during phacoemulsification. Several viscoelastics with different physical and chemical properties are available. Viscoelastics are used to stabilize the anterior chamber, to help maintain the eye pressurization, and to help absorb and dissipate thermal energy. There are two major classes of viscoelastic materials. The first type is a high viscosity, cohesive material such as sodium hyaluronate. The second is a low viscosity, dispersive material such as hydroxypropyl methylcellulose which is designed to adhere to the endothelium as a

protective coating during surgery. However, the fragile corneal endothelium is still damaged despite the use of viscoelastics [9].

Design requirements for the endo-contact lens to be successful include the need to be buoyant and transparent so as to float to the anterior-most portion of the aqueous humour as the patient lies on their back during cataract surgery and allow for the surgeon to work with full surgical access and visibility. The lens also needs to be foldable in order for the device to be able to be inserted into the aqueous humour through the cataract incisions. Finally, the lens needs to be hydrophilic so as to hydroplane across the corneal endothelium. It was determined that a polymer material would best fit the bulk of these strict requirements for the development of the endo-contact lens. However to the best of our knowledge a polymer which fits all of the device requirements, transparent, flexible, and buoyant, does not exist.

The development of the endo-contact lens has made use of the properties of PDMS as a transparent and foldable viscoelastic polymer. The historical success of silicone based biomaterials in the ocular space also makes PDMS an ideal biomaterial for this application [10–15]. PDMS, however, is not naturally buoyant and several methods have been researched for the purpose of inducing buoyancy while maintaining transparency. To this end, the PDMS endo-contact lens has been uniquely engineered to have a peripheral ring of air (Figure 3.1). The traditional method of reducing polymer density would be to incorporate microbubbles into the polymer design. However, any form of bulk microbubble infusion results in a loss of material transparency. The peripheral bubble design maintains the optical transparency of the lens through the bulk of the device and also causes the lens to become buoyant. The peripheral ring has been designed

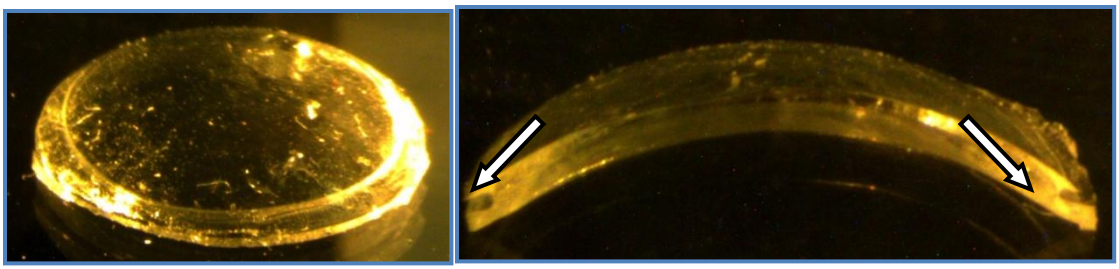

Figure 3.1. The PDMS lens is transparent and foldable with an air channel around the periphery.

to be manufactured such that it is not a fully enclosed bubble. The high contact angle of aqueous on PDMS prevents the penetration of liquid into the air chamber thus maintaining the presence of air in the channel.

The endo-contact lens is designed to be a more effective protection for the corneal endothelium than currently marketed products. Specifically, it has been designed to be a foldable 100 micron transparent shield which floats in the anterior chamber while hydroplaning and not sticking to the corneal endothelium. This allows for thermal protection of the corneal endothelium while at the same time providing surgical access. The device is designed to be a disposable implant that would protect the cornea and potentially eliminate the need for viscoelastic. This research indicates that with the use of this device, damage to the corneal endothelium will be reduced during phacoemulsification, improving surgical outcomes and could potentially wholly replace traditional viscoelastics.

Experimental

Computer Modeling

Major ocular structures including the cornea, lens, aqueous humor, and vitreous humor were modeled using COMSOL Multiphysics (4.3.0.151). A 2D-axisymmetric geometry was used for this study. Material properties for each tissue and liquid were obtained from previously published manuscripts and are tabulated in Table 3.1.

This model was used to assess the potential efficacy of the endo-contact lens in protecting the corneal endothelium prior to *in vivo* experiments. The governing equation used by COMSOL is the generalized heat transfer equation assuming time dependency and a fixed geometry was

$$\rho C_P \frac{dT}{dt} + \rho C_P \boldsymbol{u} \cdot \nabla T = \nabla \cdot (k \nabla T) + Q + Q_{bio}, \tag{3.1}$$

where ρ is density, C_P is specific heat, k is thermal conductivity, T is the temperature, Q is heat, and Q_{bio} is biological heat supplied to the system. The model of the eye was designed using anatomical measurements and is shown in Figure 3.2.

Table 3.1. Material properties of ocular domains for use in COMSOL.

Domain	Thermal Conductivity (W/m*K)	Specific Heat (J/kg*K
Cornea	0.58	3500
Lens	0.4	4200
Aqueous Humor	0.58	4200
Vitreous Humor	0.603	4200
Endo-Contact Lens	0.15	1460

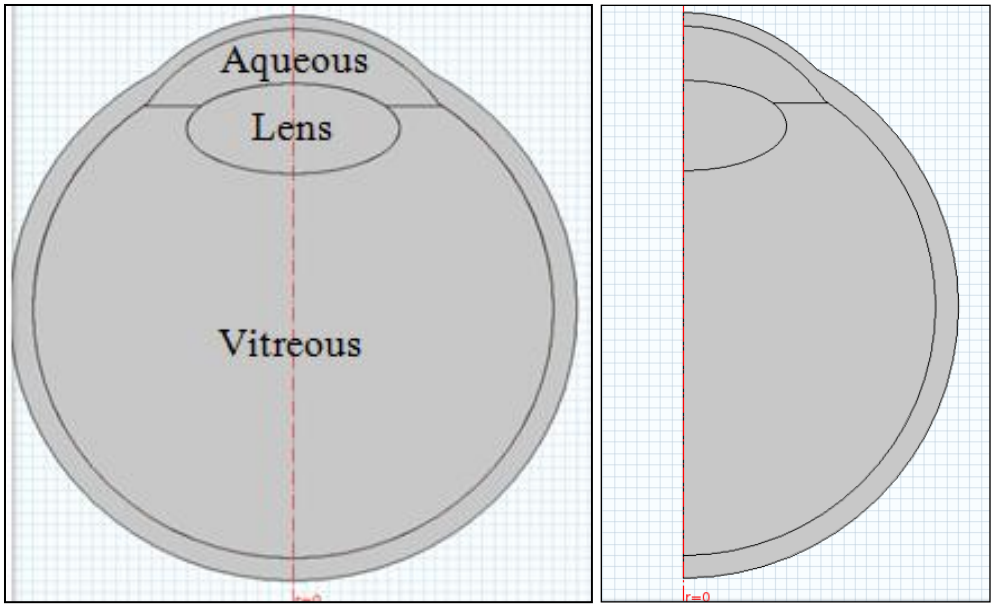

Figure 3.2. The COMSOL model generated showing the major anatomical structures, and the 2D-axisymmetric model.

Materials and Design

Polydimethylsiloxane (PDMS, Sylgard 184, Dow Corning) was used as the primary component of the endo-contact lenses. During device manufacture, the polymer was mixed at a 10:1 ratio base to curing agent. The endo-contact lenses were manufactured through a molding process. The first generation mold was manufactured using Teflon®. The mold was designed in Solidworks®, machined using a computer numerical control (CNC) machine, and aligned using four nails as shown in Figure 3.3. This original mold design generated a fully enclosed peripheral bubble in the endo-contact lens. However, this design allowed for very little variation in molding conditions. As a result the manufacturing process was unreliable. Additionally, the softness of the Teflon material used in the mold yielded microscopic machining marks which transferred to the PDMS

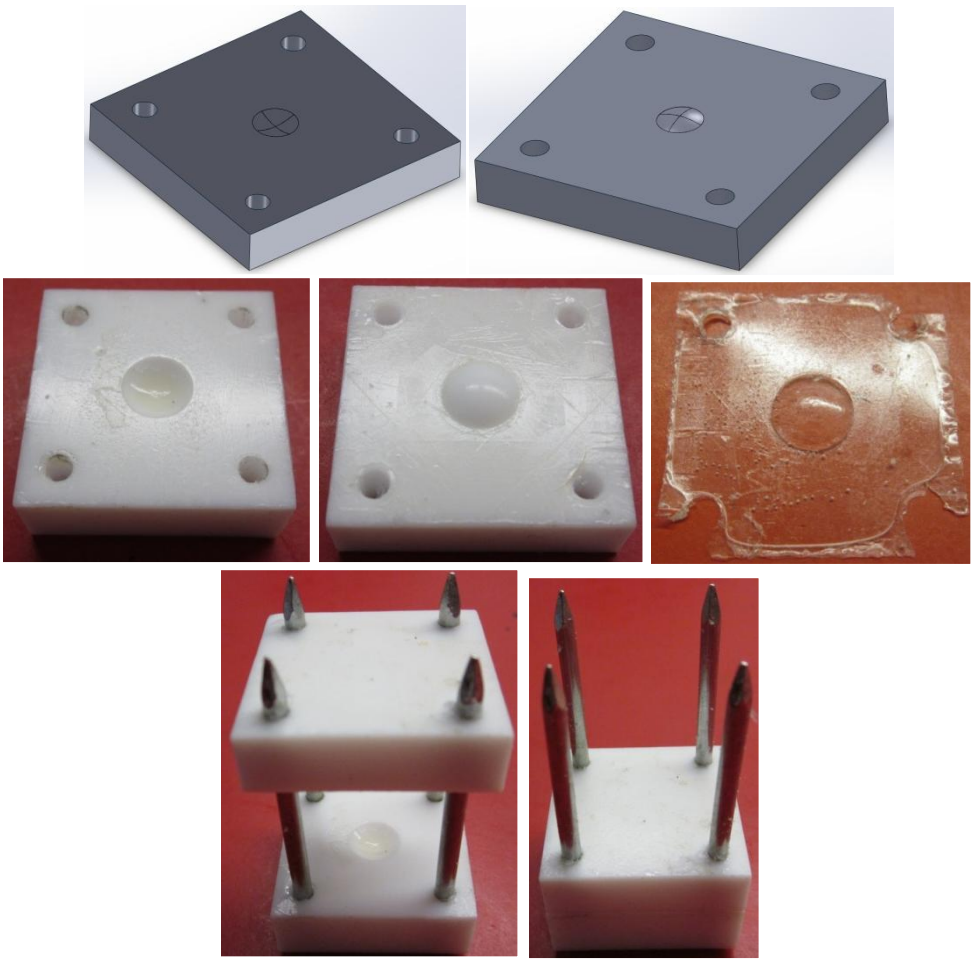

Figure 3.3. Design for the manufacture and use of the mold.

when used. This has resulted in some loss of transparency in the endo-contact lenses.

In order to address the complications involved with the Teflon mold a second generation mold was manufactured. This mold was manufactured of steel and afterwards polished. The polish was intended to improve the optical quality of the manufactured lenses. Additionally, the molding process was modified to include the use of a paper insert. This insert would be placed between the two molding pieces with a hole in the paper center; this hole was slightly smaller than the size of the endo-contact lens (~4.8 mm diameter). During the molding process the paper insert would induce the formation

of a peripheral channel in the manufactured endo-contact lenses rather than a peripheral enclosed bubble. This second mold and modified molding process was much more robust and allowed for a much higher success rate in the formation of PDMS endo-contact lenses. This molding process is shown in Figure 3.4.

Biocompatibility

In order to determine the degree of PDMS monomer leeching *in vitro* endo-contact lenses were immersed in vials of PBS and placed into sonication baths for 24 hours. The experimental negative control was a vial of sonicated PBS which was never introduced to any PDMS. The positive control was a vial of unmodified PDMS monomers. After 24 hours of sonication the endo-contact lenses were removed from solution. Mass spectrometry was used to determine the presence of PDMS monomers in each solution.

Preliminary *In vivo* biocompatibility experiments were also performed on n=2 rabbits. These data were obtained in partial fulfillment of a planned future study wherein two groups of n=7 rabbits will be assessed for the biocompatibility and efficacy of the endo-contact lens. Endo-contact lens efficacy was assessed through *in vivo* use of the lenses in rabbits used during cataract surgery. Rabbits underwent phacoemulsification and IOL insertion with ultrasound energy of 100 CDE (cumulative dissipated energy). 100 CDE of ultrasound energy was used to simulate more than the average required energy used during complex cases of cataract surgery. Two rabbits were used. One rabbit used the endo-contact lenses during surgery and the second used standard viscoelastic. Standard postoperative regimen was prescribed for both rabbits. Postoperative day 1 and 5 pachymetry was measured and corneas were photographed on those days. At

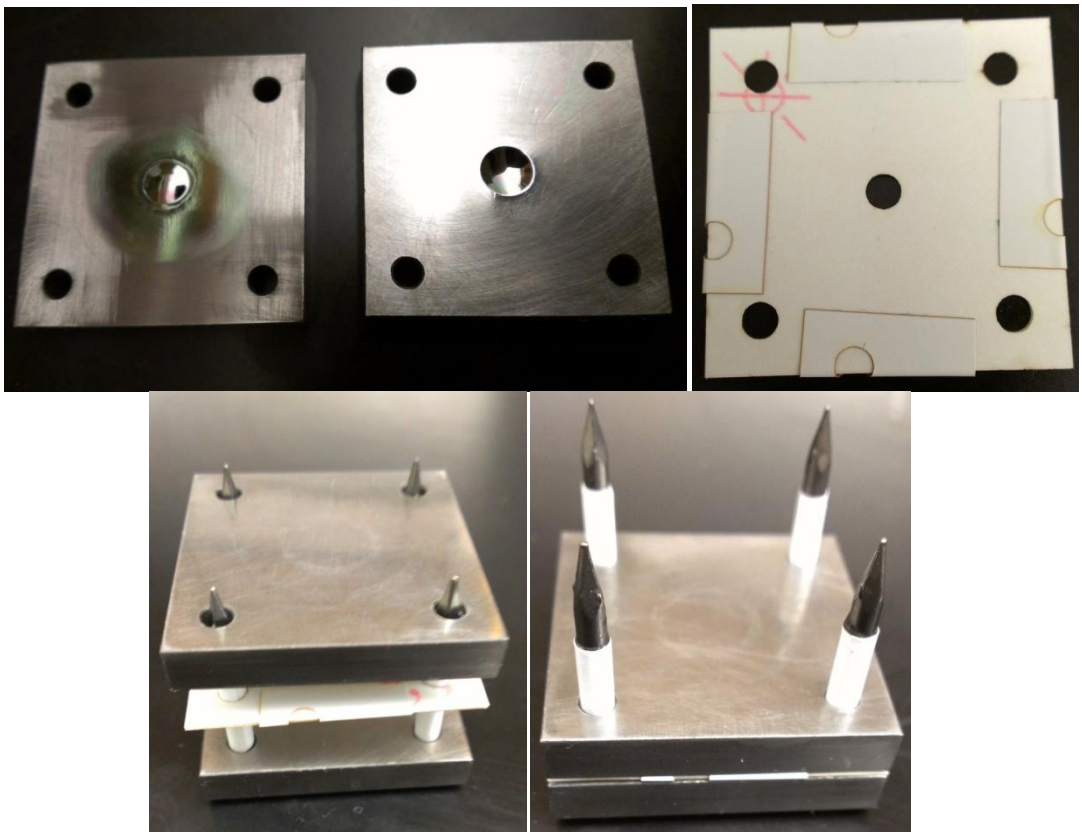

Figure 3.4. Metallic mold setup for manufacture of the PDMS lens.

postoperative day 5, eyes were harvested. Rabbit corneas underwent endothelial cell counting. Additionally, corneas and irises underwent histological analysis to evaluate postoperative morphology.

Results and Discussion

Computer Modeling

The phacoemulsive heat generation was modeled by assuming a time-averaged heat source applied to the whole of the lens. This approach of a single fixed heat source was taken due to the constraints of COMSOL modeling. It is expected that this assumption

will not negatively affect the model in a significant way as during the process of phacoemulsification a surgeon will, on average, spend time evenly throughout the whole of the lens. This model has also been simplified to not account for the physical disintegration and breakdown of the lens during phacoemulsification. The model was carried out for 60 seconds, during which time an *in vivo* lens will not yet have fully broken down. This model also takes advantage of effective phaco time (EPT). EPT is a method of accounting for the variability in ultrasound delivery during a surgery. EPT accounts for this variation by calculating the equivalent phaco time at 100% power. While an average cataract surgery may be 10-15 minutes long, due to the low duty cycle and low power used during the procedure, the EPT may be only 60 seconds. Using this method, an effective phaco time of 60 seconds and maximum probe power of 7 Watts was used. Thus the EPT method would produce an average of 4.35 MW/m^3 as a heat source across the whole of the lens. The result of the COMSOL model is shown in Figure 3.5.

The temperature change in the corneal endothelium was represented by plotting the temperature change over time at a single point at the center of the modeled corneal endothelial layer. This is shown in Figure 3.6. Over the 60 seconds EPT the endo-contact lens showed a 44.5% reduction in temperature with this model when compared to the model with no endo-contact lens.

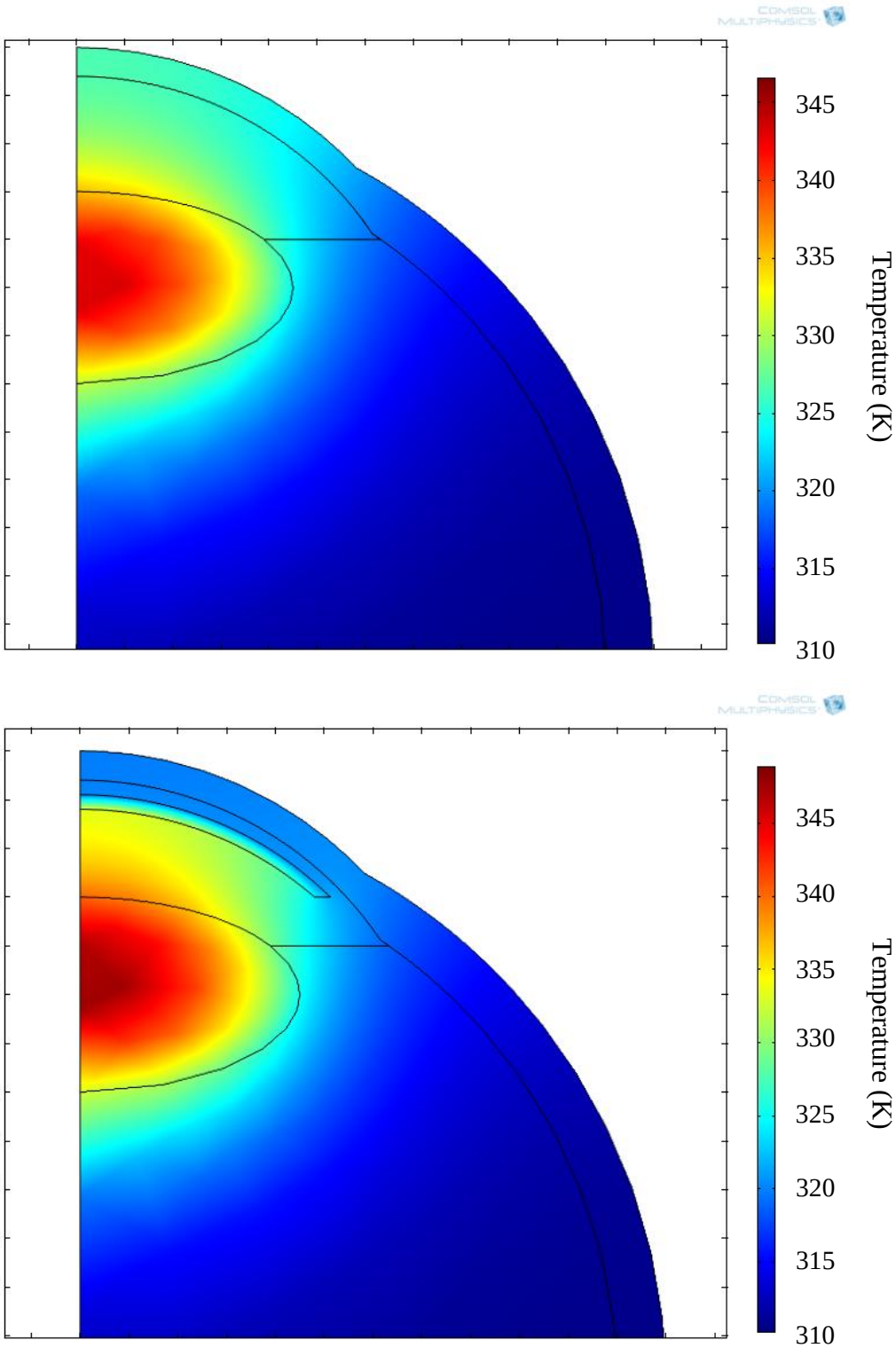

Figure 3.5. COMSOL modeling showed the effect of the endo-contact lens in the thermal protection of the cornea.

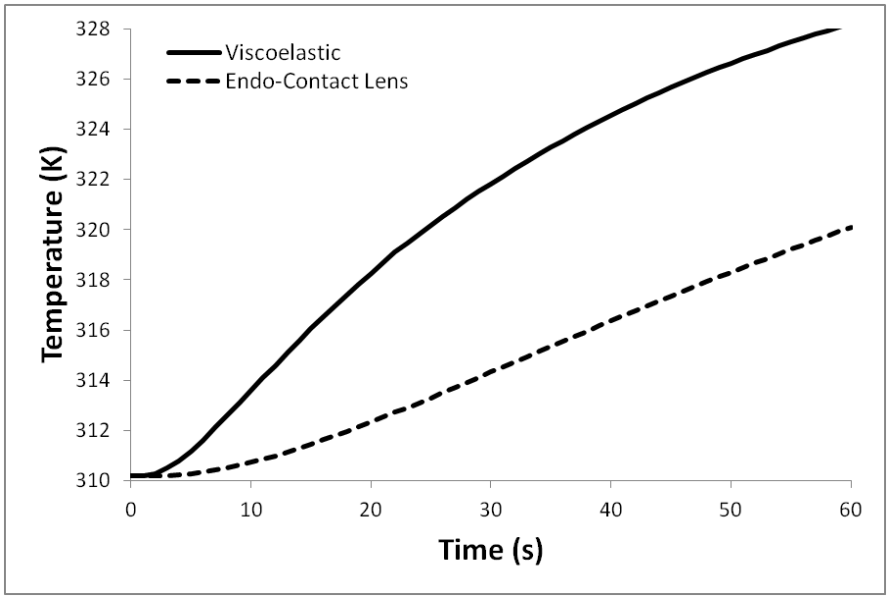

Figure 3.6. Temperature of the corneal endothelium graphed over time as a function of presence of the endo-contact lens.

PDMS Design

PDMS is a polymer with a silicone and oxygen backbone with methyl side chains. These side chains cause the polymer to be very hydrophobic. Contact angles of water on unmodified PDMS are ~90°. However, PDMS surface wettability can be improved by oxygen plasma treatment. This process replaces surface methyl groups with hydroxyl groups through hydrogen abstraction. After plasma treatment, contact angles decrease to <10°. This wettability change is not permanent and the PDMS will undergo hydrophobic recovery after a period of hours. Since the shelf life of this device is only as long as its ability to maintain high wettability a series of experiments were performed with the intent of increasing the time required for hydrophobic recovery.

Work by Vickers et al. showed promise with maintaining wettability by dramatically swelling the PDMS thereby allowing for unreacted monomers to diffuse out of the

polymer [16]. PDMS is first caused to swell by immersion into a high swelling solvent. The polymer is allowed to stay swollen for 24 hours. The sample is then brought back to its original size by immersion into lower swelling solvents. To test this hypothesis with the endo-contact lens, PDMS was first swollen in chloroform (swelling ratio 1.39). It was then returned to its original size through immersion in chlorobenzene (swelling ratio 1.22), 1-propanol (swelling ratio 1.09), and finally water (swelling ratio 1.00). These samples were then compared to unmodified PDMS. Both sample group surfaces were modified by oxygen plasma treatment and contact angles were monitored over time (Table 3.2). The results of the experiment showed that the swelling protocol did not improve the longevity of surface wettability.

During the PDMS swelling experiments it was observed that when the polymer surfaces maintained contact with water through immersion over long periods of time wettability was maintained. Subsequently, PDMS surfaces that did not undergo the swelling protocol were immersed in water immediately after oxygen plasma treatment and stored in water for the duration of an additional experiment. The wettability of these

Table 3.2. Wettability of PDMS over time.

	Unmodified PDMS	PDMS After Swelling	PDMS in Water
Prior to Plasma Treatment	92.3° ± 1.4°	95.75° ± 2.3°	-
Plasma Treatment +0 hrs	7.3° ± 1.6°	9.0° ± 2.6°	7.0° ± 1.8°
Plasma Treatment +24 hrs	47.4° ± 1.7°	41.7° ± 2.4°	7.7° ± 1.5°
Plasma Treatment +1 week	-	-	7.4° ± 2.1°
Plasma Treatment +2 weeks	-	-	8.3° ± 1.1°

polymer surfaces was measured and is also shown in Table 3.2. This experiment showed that PDMS would maintain a hydrophilic surface over long periods of time when immersed in water.

Biocompatibility

ISO 10993 is a set of international standards for use in evaluating the biocompatibility of medical devices and biomaterials. The FDA considers these standards to be generally comprehensive but also recognizes that each medical device's biocompatibility needs should be evaluated individually. Due to the diversity of medical devices it may be that despite falling into a specific category, additional tests should be considered. It could also be that not all tests will be necessary for any given device. Medical device developers are expected to use ISO 10993 as a set of guidelines from which to determine the specific needs of each device. This set of standards contains both *in vitro* and *in vivo* tests for evaluating the biocompatibility of medical devices.

ISO 10993 confines required testing for a short term implant (<24 hours) for use in nonblood contacting tissue to sensitization, irritation, and cytotoxicity evaluations. Sensitization tests for adverse reactions in animals by exposing the animal to the biomaterial in question. The animal is then observed for sensitization reactions by observing redness and swelling as signs that the biomaterial is causing a reaction from the host's immune system. Irritation tests are similar to sensitization tests in many ways. To test for irritation, the reaction to a single, repeated, or continual exposure from device materials is assessed. The host is evaluated for signs of irritation not involving the immune system. Therefore, sensitization and irritation are both evaluated through *in vivo*

methods. The focus of *in vitro* biocompatibility assessments are cytotoxicity testing. Cytotoxicity evaluations are generally available as rapid, standardized tests such as the Agar Overlay, MEM Elution, and Direct Contact tests. Cytotoxicity tests seek to determine if a biomaterial contains significant quantities of harmful extractables or if the biomaterial has other significant cytotoxic effects.

PDMS has long been used in biological systems with good biocompatibility. The Whitesides group at Harvard showed in 2004 that the growth of mammalian cells on PDMS was comparable to growth on tissue culture-treated polystyrene for most cell types [17]. Therefore our evaluation of *in vitro* biocompatibility of the PDMS endo-contact lens did not focus on sensitization, irritation, and traditional cytotoxicity. It was determined that a long term tissue exposure to PDMS was possible due to the leeching of PDMS monomers from the lens during cataract surgery. Experimental results showed that the presence of PDMS monomers yielded distinct peaks at 221.4 and 222.0 Da. These results are clearly seen in the positive control but are absent in each of the other samples (<5E4 cps) (Figure 3.7).

Normal rabbit corneal thicknesses range from 250 to 330 μm. We found the following corneal thicknesses; both eyes of each rabbit underwent high-energy phacoemulsification, one with and one without the endo-contact lens (Table 3.3). The average corneal thickness increase without endo-contact lens was 29.5%, while increase with endo-contact lens was 10.4%.

Two rabbits had cataract surgeries performed on them. One eye for each rabbit used the endo-contact lens during phacoemulsification. The control eyes had cataract surgery performed on them using the current standard of care with viscoelastic. After sacrifice,

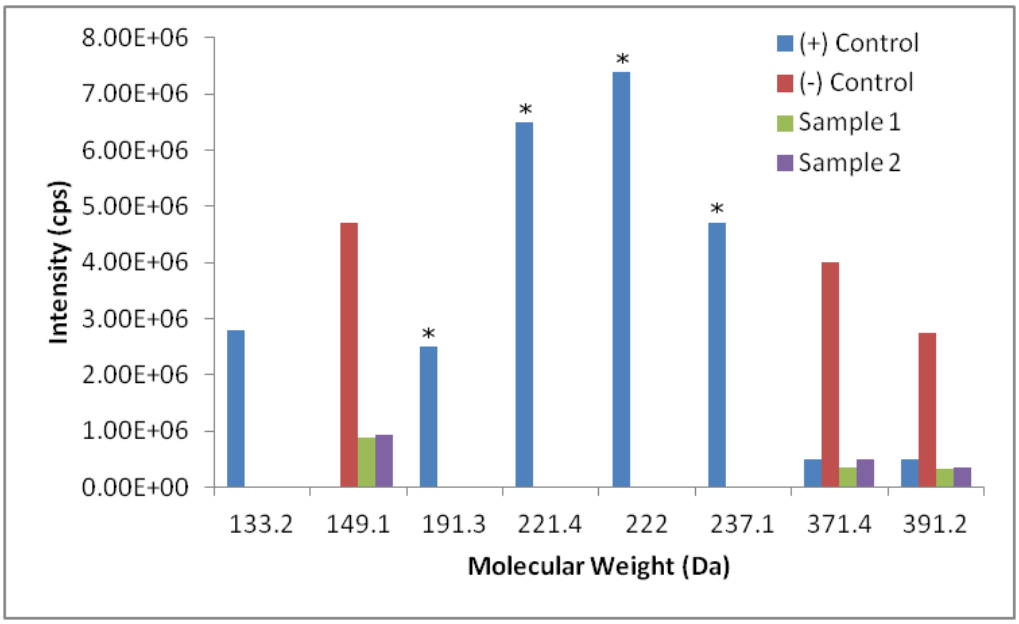

Figure 3.7. Mass spectrometry of PDMS monomers, PBS, and PDMS solutions showing no leaching of silicone monomers.

Table 3.3. Corneal thicknesses measured prior to and after cataract surgery.

	Rabbit 1		**Rabbit 2**	
	Pre-op	**Post-op**	**Pre-op**	**Post-op**
Endo-contact lens	297 µm	344 µm	314 µm	330 µm
No Endo-contact lens	325 µm	389 µm	247 µm	344 µm

pachymetry was performed and the corneas were imaged (Figure 3.8). The cellular morphology of the cell layers is visible and shows evidence to the increased efficacy of the endo-contact lens in the protection of the corneal endothelium. The endothelial cells also show a more natural morphology for the eyes that the endo-contact lenses were used on than the cells of the eyes where the lenses were not used as seen in Figure 3.8. The

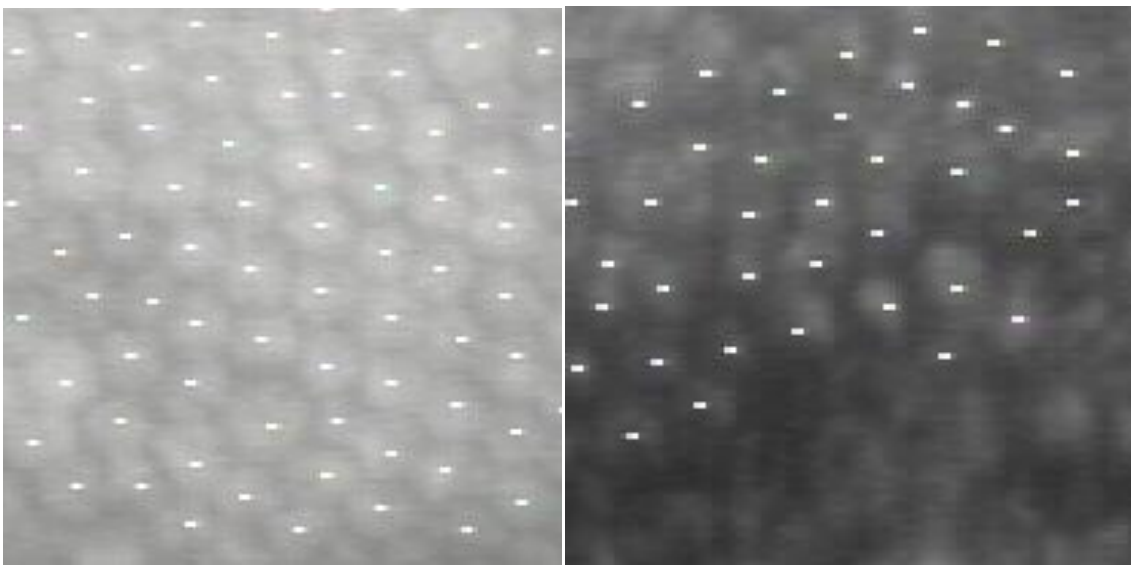

Figure 3.8. Cellular morphology of the corneal endothelium after 100 CDE cataract surgeries for eyes with the endo-contact lens **(left)** and without **(right)**.

resultant endothelial cell counts showed an endothelial cell count of 64 and 66 for the eyes with endo-contact lenses and 31 and 38 for the eyes without the lenses over the same area.

Conclusions

Within the United States there are 3 million cataract surgeries annually. These surgeries can damage the patient's corneal endothelium. This damage results in decreased corneal clarity and can potentially result in the need for corneal transplantations. The endo-contact lens has been developed for the purpose of shielding the cornea for the thermal and fluidic injury that can result from cataract surgery.

The development of the endo-contact lens continues to be a work in progress but this research has shown the successful design and development of key aspects of the device

including device transparency, flexibility, polymer composition, and buoyancy. Experiments indicate that the device would be biocompatible in the ocular space for the short duration purpose of protecting the corneal endothelium. Computer modeling and experiments have also indicated that the device would be efficacious in the protection of the corneal endothelium during surgery by reducing thermal exposure by 45%. The results of this study also show a significant reduction in corneal swelling and an increase in endothelial cell counts after surgery. The next step for the development of this device would be for the statistically powered *in vivo* experiment verifying the results seen in this preliminary study. It is expected that the development of this device will be a great benefit to patients and healthcare providers as the number of operations increase.

References

[1] Moreau KL, King JA. Protein misfolding and aggregation in cataract disease and prospects for prevention. Trends in Molecular Medicine 2012;18:273–82.

[2] Han YK, Miller KM. Heat production: Longitudinal versus torsional phacoemulsification. Journal of Cataract and Refractive Surgery 2009;35:1799–805.

[3] Lee Y. Thermal burns caused by ophthalmic viscosurgical device occlusion in torsional phacoemulsification. Tzu Chi Medical Journal 2010;22:229–31.

[4] Yang RM, Sha X, Zeng M, Tan Y, Zheng Y, Fan F. the influence of phacoemulsification on corneal endothelial cells at varying blood glucose levels. Eye Science 2011;26:91–5.

[5] Gogate P, Ambardekar P, Kulkarni S, Deshpande R, Joshi S, Deshpande M. Comparison of endothelial cell loss after cataract surgery: phacoemulsification versus manual small-incision cataract surgery: six-week results of a randomized control trial. Journal of Cataract and Refractive Surgery 2010;36:247–53.

[6] Peh GSL, Beuerman RW, Colman A, Tan DT, Mehta JS. Human corneal endothelial cell expansion for corneal endothelium transplantation: an overview. Transplantation 2011;91:811–9.

[7] Tabandeh H, Chaudhry NA, Boyer DS, Kon-Jara VA, Flynn HW. Outcomes of cataract surgery in patients with neovascular age-related macular degeneration in the era of anti-vascular endothelial growth factor therapy. Journal of Cataract and Refractive Surgery 2012;38:677–82.

[8] Keay L, Gower EW, Cassard SD, Tielsch JM, Schein OD. Postcataract surgery endophthalmitis in the United States: analysis of the complete 2003 to 2004 Medicare database of cataract surgeries. Ophthalmology 2012;119:914–22.

[9] Van den Bruel A, Gailly J, Devriese S, Welton NJ, Shortt AJ, Vrijens F. The protective effect of ophthalmic viscoelastic devices on endothelial cell loss during cataract surgery: a meta-analysis using mixed treatment comparisons. The British Journal of Ophthalmology 2011;95:5–10.

[10] Hall DL. Silicone intraocular lens implants and circular anterior capsulotomy (capsulorhexis). The Journal of the Louisiana State Medical Society: 1989.

[11] Apple DJ, Federman JL, Krolicki TJ, Sims JCR, Kent DG, Hamburger HA, et al. Irreversible silicone oil adhesion to silicone intraocular lenses: A clinicopathologic analysis. Discussion. Ophthalmology 1996;103:1555–62.

[12] Boswell CA, Noecker RJ, Mac M, Snyder RW, Williams SK. Evaluation of an aqueous drainage glaucoma device constructed of ePTFE. Journal of Biomedical Materials Research 1999;48:591–5.

[13] Li PY, Shih J, Lo R, Adams B, Agrawal R, Saati S, et al. An electrochemical intraocular drug delivery device. Sensors and Actuators A: Physical 2008;143:41–8.

[14] Saati S, Lo R, Li PY, Meng E, Varma R, Humayun MS. Mini drug pump for ophthalmic use. Trans Am Ophthalmol Soc 2009;107:60–71.

[15] Yasukawa T, Ogura Y, Sakurai E, Tabata Y, Kimura H. Intraocular sustained drug delivery using implantable polymeric devices. Advanced Drug Delivery Reviews 2005;57:2033–46.

[16] Vickers JA, Caulum MM, Henry CS. Generation of hydrophilic poly(dimethylsiloxane) for high-performance microchip electrophoresis. Analytical Chemistry 2006;78:7446–52.

[17] Lee JN, Jiang X, Ryan D, Whitesides GM. Compatibility of mammalian cells on surfaces of poly (dimethylsiloxane). Langmuir 2004:11684–91.

CHAPTER 4

POLYETHYLENE GLYCOL FOR A REDUCTION IN PROTEIN ADSORPTION

Abstract

Biocompatibility is a major concern for medical device development. One of the first steps involved in the host response is that of protein adsorption. Polyethylene glycol (PEG) surfaces have been developed for the purpose of reducing protein adsorption with the intent of improving a device's biocompatibility. However, the protein inert qualities of PEG are not clearly understood. This study aims to elucidate the impact of PEG surface density in reducing protein adsorption. Two forms of PEG surface gradients were evaluated for the adsorption and desorption of albumin and fibrinogen, two common blood proteins. This study shows that as the concentration of protein increases, polymer surface density become increasingly important.

Introduction

The interactions between host and biomaterial have long been studied [1–21]. Although much progress has been made in the development of biomaterials, successful applications have been limited in scope due to a lack of consistency and understanding of biocompatibility [13,15–17,22,23]. Medical device biocompatibility is a complex issue,

but when these devices are blood-contacting the situation becomes significantly more complex. Typically a biomaterial, after being exposed to a protein solution (e.g., blood), will become coated with a protein layer within seconds [9,15,24–32]. The adsorption of certain blood proteins prompts the adherence and activation of blood cells and platelets [8,9,13,15,16,19,30,33–35]. These interactions can initiate two of the major biomaterial problems: the foreign body reaction and inflammation [15,16,18,19]. Platelet initiated fibrin formation and cross-linking can also cause fouling or disruption of a biomedical device and its function. These factors determine a biomaterial's biocompatibility.

A great deal of research has focused on the protein inert properties of polyethylene glycol (PEG) [34,36–43]; however, despite the investigation of many different underlying mechanisms, the protein inert qualities of PEG are still not fully understood. This research has prompted the understanding that the protein inert properties of PEG-containing molecules are due to a combination of phenomena. The large extended volume which the hydrophilic polymer occupies in water based media forms an enthalpic and entropic favored state [24,30,36–38,41,44–49]. In order to adsorb to a biomaterial surface, a protein would need to disrupt the entropic and enthalpic favored state of the fully extended PEG polymers. This and the absence of strong attractive interactions between most proteins and PEG-containing coatings appear to be the most influential adsorption-reducing properties. The protein inert properties of PEG-containing coatings depend on a range of parameters including molecular weight, interfacial chain density, and polymer chain structure [25,44,50,51]. This study intends to elucidate the impact of PEG grafting density on the inhibition of protein adsorption.

Materials and Methods

Sulfhydryl Surface Formation

The initial substrates for the gradient surfaces were 3”x1”x1mm fused silica microscope slides (Ted Pella). After cleaning with Millipore® water and Alconox® solution the slides were soaked in Piranha solution (70% H_2SO_4, 30% H_2O_2) for 1 hour. The slides were then rinsed again with Millipore® water, dried, and oxygen plasma (Plasmod, Tegal Inc., 50 W @200 mTorr) treated. Oxygen plasma treatment resulted in uniform surface coverage with reactive silanol groups. These surfaces were then immersed in a 1% solution of 3-mercaptopropyltrimethoxysilane (MTS) (M8500, UCT) in toluene for 4 hours. The result was the formation of surface sulfhydryl chemistry. This process is diagramed in Figure 4.1.

PEG Gradient Formation

Two methods were compared for the formation of PEG density gradients. The first method of surface gradient formation was controlled exposure of uniform sulfhydryl surfaces, generated as described in the previous section, with maleimide-terminated PEG (5 kDa, 63187, Sigma-Aldrich). A 0.1 mg/mL (1.8E-5 M) solution of a maleimide-

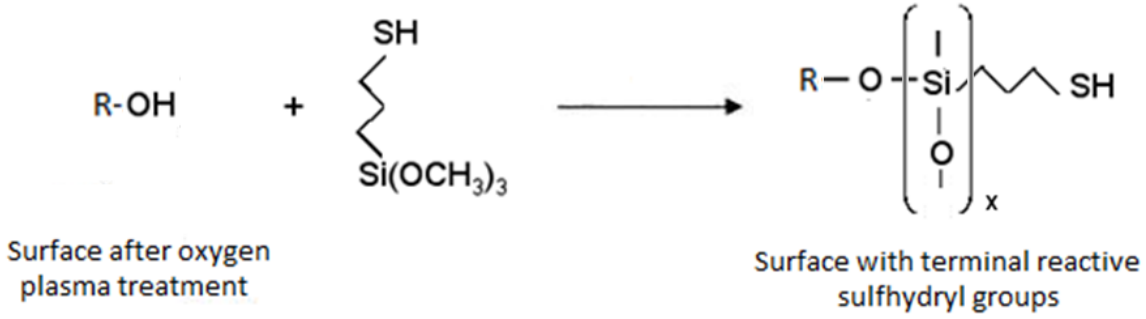

Figure 4.1. Diagram of the MTS reaction forming uniform sulfhydryl surfaces. “R” represents solid fused silica with silanol groups on its surface.

terminated PEG was progressively added to the sulfhydryl surfaces in a vertical flow cell over the course of 1 minute to generate a reaction gradient dependent on transportation rate kinetics. The maleimide-sulfhydryl reaction (Figure 4.2) gradient is stochastically controlled by the duration of time during which the surface is exposed to PEG. The PEG solution was introduced into the bottom of the flow cell. It was then flowed upwards along the length of the slide. The bottom third of the surface was immersed in PEG for 5 minutes prior to the introduction of such flow to generate a uniformly coated PEG region to be used as a control. By this method, the PEG solution was in contact with the bottom third of the surface for a total of 7 minutes, a gradient of 2 minutes to transient contact in the central third, and no contact in the upper third of the surface. This method was used to successfully form a gradient of high PEG surface density near the bottom of the flow cell and progressively lower PEG surface density along the length of the slide. This method is shown in Figure 4.3.

The second method generated the gradient through a gradual oxidation of reactive species (Figure 4.4). After the formation of uniform sulfhydryl surfaces, the surface

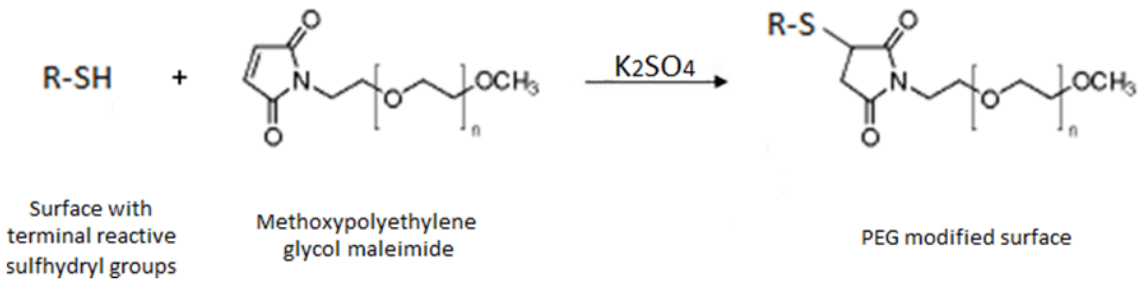

Figure 4.2. Diagram of the method for the generation of PEG surface gradients. K_2SO_4 11% (w/w) was used as a salt to increase grafting density. "R" represents solid fused silica with sulfhydryl groups on its surface.

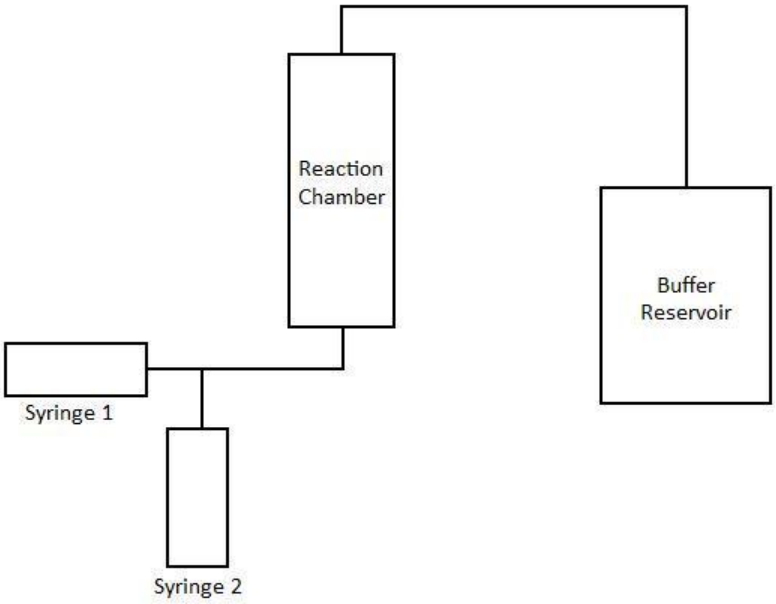

Figure 4.3. Diagram showing the flow method of gradient formation. Syringe 1 is used to fill the system with buffer solution. Syringe 2 is used to flow maleimide PEG solution into the reaction chamber creating a gradient based on PEG-sulfhydryl exposure time.

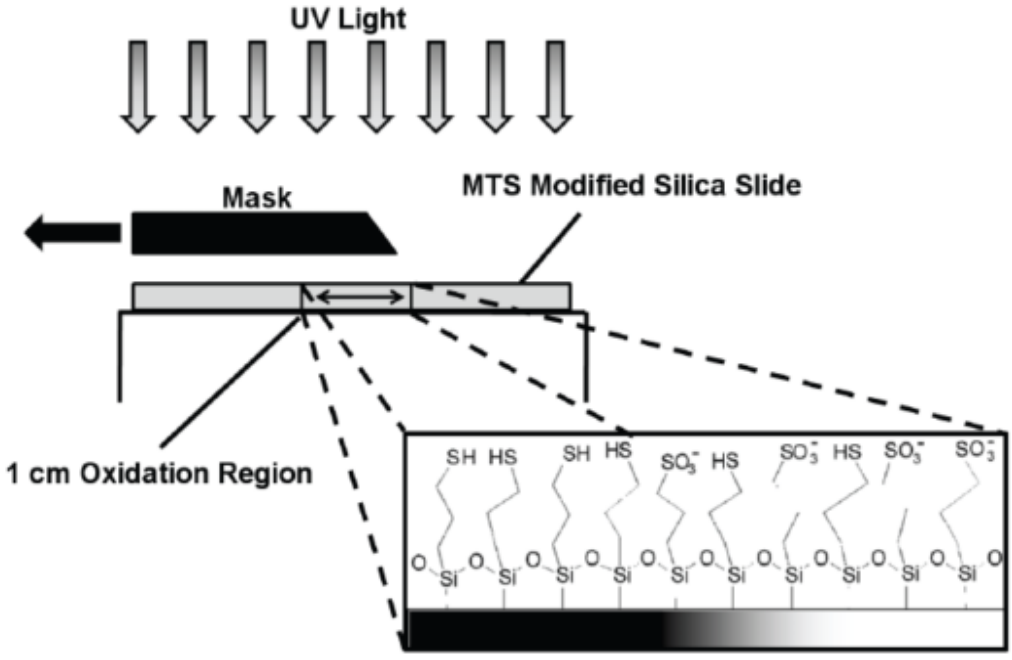

Figure 4.4. Diagram showing the progressive oxidation of surface sulfydryl groups for the formation of PEG gradients [52].

chemistry was modified so as to generate a gradient of reactivity to maleimide-terminated poly (ethylene glycol) (PEG) (5 kDa, 63187, Sigma-Aldrich) through UV oxidation. This was performed by placing the uniform sulfhydryl surface into a slide holder and exposed to UV light (ELC-4000, Electrolite Corp.). UV light oxidation was performed such that the central 1 cm region of the 3" fused silica slide was gradually exposed by the linear translation of a mask at a constant rate of 0.25 cm/min for 4 minutes. Afterwards, the slides were uniformly immersed in maleimide-PEG solution (0.1 mg/mL [1.8E-5 M]) for 5 minutes.

Surface Characterization

X-ray Photoelectron Spectroscopy (XPS) was performed at the University of Utah nanofabrication laboratory. The mono Al source was operated at 150 W (10 mA, 15 kV) for all samples and the charge neutralizer was optimized at 2.15-1.95 A on the filament and 3.05 V on the charge balance depending on the sample. Survey scans were collected using 1 eV steps, 200 ms dwell time at a pass energy of 160 eV. High resolution regional scans were collected using 0.1 eV steps, 300 ms dwell time at a pass energy of 40 eV.

Equilibrium, advancing, and receding water contact angles were measured by the sessile drop method using a contact angle goniometer (CAM 100, KSV Instruments). Five μL Milipore filtered water droplets were dispensed along the length of the samples and imaged using the instrument camera. The KSV software was used to calculate the contact angle of the water droplet using the image of the drop.

Protein Adsorption Kinetics

Albumin (HSA) (fraction V, fatty acid free) from human serum and fibrinogen (FGN) were purchased from Sigma-Aldrich and used as received. Protein solutions were prepared for fluorescent labeling by mixing purchased protein with Dulbecco's Phosphate-Buffered Saline (DPBS). Each protein solution was fluorescently labeled using Alexa Fluor 488 carboxylic acid, succinimidyl ester (A20000) which was purchased from Invitrogen. After conjugation of protein and Alexa Fluor 488, the solution was passed through a column (PD-10 desalting column, GE Healthcare, 17-0851-01) to separate the free probe from the conjugated protein fraction. The concentration of fluorescently labeled protein was determined by a 3-step process. First, the protein solution's absorbance at 280nm and 496nm was quantified using a spectrophotometer [53]. Next, the concentration of free fluorescent probes was calculated as shown in equation 4.1; and the concentration of fluorescently tagged protein was calculated as shown in equation 4.2. The degree of labeling was determined as shown in equation 4.3. DPBS was then added as needed to these solutions to generate protein solutions at 1% and 10% human plasma concentrations.

$$[Flourescent\ Probe] = \frac{I_{496}}{71000} \tag{4.1}$$

$$[Flourescent\ Protein] = \frac{I_{280} - (0.11 * I_{496})}{35279} \tag{4.2}$$

$$Labeling\ Degree = \frac{[Flourescent\ Probe]}{[Flourescent\ Protein]} \tag{4.3}$$

Total Internal Reflection Fluorescence Spectroscopy (TIRF) is a surface analysis technique which is based on the excitation of fluorophores by an exponentially decaying evanescent wave [54]. When the incident light wave strikes the interface between the two media at an angle larger than the critical angle the light wave forms an evanescent wave

before being completely reflected back into the first medium. The evanescent wave is formed only at the interface between two media with sufficiently different refractive indices; in this case between silica with the PEG gradient and the buffer solution. The evanescent wave allows for excitation of fluorophores 200 nm deep into the buffer solution. The excitation light source was a 0.5 mW Ar^{+}-ion laser beam. This light was sent through attenuation filter before being expanded and collimated into a Gaussian profile beam of light (~2 cm diameter). The beam was then passed through a 1cm x 1mm rectangle mask before being used for total internal reflection. The quartz slide with the PEG gradient surface was optically coupled with a quartz prism using glycerol to maintain optical refraction properties. A silicon rubber gasket was used to separate the fused silica slide from a black-anodized aluminum support. This created an open space (thickness 0.5 mm) which was used to flow protein and buffer solutions across the PEG modified surface (Figure 4.5). Solutions were allowed to flow in and out of the space through two holes in the bottom and two holes in the top of the aluminum support. Solutions were injected into the flow cell at 0.7 mL/min using a syringe pump.

The fluorescence emitted from the PEG surface was imaged through the quartz prism using a thermo-cooled charge-coupled device (CCD, C200, Photometrics) camera. The wavelength of the emitted fluorescence light was selected using a monochromator (1681C, SPEX Industries Inc., f /4, 2 mm slit, 300 grooves mm^{-1} grating). The CCD camera was cooled to -46 degrees C to minimize dark current. Both the light source and CCD camera were controlled using a computer (Mac II, Apple) for data acquisition. The CCD camera was connected to the computer using a DMA board (National Instrument, NB-DMA-8). The fluorescence signal was binned across a wavelength range by

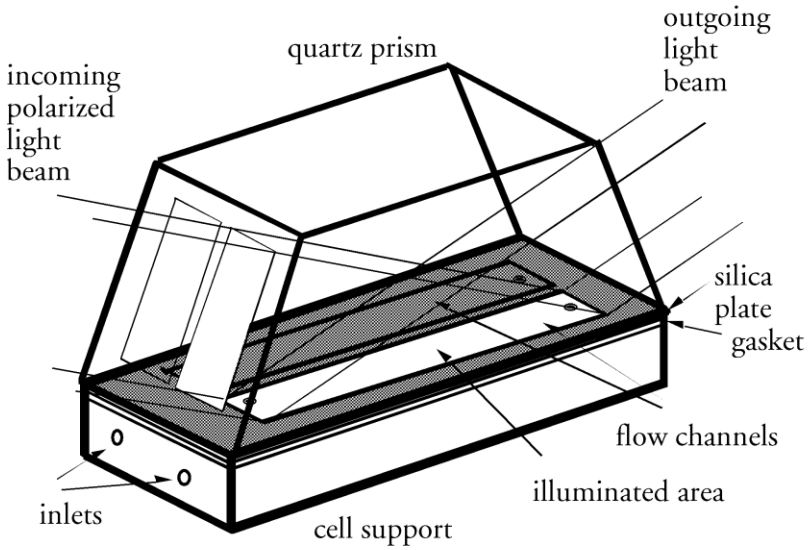

Figure 4.5. The schematics of the TIRF flow cell, comprising the cell support, gasket, and silica plate with the PEG gradient, and the quartz prism [55].

combining adjacent pixels in the CCD camera during an exposure of 1 second in order to improve the S/N ratio and allow for a quicker readout of the camera signal. The shutter was then closed and data recorded for 1 second to provide a blank which was used to subtract background noise from the fluorescence data at each data acquisition time point. The resulting profiles of fluorescence vs. gradient length vs.time were then combined in a single data file. Twenty instances of binned data from such a file were then integrated and combined to form the protein adsorption and desorption kinetics or adsorbed protein gradient profiles depending on whether protein solution or buffer solution was being flowed past the PEG modified surface. Adsorption and desorption data were separately gathered in series for 10 minutes each. Prior to the gathering of experimental data a laser profile was obtained using a uniformly fluorescent liquid. This was necessary due to the laser light not being completely uniform in intensity. This laser profile was used to flat-field the obtained adsorption and desorption data to remove the effects of uneven spatial

intensity of the expanded and collimated laser beam.

Results and Discussion

Surface Characterization

PEG surface gradients were formed in two ways. Each method began with the formation of a uniform sulfhydryl terminated surface through an MTS reaction. The first method of gradient formation utilized the control of the reaction time between PEG and surface sulfhydryl groups through a flow method. However, as will be shown below, the flow method did not successfully form a smooth gradient effect of PEG surface density on protein adsorption and instead formed a step profile PEG gradient. In order to form a less steep PEG gradient surface, the second method was utilized. The second method limited PEG reaction sites by UV oxidation of the surface sulfhydryl groups to sulfonate groups. Only where sulfhydryl groups persisted could the maleimide-terminated PEG be grafted to the surface. The generation of sulfhydryl-sulfonate gradients resulted in changes in surface wettability. Water contact angle measurements (advancing, receding, and equilibrium) showed the existence of a wettability gradient which is indicative of a sulfhydryl-sulfonate gradient as shown in Table 4.1 and Figure 4.6. Figure 4.6 is representative of the generated gradients showing the expected contact angles for sulfonate, sulfhydryl, and PEG regions [52,56]. Prior to PEG grafting, the gradient region of the surface gradually increased from ~12° on the sulfonate side to ~66° on the sulfhydryl side which is consistent with previous reports [57–60].

Since contact angle measurements were only an indirect indicator of surface chemistry, high resolution XPS spectra of C1s and S2p peaks were performed to verify

Table 4.1. Water contact angle measurements comparing sulfhydryl and sulfonate regions on MTS gradient surfaces.

	Sulfhydryl Region	Sulfonate Region
Advancing	69.1 ± 4.2°	32.3 ± 4.9°
Receding	52.5 ± 3.5°	10.4 ± 2.8°
Equilibrium	66.0 ± 2.8°	13.1 ± 3.0°

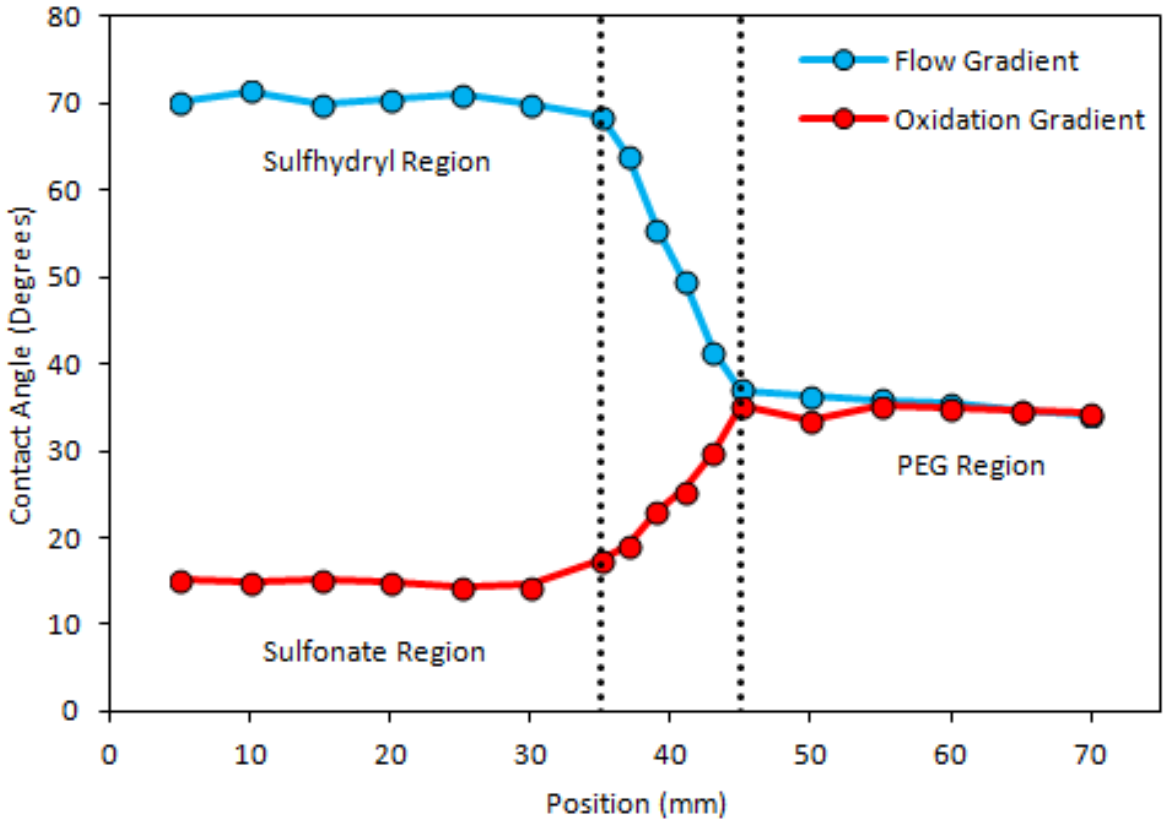

Figure 4.6. Water contact angles showing the generated PEG gradients.

the formation of surface sulfhydryl-sulfonate gradients and subsequent PEG-sulfonate gradients (Figure 4.7). Surfaces were UV oxidized for 0, 1, or 2 minutes and subsequently immersed in maleimide-terminated PEG solution for 5 minutes. The relative changes between the ~284 eV C-C carbon peak and the ~286 eV C-O carbon peak show a progressive increase of C-O concentration, and thus PEG concentration, as oxidation time decreases (Figure 4.7, top). The magnitudes of the ~163 eV S2p sulfur (-SH) peak and the ~168 eV oxidized sulfur (SO_3^-) peak (Figure 4.7, bottom) change as a function of the UV oxidation time indicating the change in reactive (-SH) surface chemistry over time thus matching the XPS spectra reported in the literature [57,59,60]. As oxidation time increases the relative concentration of SO_3^- increases. These results corroborate the contact angle measurements indicating the formation of sulfhydryl-sulfonate and subsequent PEG-sulfonate gradients.

XPS was also performed on sulfhydryl surfaces which were immersed in 0, 0.1, and 1 mg/mL PEG solutions (Figure 4.8). This was performed to determine which concentration of PEG would be most effective for the generation of our gradient and additionally to show the effect of increasing PEG concentration on the surface composition. Data from the graphs show that the maleimide-sulfhydryl reaction occurs quickly and that despite the 10-fold difference in concentration little change is seen in the resultant surface composition. For this reason it was determined to use a PEG solution of 0.1 mg/mL for the generation of the gradients.

Protein adsorption and desorption to PEG gradients were measured using fluorescently labeled albumin (HSA) and fibrinogen (FGN) and TIRF. These proteins were chosen because of their abundance and significance in the blood. Albumin was

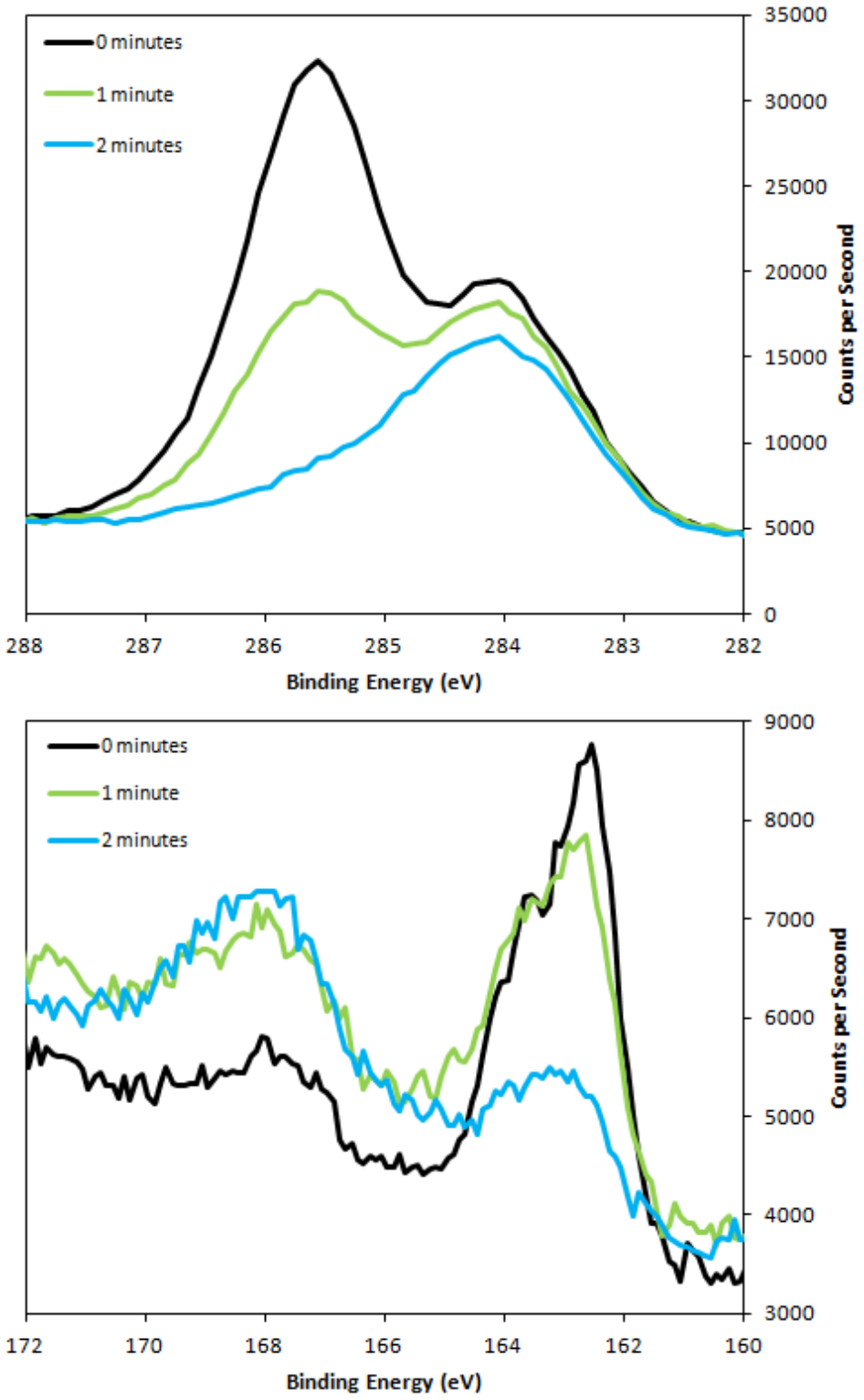

Figure 4.7. XPS spectra of the C1s carbon peak and S2p sulfur peak showing the relative changes in concentration of C-C to C-O and S-H to $S\text{-}O_3^-$

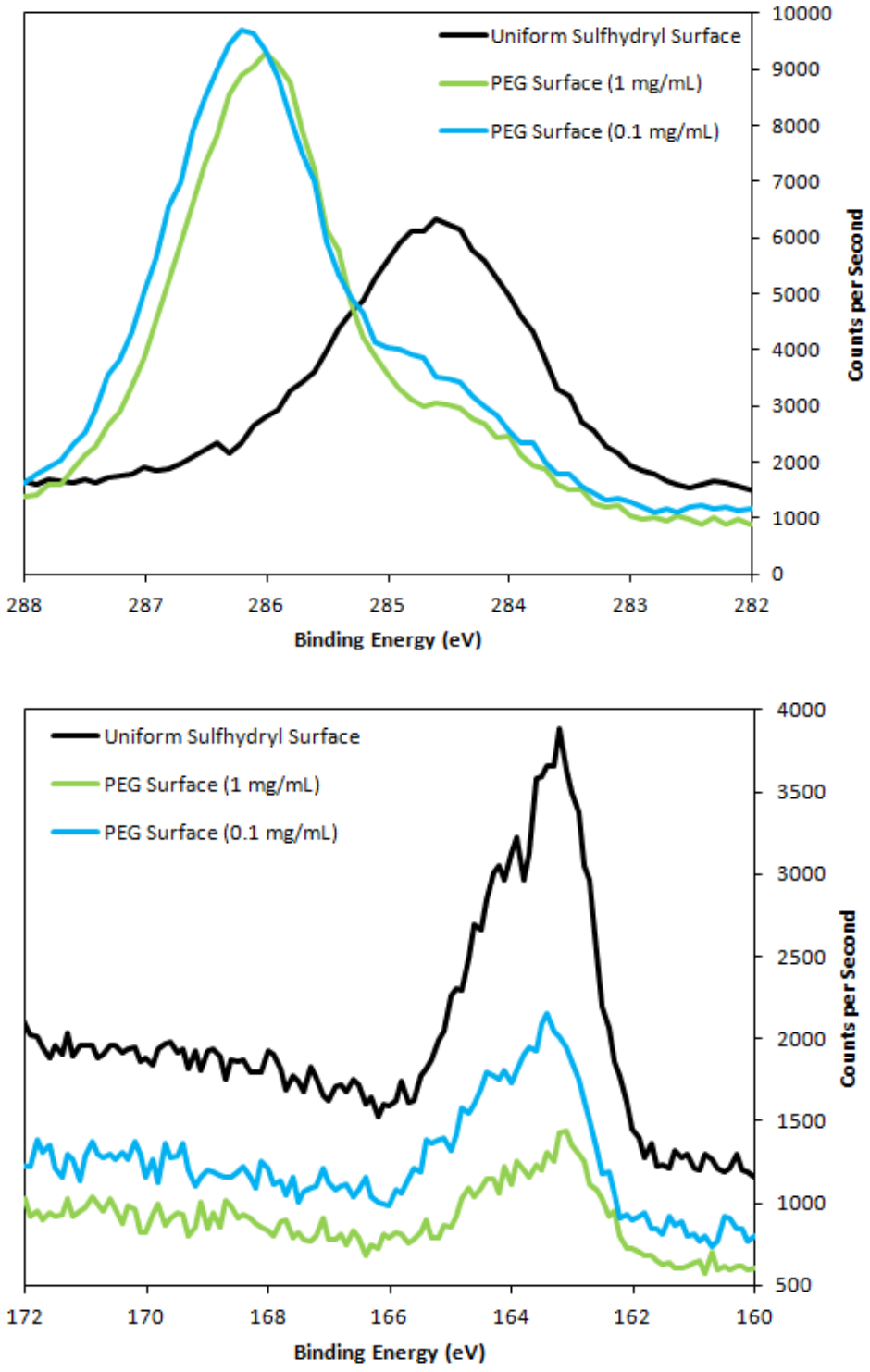

Figure 4.8. XPS spectra of the C1s carbon peak and S2p sulfur peak showing the relative changes in concentration of C-C to C-O and S-H to $S\text{-}O_3^-$

tested at concentrations of 0.4 and 4 mg/mL. Fibrinogen was tested at concentrations of 0.03 and 0.3 mg/mL. These concentrations correspond to 1% and 10% of their blood concentrations.

HSA and FGN were both independently tested on PEG gradient surfaces to show adsorption and desorption properties. Figure 4.9 shows the effect that PEG surface gradient has on 1% blood protein concentrations. At these low concentrations both HSA and FGN initial adsorption rate are expected to be largely limited by transport.

One difficulty in a study of this nature is the quantified determination of the protein surface adsorption. This study takes the approach of determining protein surface coverage as a measure of protein adsorption quantification as a function of time. For each surface and protein the surface adsorption becomes a function of the protein's transport to the surface and secondly, the actual adsorption to the surface. Therefore, for each protein and surface the surface coverage can be either transport limited or adsorption limited. For these experiments we consider protein in solution which is made to flow through a controlled channel with a rectangular cross-section. For a transport limited regime the flux of protein molecules to the surface (J_P) is shown in equation 4.4 where D_P is the diffusion coefficient of the protein, c_P is the concentration of protein in solution, [Γ(4/3)] is the gamma function of 4/3, l is the distance of the flow channel, b is the channel thickness, and w is the channel width, q is the volumetric flow rate of the protein solution.

$$J_P = [\Gamma\left(\frac{4}{3}\right)]^{-1} \cdot 9^{-\frac{1}{3}}\left(\frac{6q}{b^2 w l D_P}\right)^{\frac{1}{3}} D_P c_P \tag{4.4}$$

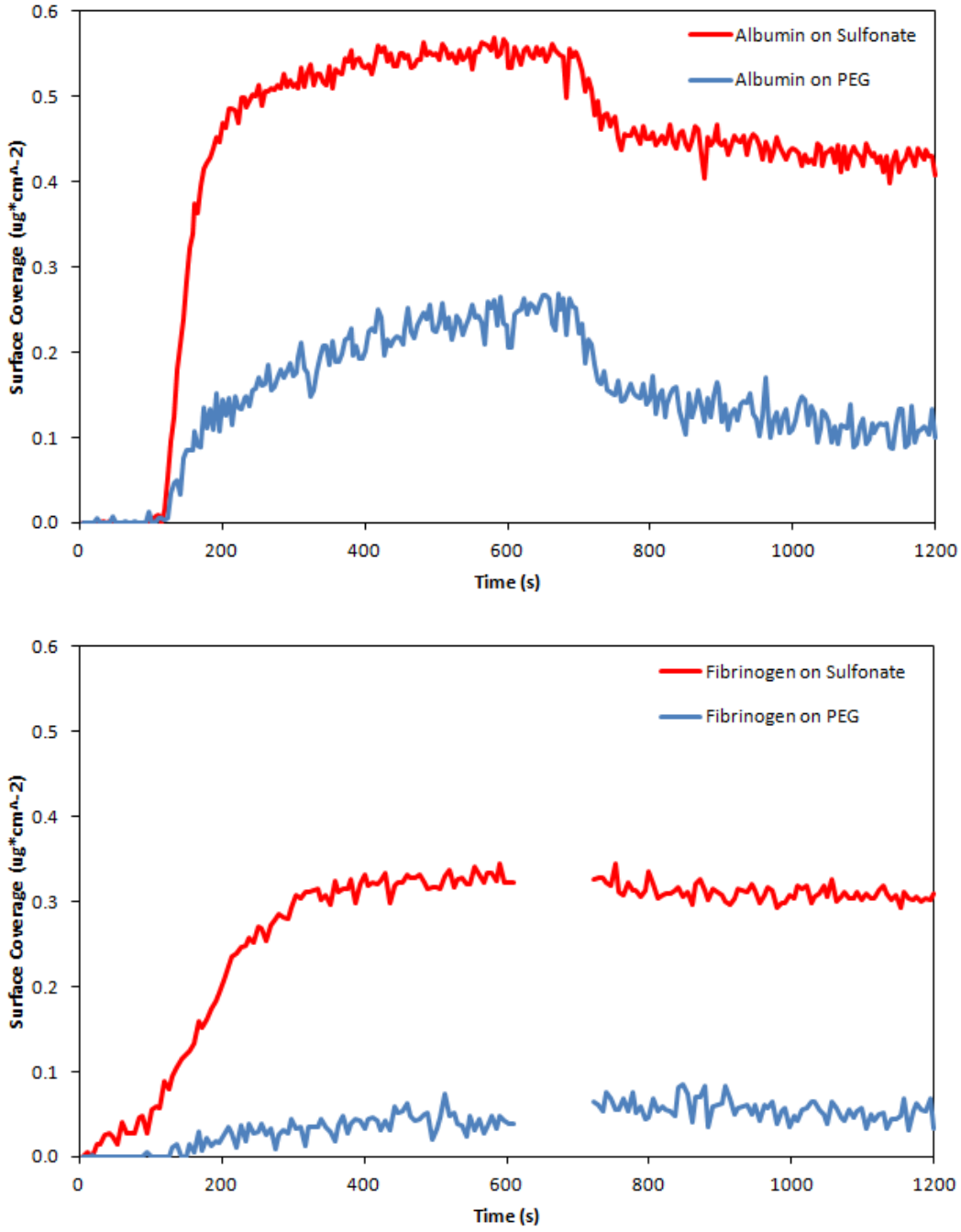

Figure 4.9. Human serum albumin and fibrinogen adsorption kinetics from the solutions equivalent to 1% blood protein concentrations to sulfonate and PEG surface regions of the PEG gradient generated by the UV exposure method. Artifact data was removed between 600-700 seconds.

In a transport limited regime, J_P from equation 4.4 equals the adsorption rate dΓ/dt. Data obtained from TIRF experiments were in the form of fluorescence and were converted into surface coverage through the use of this relationship with the 1% fibrinogen data. This relationship is shown in equation 4.5 where X is a constant with units of $kg \cdot m^{-2} \cdot counts^{-1}$.

$$X = J_P \cdot \left(\frac{dF_i}{dt}\right)^{-1} \tag{4.5}$$

This constant is used to convert fluorescence intensity (F_i) to surface coverage at all time points. Data obtained from this method agree with literature which was verified with autoradiography [56]. Albumin was determined to not be fully transport limited for these experiments and was converted to surface coverage using the calibration from the same study.

At low concentrations, very little change is seen when buffer is flowed through the system during the second half of the TIRF experiment. HSA shows some degree of desorption when buffer is flowed through the system, but that is not seen in the case of FGN adsorption. These data show that for both HSA and FGN, grafted surface PEG chains are effective at reducing protein adsorption.

Gradients are very well pronounced at low concentrations. The data from Figure 4.10 show the central region of the PEG-Sulfonate surfaces and the success of the gradient generation using the oxidation method. The protein surface coverage is shown for the periods of adsorption (protein solution is flowed) and desorption (buffer is flowed). Figure 4.11 shows the adsorption and desorption adsorbed kinetics from the protein solutions equivalent to their 10% blood concentration on step PEG gradient surfaces generated by the flow method. As with the 1% solutions, during flow of protein solutions,

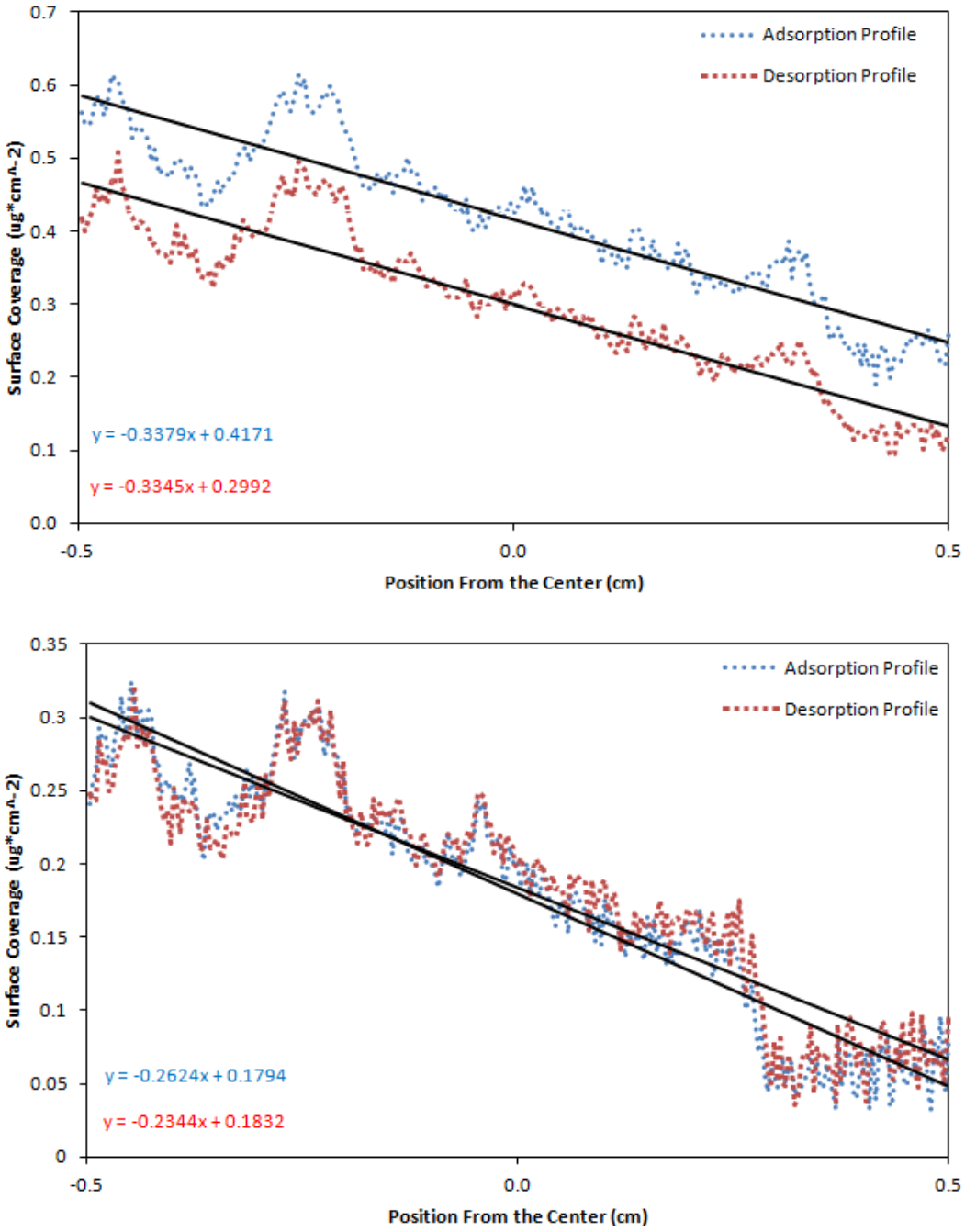

Figure 4.10. Human serum albumin and fibrinogen adsorption profiles along the UV exposure generated PEG gradient at the end of the adsorption and desorption cycles from the solutions equivalent to 1% blood protein concentrations.

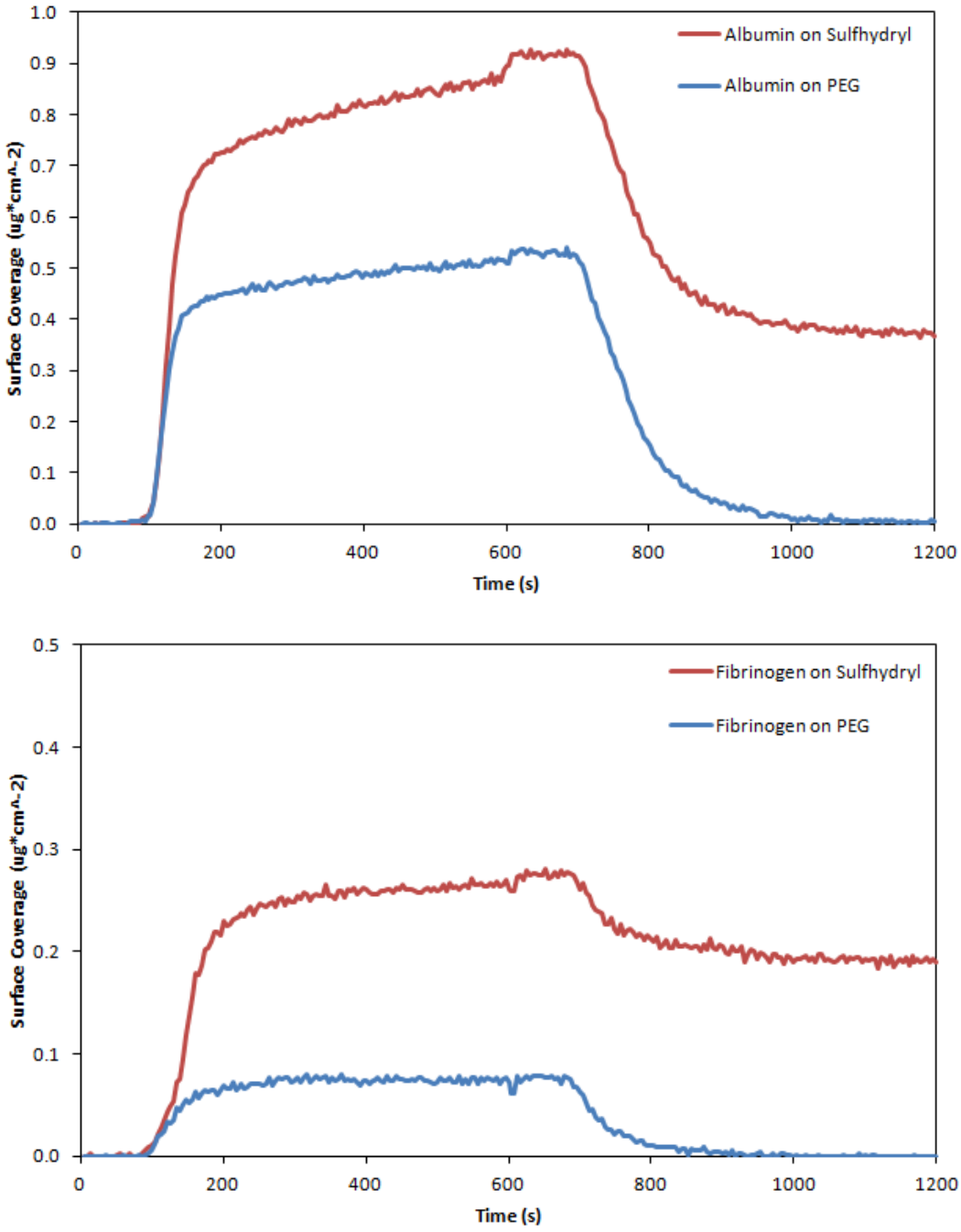

Figure 4.11. Human serum albumin and fibrinogen adsorption kinetics from the solutions equivalent to 10% blood protein concentrations to MTS and PEG surface regions of the step PEG gradient generated by the flow method .

protein surface adsorption is apparent. However, once protein solution is replaced with buffer solution much of the fluorescence intensity is removed on the PEG side of the gradient. This is due in large part to the removal of bulk solution fluorescence excited by the evanescent wave. However, this behavior is also similar to what is shown in recent protein adsorption models [25,30,42,50,51]. During buffer flow, proteins immediately desorb in large quantities and after a few minutes are desorbed from the grafted PEG region to such a degree as to render them undetectable by TIRF, near-zero surface adsorption. The adsorption proteins to the sufhydryl region of the step PEG gradient remained at the levels comparable to previously reported data [56].

The flow gradient used for 10% protein concentrations was not as successful as was seen for the oxidation gradient. Figure 4.12 shows the region of the surface which was intended to have the gradient from sulfhydryl to PEG. However, for these surfaces we see something more similar to a step function wherein the surface adsorption of protein drops off completely on the PEG side.

It has been demonstrated that the primary parameter which governs protein adsorption to surfaces is polymer surface coverage [25,30,42,46,50,51,61,62]. While the formation of PEG surface density gradients was confirmed using contact angle and XPS methods these data suggest that the importance of PEG surface density becomes more pronounced with increasing protein concentration. To evaluate the effect of PEG surface density on protein adsorption two different gradient surfaces were utilized. Initially, a flow based gradient approach was attempted. This method appeared to develop the gradient went characterized using contact angle analysis. However, the surface adsorption data show a step function rather than a gradient (Figure 4.12). This could indicate that at

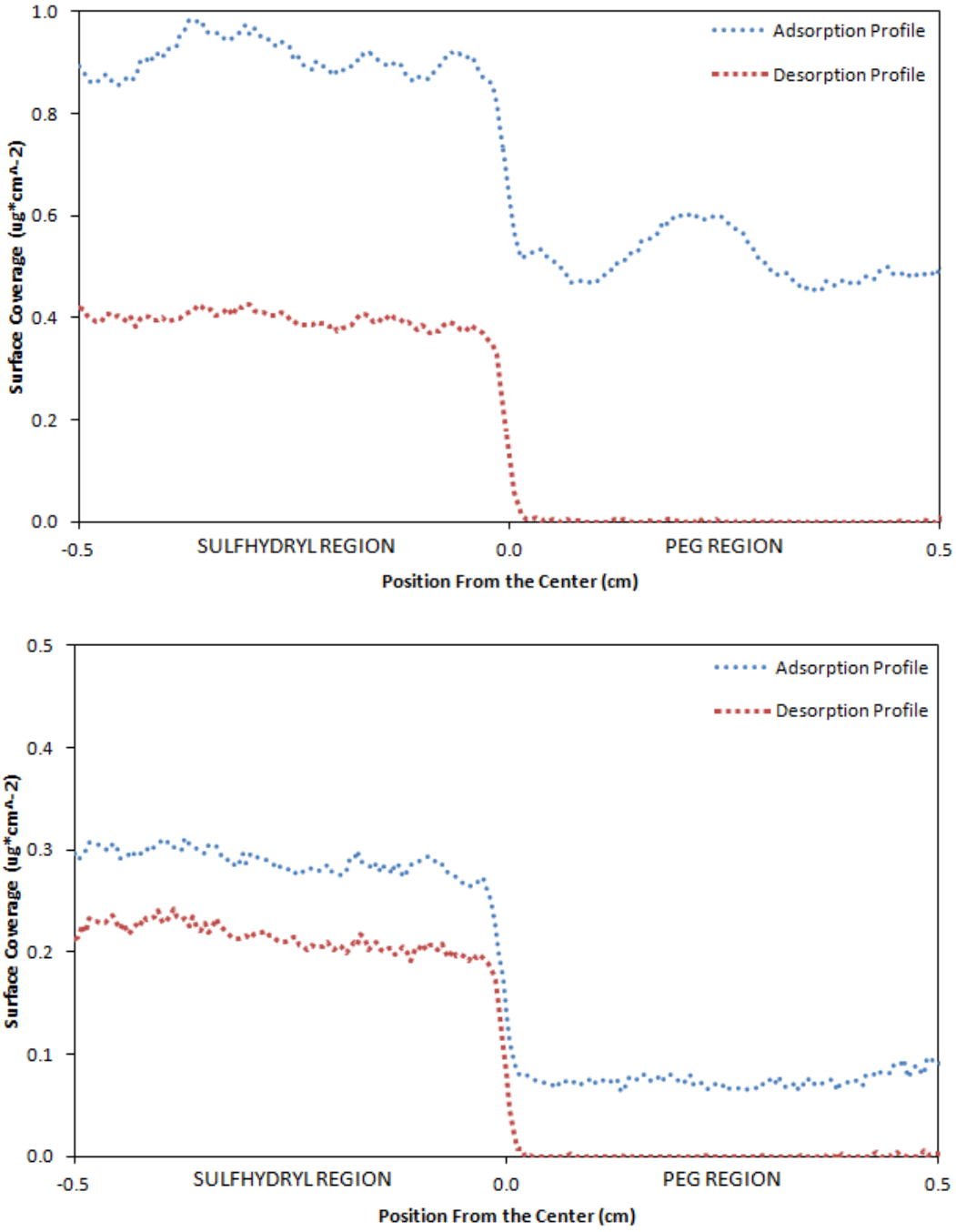

Figure 4.12. Human serum albumin and fibrinogen adsorption and desorption profiles along the flow generated PEG gradient at the end of the adsorption and desorption cycles from the solutions equivalent to 10% blood protein concentrations.

higher concentrations PEG showed a more significant impact or it could indicate that the development of the gradient was unsuccessful. Additionally, the data show that neither fibrinogen or albumin irreversibly bound to the PEG surfaces (Figure 4.11). The oxidation approach prevented the maleimide-PEG from reacting with the surface by oxidizing sulfhydryl chemistry to unreactive sulfonate in a progressive manner. This method appears to have been more successful in the formation of the gradient and was confirmed with contact angle analysis and XPS. These surfaces showed a progressive increase in protein adsorption consistent with the gradient profile.

Differences can be seen between the adsorption and desorption profiles of albumin and fibrinogen which are consistent with previous work [56]. The 1% fibrinogen profiles show that the protein is transport limited and show very little desorption during the flow of buffer. In contrast, 1% albumin data show the protein is not strictly transport limited. 1% fibrinogen surface coverage settles at about 0.3 $\frac{\mu g}{cm^2}$ which agrees with autoradiography confirmed data [56].

Ten percent data for both proteins show that the shape of adsorption profiles are similar for both sulfhydryl and PEG surface regions. Initally albumin adsorbs to a surface coverage of ~0.9 $\frac{\mu g}{cm^2}$, but desorbs to ~0.4 $\frac{\mu g}{cm^2}$ on sulfhydryl surface regions. The PEG regions show a similar rise up to ~0.5 $\frac{\mu g}{cm^2}$ and full desorption during buffer flow. Protein fully desorbs from the PEG surface during buffer flow for both proteins. Fibrinogen adsorbs to the sulfhydryl region up to 0.28 $\frac{\mu g}{cm^2}$ and then desorbs to 0.2 $\frac{\mu g}{cm^2}$. In the PEG region the protein adsorbs to 0.8 $\frac{\mu g}{cm^2}$ and then fully desorbs. The same amount of desorption is seen in both regions. With this 10-fold increase in protein concentration the

adsorption is no longer strictly transport limited for either protein.

As few, if any, natural biological protein solutions contain only a single protein additional work includes the determination of surface adsorption of more complex protein mixtures. Protein adsorption of binary mixtures has been examined in previous studies [56]. If similar data could be projected on these gradient surfaces it could be expected to see initial albumin adsorption in high quantities only to be replaced in some degree with fibrinogen due to the Vroman Effect. Ternary solutions were evaluated in previous work [56] wherein the effect of the ternary solution was first modeled and then confirmed using experimental data.

Conclusions

Polymer coatings, especially PEG, have long been studied for the purpose of improving medical device biocompatibility. While many techniques have been developed for the grafting of PEG to biomaterials, none have been able to produce a perfectly biocompatible surface. In order to further understand the mechanisms of PEG's protein inertness, polymer density gradient surfaces were generated and characterized using contact angle measurements and XPS. TIRF was used in conjunction with fluorescently-labeled HSA and FGN to measure protein adsorption onto two types of PEG surface density gradients.

It has been shown that properties such as molecular weight and particularly surface density have an effect on the efficacy of PEG surface coatings [25,44,50,51]. In this study two major blood proteins, HSA and FGN, were used to determine the efficacy of PEG density gradients. TIRF data were consistent with that of previous work in surface

coverage and profile over time [56]. Surface gradients were successfully generated through oxidation and exposure based methods. Surfaces were characterized using contact angle and XPS techniques. Each protein was diluted to 1% and 10% of normal blood concentration. Protein adsorption to PEG surfaces at 1% concentrations was very low and the polymer surface density gradient was shown to have a nearly linear effect on protein adsorption. When the concentration of protein was increased to 10% blood concentration, the gradients showed the characteristics of a step function rather than a progressive gradient. This could be due to the incorrect formation of the gradient or to an increased effectiveness of PEG at higher protein concentrations.. It is not clear if this is due to the actual step profile of PEG grafting density (note that the contact angle data in Figure 4.6 do not show a steep gradient) of the efficacy of grafted PEG chains to resist protein adsorption from more concentrated solutions. If the latter is the case then this result may indicate that a critical polymer surface density may be required for prevent adsorption from solutions of higher protein concentrations in order to maintain a protein inert surface property.

References

[1] Apple DJ, Mamalis N, Brady SE, Loftfield K, Kavka-Van Norman D, Olson RJ. Biocompatibility of implant materials: a review and scanning electron microscopic study. Journal-American Intra-Ocular Implant Society 1984;10:53.

[2] Elwing H, Welin S, Askendal A, Nilsson U, Lundstrom I. A wettability gradient method for studies of macromolecular interactions at the liquid/solid interface. Journal of Colloid and Interface Science 1987;119:203–10.

[3] Langer R. Biomaterials and biomedical engineering. Chemical Engineering Science 1995;50:4109–21.

[4] Fitton JH, Clayton AB, Hicks CR, Ziegelaar BW, Vijayasckaran S, Dalton PD, et al. Increasing the Biocompatibility of Keratoprosthesis Materials. Fifth World Biomaterials Congress 1996:491.

[5] Van Kooten TG, Klein CL, Köhler H, Kirkpatrick CJ, Williams DF, Eloy R. From cytotoxicity to biocompatibility testing in vitro: cell adhesion molecule expression defines a new set of parameters. Journal of Materials Science Materials in Medicine 1997;8:835–41.

[6] Mathur A, Collier T, Kao W, Wiggins M, Schubert M, Hiltner A, et al. In vivo biocompatibility and biostability of modified polyurethanes. Journal of Biomedical Materials Research 1997;36:246–57.

[7] Elwing H. Protein absorption and ellipsometry in biomaterial research. Biomaterials 1998;19:397–406.

[8] Lee JH, Lee HB. Platelet adhesion onto wettability gradient surfaces in the absence and presence of plasma proteins. Journal of Biomedical Materials Research 1998;41:304–11.

[9] Tsai WB, Grunkemeier JM, Horbett TA. Human plasma fibrinogen adsorption and platelet adhesion to polystyrene. Journal of Biomedical Materials Research 1999;44:130–9.

[10] Robitaille R, Pariseau JF, Leblond FA, Lamoureux M, Lepage Y, Hallé JP. Studies on small alginate-poly-L-lysine microcapsules. III. Biocompatibility of smaller versus standard microcapsules. Journal of Biomedical Materials Research 1999;44:116–20.

[11] Alauzun JG, Young S, D'Souza R, Liu L, Brook MA, Sheardown HD. Biocompatible, hyaluronic acid modified silicone elastomers. Biomaterials 2010;31:3471–8.

[12] Wei J, Igarashi T, Okumori N, Maetani T, Liu B, Yoshinari M. Influence of surface wettability on competitive protein adsorption and initial attachment of osteoblasts. Biomedical Materials 2009;4:1–7.

[13] Rivera J, Lozano ML, Navarro-Núñez L, Vicente V. Platelet receptors and signaling in the dynamics of thrombus formation. Haematologica 2009;94:700–11.

[14] Low SP, Voelcker NH, Canham LT, Williams KA. The biocompatibility of porous silicon in tissues of the eye. Biomaterials 2009;30:2873–80.

[15] Anderson JM, Rodriguez A, Chang DT. Foreign body reaction to biomaterials. Seminars in Immunology 2008;20:86–100.

[16] Ratner BD. The catastrophe revisited: Blood compatibility in the 21st Century. Biomaterials 2007;28:5144–7.

[17] McGuigan AP, Sefton MV. The influence of biomaterials on endothelial cell thrombogenicity. Biomaterials 2007;28:2547–71.

[18] Ward KW. The inflammatory response in implanted materials; a review of the foreign body response. Trends in Inflammation Research 2005:137–53.

[19] Gorbet MB, Sefton MV. Biomaterial-associated thrombosis: roles of coagulation factors, complement, platelets and leukocytes. Biomaterials 2004;25:5681–703.

[20] Anderson JM. Biological responses to materials. Annual Review of Materials Research 2001;31:81–110.

[21] Sefton MV, Gemmell CH, Gorbet MB. What really is blood compatibility? Journal of Biomaterials Science. Polymer Edition 2000;11:1165– 1182.

[22] Anderson JM. Multinucleated giant cells. Current Opinion in Hematology 2000;7:40–7.

[23] Williams DF. On the mechanisms of biocompatibility. Biomaterials 2008;29:2941–53.

[24] Efremova N, Bondurant B, O'Brien D, Leckband D. Measurements of interbilayer forces and protein adsorption on uncharged lipid bilayers displaying poly(ethylene glycol) chains. Biochemistry 2000;39:3441–51.

[25] Szleifer I. Protein adsorption on surfaces with grafted polymers: a theoretical approach. Biophysical Journal 1997;72:595–612.

[26] Holmberg M, Hou X. Competitive protein adsorption of albumin and immunoglobulin G from human serum onto polymer surfaces. Langmuir : the ACS Journal of Surfaces and Colloids 2010;26:938–42.

[27] Hansson KM, Tosatti S, Isaksson J, Wettero J, Textor M, Lindahl TL, et al. Whole blood coagulation on protein adsorption-resistant PEG and peptide functionalised PEG-coated titanium surfaces. Biomaterials 2005;26:861–72.

[28] Hlady V, Buijs J. Protein adsorption to solid surfaces. Current Opinion in Biotechnology 1996;7:72–7.

[29] Leibner ES, Barnthip N, Chen W, Baumrucker CR, Badding JV, Pishko M, et al. Superhydrophobic effect on the adsorption of human serum albumin. Acta Biomaterialia 2009;5:1389–98.

[30] Latour RA. Biomaterials: protein-surface interactions. Encyclopedia of Biomaterials and Biomedical Engineering New York: Marcel Dekker 2004:1–15.

[31] Agnihotri A, Siedlecki CA. Time-dependent conformational changes in fibrinogen measured by atomic force microscopy. Langmuir 2004;20:8846–52.

[32] Luttikhuizen D, Harmsen M, Van Luyn M. Cellular and molecular dynamics in the foreign body reaction. Tissue Engineering 2006;12:1955–70.

[33] Jackson SP. The growing complexity of platelet aggregation. Blood 2007;109:5087–95.

[34] Lee JH, Jeong BJ, Lee HB. Plasma protein adsorption and platelet adhesion onto comb-like PEO gradient surfaces. Journal of Biomedical Materials Research 1997;34:105–14.

[35] Ruggeri ZM, Mendolicchio GL. Adhesion mechanisms in platelet function. Circulation Research 2007;100:1673–85.

[36] Jeon S, Lee J, Andrade J, De Gennes P. Protein–surface interactions in the presence of polyethylene oxide:: I. Simplified theory. Journal of Colloid and Interface Science 1991;142:149–58.

[37] Lee H, Lee J, Andrade J. Blood compatibility of polyethylene oxide surfaces. Progress in Polymer Science(UK) 1995;20:1043–79.

[38] Kingshott P, Griesser HJ. Surfaces that resist bioadhesion. Current Opinion in Solid State & Materials Science 1999;4:403–12.

[39] Alcantar N, Aydil E, Israelachvili J. Polyethylene glycol-coated biocompatible surfaces. Journal of Biomedical Materials Research 2000;51:343–51.

[40] Morra M. Poly(ethylene oxide) coated surfaces. Water in Biomaterials Surface Science, Wiley; 2001, p. 1–44.

[41] Dalsin JL, Messersmith PB. Bioinspired antifouling polymers. Materials Today 2005:38–46.

[42] Fang F, Satulovsky J, Szleifer I. Kinetics of protein adsorption and desorption on surfaces with grafted polymers. Biophysical Journal 2005;89:1516–33.

[43] Kim M, Khang G, Lee H. Gradient polymer surfaces for biomedical applications. Progress in Polymer Science 2008;33:138–64.

[44] Bhat R, Timasheff SN. Steric exclusion is the principal source of the preferential hydration of proteins in the presence of polyethylene glycols. Protein Science : a Publication of the Protein Society 1992;1:1133–43.

[45] Sheth S, Leckband D. Measurements of attractive forces between proteins and end-grafted poly(ethylene glycol) chains. Proceedings of the National Academy of Sciences of the United States of America 1997;94:8399–404.

[46] Sofia S, Premnath V, Merrill E. Poly(ethylene oxide) grafted to silicon surfaces: grafting density and protein adsorption. Macromolecules 1998;31:5059–70.

[47] Malmsten M, Emoto K, Van Alstine JM. Effect of chain density on inhibition of protein adsorption by poly (ethylene glycol) based coatings. Journal of Colloid and Interface Science 1998;202:507–17.

[48] Leckband D, Sheth S, Halperin A. Grafted poly (ethylene oxide) brushes as nonfouling surface coatings. Journal of Biomaterials Science, Polymer Edition 1999;10:1125–47.

[49] Li D, Chen H, Mcclung WG, Brash JL. Lysine-PEG-modified polyurethane as a fibrinolytic surface: Effect of PEG chain length on protein interactions, platelet interactions and clot lysis. Acta Biomaterialia 2009:1–8.

[50] Fang F, Szleifer I. Effect of molecular structure on the adsorption of protein on surfaces with grafted polymers. Langmuir 2002:5497–510.

[51] Fang F, Szleifer I. Kinetics and thermodynamics of protein adsorption: a generalized molecular theoretical approach. Biophysical Journal 2001;80:2568–89.

[52] Corum L, Hlady V. screening platelet - surface interactions using negative surface charge gradients. Biomaterials 2012;31:3148–55.

[53] Haugland RP. Coupling of monoclonal antibodies with fluorophores. Methods in Molecular Biology 1995;45:205–21.

[54] Axelrod D, Burghardt TP, Thompson NL. Total internal reflection fluorescence. Annual Review of Biophysics and Bioengineering 1984;13:247–68.

[55] Hlady V. Spatially resolved adsorption kinetics of immunoglobulin G onto the wettability gradient surface. Applied Spectroscopy 1991;45:246–52.

[56] Ding Y, Hlady V. Competitive adsorption of three human plasma proteins onto sulfhydryl-to-sulfonate gradient surfaces. Croatica Chemica Acta 2011;84:193–202.

[57] Vasilev K, Mierczynska A, Hook AL, Chan J, Voelcker NH, Short RD. Creating gradients of two proteins by differential passive adsorption onto a PEG-density gradient. Biomaterials 2009;31:392–7.

[58] Jo S, Park K. Surface modification using silanated poly (ethylene glycol) s. Biomaterials 2000;21:605–16.

[59] Corum L, Hlady V. Screening platelet-surface interactions using negative surface charge gradients. Biomaterials 2010;31:3148–55.

[60] Lin YS, Hlady V, Golander C. The surface density gradient of grafted poly(ethylene glycol): preparation, characterization and protein adsorption. Colloids and Surfaces 1994;3:49–62.

[61] McPherson T, Kidane A, Szleifer I, Park K. Prevention of protein adsorption by tethered poly(ethylene oxide) layers: experiments and single-chain mean-field analysis. Langmuir 1998;14:176–86.

[62] Bhat RR, Tomlinson MR, Wu T, Genzer J. Surface-grafted polymer gradients: formation, characterization, and applications. Advances in Polymer Science 2006;198:51–124.

CHAPTER 5

CONCLUSION

This work has demonstrated the design, fabrication, and characterization of two new biomedical devices: (i) the capsular drug ring (CDR); and (ii) the endo-contact lens. These two devices are designed to improve patient outcomes with ocular diseases, specifically age-related macular degeneration, glaucoma, and cataracts. This work also discusses the impact of polyethylene glycol (PEG) surface density on the adsorption of proteins to a surface, regarded as the first step in determining an implant's biocompatibility.

AMD is the leading cause of blindness and significant visual impairment in developed nations. Significant improvement in patient health outcomes can be made through the development of an extended release device, the CDR. This work has demonstrated the successful design and manufacture of the device. It was also shown that the device is able to deliver Avastin for clinically relevant durations (i.e., 90+ days) and it was able to do so while showing acceptable biocompatibility. *In vitro* direct contact assays show little difference in migration, proliferation, and proinflammatory cytokine generating behaviors when compared to gold standard culture methods. The CDR continues to be a work in progress, but key *in vitro* device biocompatibility and efficacy assessments demonstrate the potential of the device.

Three million cataract surgeries are performed annually within the United States. Within the eye, a delicate monolayer of cells known as the corneal endothelium is damaged to various degrees during surgery. This damage results in decreased corneal clarity and can potentially result in the need for corneal transplantations. The endo-contact lens has been developed as a simple and easy to use device for the purpose of shielding the cornea during cataract surgery. It specifically shields the corneal endothelium from thermal and fluidic injury that is caused by phacoemulsification.

This research has shown the successful design and development of key aspects of the endo-contact lens. *In vitro* and preliminary *in vivo* results indicate that the device would be biocompatible in the ocular space within its intended purpose. Computer modeling shows device efficacy in the protection of the corneal endothelium during surgery by reducing thermal exposure by 45%. Preliminary *in vivo* results show a significant reduction in corneal swelling and an increase in endothelial cell counts after surgery.

The biocompatibility of biomedical implants is highly dependent on the interaction of the implant surface with the proteins and cells of the body. Polymer coatings, especially PEG, have long been studied for the purpose of improving medical device biocompatibility. This work attempted to further understand the mechanisms of PEG's protein inert qualities. In order to do so, polymer density gradient surfaces were generated and characterized. Total internal reflection fluorescence (TIRF) was used in conjunction with fluorescently-labeled albumin and fibrinogen to quantify the adsorption of these proteins to the PEG gradient surfaces. One percent protein concentrations showed very low adsorption to surfaces. In addition, the polymer surface density gradient was shown to have a nearly linear effect on protein adsorption. At 10% protein

concentrations the effect of PEG was more pronounced and a step function of protein adsorption was observed. When buffer was flowed over the surface after 10 minutes of exposure no detectable protein remained adsorbed to the surface.

The important contributions of this dissertation work are listed below.

1. A comprehensive review of the management of ocular diseases including age-related macular degeneration, glaucoma, and cataracts.
2. A comprehensive review of the state of the field of implantable ocular drug delivery devices.
3. The development and manufacture of the CDR showing Avastin drug release *in vitro* out to 90+ days.
4. An assessment of the *in vitro* ocular biocompatibility of the CDR.
5. The development and manufacture of the endo-contact lens.
6. COMSOL modeling showing the efficacy of the endo-contact lens in reducing exposure of the corneal endothelium to thermal energy by 45%.
7. Manufacture methods of the endo-contact lens showing no PDMS monomer leaching preventing long term exposure of ocular tissues to the biomaterial.
8. Preliminary *in vivo* results showing efficacy of the endo-contact lens showing a 39.1% reduction in postsurgical corneal thickening and 1.91 times the number of postsurgical viable corneal endothelial cells.
9. Preliminary *in vivo* results showing healthy cellular morphologies postsurgery with the use of the endo-contact lens.
10. The methods for the formation of two different types of PEG density gradients for use in the study of PEG and protein adsorption.

11. Results showing protein adsorption to PEG surfaces at 1% and 10% blood concentrations.

Future Work

While this dissertation has answered important questions and shown successful development of two ocular biomedical devices, it has opened up a number of new areas that need to be explored and developed in the future.

Capsule Drug Ring

The development of the CDR has progressed through the majority of its *in vitro* work. Up to this point, the CDR biocompatibility assays have all be performed in absence of Avastin, the expected drug of choice for this device. Future work will include the incorporation of Avastin into *in vitro* biocompatibility assays to determine the effect of the drug presence. In addition, improved drug release kinetics to improve the long term efficacy of the device will need to be developed. In order to complete this task an effective model for the determination of required daily dosage will need to be developed. With the end goal of advancing this device into clinical use, the complete statistically powered *in vivo* biocompatibility and efficacy assessment of the device will need to be completed.

Endo-contact Lens

The safety and efficacy of the endo-contact lens can best be elucidated through *in vivo* animal models. Through *in vivo* testing it is expected that the potential inflammatory

and immune response that may develop hours or days after the use of the device can be quantified. *In vivo* endo-contact lens assessments should make use of slit lamp examination, measurement of intraocular pressure, and indirect ophthalmoscopy to evaluate possible toxic effects of the use of the endo-contact lens postsurgery. Histopathological examination will further this determination and will also quantify the efficacy of the endo-contact lens *in vivo*. In order to simulate a complex case of cataract surgery, phacoemulsification should be performed until at least 100 cumulative dissipated energy (CDE) has been exerted. Harvested corneas and irises which undergo histological analysis (hematoxylin and eosin (H & E)) to evaluate morphology and anatomic toxicity will better elucidate the biocompatibility and efficacy of this device.

Polyethylene Glycol Surfaces

Gradient surfaces were studied using protein solutions of 1% and 10% blood concentrations. Additionally, each experiment was carried out for only a single protein at a time. Biological conditions include higher protein concentrations and complex protein and cellular conditions. In order to better understand the effect of PEG on protein adsorption under biological conditions, higher protein concentrations and more complex protein mixtures need to be studied. The next step in this study is to quantify protein adsorption to surfaces under mixtures of the albumin, fibrinogen, and IgG and to study these protein mixtures at 1%, 10%, and 100% that of blood concentrations. Further studies would include the evaluation of platelet-free plasma on gradient surfaces.

In summary, for the development of biomedical devices including the CDR and endo-contact lens to progress into clinical use, statistically powered *in vivo* biocompatibility

and efficacy assessments need to be completed. These assessments as well as the study of protein surface adsorption can contribute to development in theoretical understanding, and specific application based biocompatibility.